Design and Performance Analysis of Photonic Crystal Waveguide for Bio – Chemical Sensing Applications

Thesis Submitted
by

Balveer Painam
(Regd. No. 901306004)

In fulfillment of the requirement for
the degree of
Doctor of Philosophy

Supervisors

Dr. R. S. Kaler
Sr. Professor
ECE Department
Thapar Univeristy, Patiala, Punjab

Dr. Mukesh Kumar
Asst. Professor
EE Department
IIT, Indore, Madhya Pradesh

Department of Electronics and Communication Engineering
Thapar University, Patiala – 147004
Punjab, India

Dedicated to

My

Grandparents, Parents

&

Teachers

Certificate

I, Balveer Painam hereby certify that the work presented in this thesis entitled "**Design and Performance Analysis of Photonic Crystal Waveguide for Bio-Chemical Sensing Applications**" in fulfillment of requirement for the award of the Degree of the Doctor of Philosophy in Electronics and Communication Engineering Department, Thapar University, Patiala, is an authentic record of my own work carried out under the supervision of **Dr. R. S. Kaler**, Sr. Professor, Electronics and Communication Engineering Department, Thapar University, Patiala, India and **Dr. Mukesh Kumar**, Asst. Professor, Electrical Engineering Department, IIT, Indore, India.

The matter presented in this thesis has not been submitted in any other university or institute for the award of any degree or diploma.

Date: 18th August, 2017

Balveer Painam
Signature of the candidate

This is certified that the above statement made by the candidate is correct to the best of my knowledge.

Date: 18th August, 2017

Dr. R. S. Kaler
Senior Professor,
ECE Department
Thapar University, Patiala

CONTENTS

ACKNOWLEDGEMENTS

The real spirit of achieving a goal is through the way of excellence and austere discipline. I would have never succeeded in completing my task without the cooperation, encouragement and help provided to me by various personalities. With deep sense of gratitude I express my sincere thanks to my esteemed and worthy supervisor, Dr. R. S. Kaler, Senior Professor, Department of Electronics and Communication Engineering, Thapar University, Patiala and Dr. Mukesh Kumar, Assistant Professor, Electrical Engineering Department, IIT, Indore, for their valuable guidance in carrying out the work under their effective supervision, encouragement, enlightenment and cooperation. Most of the novel ideas and solutions found in this thesis are the result of our numerous stimulating discussions. Their feedback and editorial comments were also invaluable for writing of this thesis.

Out of a deep sense of gratefulness, I express my sincere thanks to Dr. O.P. Pandey, Dean (RSP), Dr. Alpana Aggarwal, Head ECED for continuous appreciation and support. I am also thankful to my doctoral committee members Dr. Kulvir, Dr. Sanjay Kumar and Dr. Hardeep Singh for their encouragement, constructive criticism and inspirations.

A special thanks to my lab mates, Mr. Pradeep, Ms. Gurpreet, Mrs. Rajan, Mrs. Shivani, Ms. Jiwan, Ms. Mukti, Ms. Madhavi, Mr. Sarabjit, Ms. Rupinder and Ms. Harshita ensured me to never feel bored and helped at each and every step of my research work. Together, we have undertaken many tasks and completed successfully with good team spirit. I gained a lot from them, through their personal and scholarly interactions, their suggestions at various points in my research program.

The experimental work in the thesis during my research work would not be possible without the necessary guidance of Ms. Tanu Shree of SCBC and Dr. M. S. Reddy Sir, Mrs. Bharati and Mr. Arkadeep from DBT and Ms. Megha from CSED. I would like to extend my thanks to SAI labs, Thapar University, Patiala and this work was supported by the grant from Department of Biotechnology under the Ministry of Science and Technology, Government of India.

I am indebted to all my seniors, Dr. Suresh, Dr. Ranvir, Dr. Simran, Dr. Rakesh, Dr. Dewra, Dr. Bhupinder, Dr. Tarun, Dr. Nidhi and Mr. Varun for their valuable suggestions. I would like to thank all my friends Mr. Ravi, Mr. Rajesh, Ms. Rajni, Mr. Satish, Mr. Gopi, Mr. Sravan and Mr. Phanindra who supported me throughout the course of this work. I would like to thank Ms. Prathyusha for providing support and suggestions in the research work. Last but not the least, I would like to thank all my relatives and those who have provided their help in a direct or indirect manner to achieve this goal.

I would like to pay my gratitude towards my parents, who have always supported me in doing the things my way and whose everlasting desires, encouragement, affectionate blessings and help made it possible for me to complete my degree. I would also like to render my gratitude to the Almighty God who bestowed self-confidence, ability and strength in time to complete this task and for not letting me down at the time of crisis and showing me the silver lining in the dark clouds.

Finally, words are not adequate to express my gratitude to my brother Mr. Raghuveer and my sister Ms. Srilaxmi for their patience, support and active assistance in many ways.

Balveer Painam
901306004

ABSTRACT

The consistent progress of electronic equipments in different fields, especially in control technology has brought a positive impact on communication and sensing technology. Fiber optic technology has historically dominated the communication field and recently tending towards the sensing field. Sensing devices are underway to build their own optical devices in place of electronic devices due to selectivity and specificity. Derived from the same fiber optic sensor family, photonic crystal (PC) sensor technology is rapid, pathogen-specific, and does not require chemical modification of the test sample. PCs offer the possibility of controlling and manipulating light by opening a gap in the waveguide within a given range of frequencies and it may hold the key to the continued progress.

In this thesis, we proposed different PC sensor designs to exploit the applications in the field of biochemical such as chemicals and food testing. Photonic crystal waveguide (PCW) design for chemical concentration detection is performed on sulfuric acid (H_2SO_4) and hydrogen peroxide (H_2O_2) as they are highly useful in industrial and research applications. Design of PCW for foodborne pathogen detection is performed on *Escherichia coli* (*E. coli*) as it is one of the most dangerous agent of foodborne diseases.

Various semiconductor materials and insulator with higher to lower refractive indices (Si, GaAs, Si_3N_4, and SiO_2) are analyzed to fix the choice of material for PCW design. The design and analysis are performed using the finite difference time domain (FDTD) simulation method. The design exhibits two inverted J-shaped defects with center cavity designed in the shape of *E. coli*. In this research, DH5α strain of *E. coli* foodborne pathogen is considered as a model due to its shape. Simulation of PCW design is performed using infrared radiation wavelengths. Simulation analysis reports larger resonance wavelength shifts, higher sensitivities, and quality factors for Si-based PCW biosensor at an operating wavelength of 1.55 μm.

Another proposed PCW design of biochemical sensor is to identify the chemical component's acid concentrations with a greater accuracy. The experiment is also performed to identify the refractive indices of H_2SO_4 and H_2O_2 chemical components using refractometer. The proposed design consists of circular air holes of radius 0.44a (where 'a' is the lattice constant of 0.45 μm), arranged in a hexagonal structure on silicon on insulator (SOI). Due to the change in refractive index of the sample, resonance wavelength shifts towards higher wavelengths (red shift) with a higher coefficient of determination. The proposed design allows desired input wavelength of

1550 nm to be guided in the waveguide for an effective identification of chemical component's concentrations. Resolution and limit of detection are calculated as 1.2 nm and 4×10^{-2} RIU for H_2SO_4 solution and 0.2 nm and 2×10^{-2} RIU for H_2O_2 solution. Improved sensitivities with increased standard deviations are achieved after structural optimization.

Further, we proposed a design of PCW sensor for chemical sensing applications at sodium doublet line (Sodium-D-line). The proposed PCW sensor is patterned on 10×10 µm silicon on insulator (SOI) wafer. PCW designed with circular air holes of radius r = 0.35a where 'a' is the lattice constant of 0.45 µm, arranged in hexagonal structure. The principle of measurement is based on variation in refractive index of sample that causes change in effective refractive index (ERI) in guided mode leading to blue shift. Experimental results of refractive index are used in sensing analysis. The proposed design is capable of allowing sodium-D-line wavelength through structure to work as chemical and biochemical sensor.

In the final design for foodborne pathogen detection, we considered *E. coli* cell is trapped in the middle of the PCW biosensor having three different types of waveguides, i.e., gallium arsenide/silicon dioxide ($GaAs/SiO_2$), silicon/silicon dioxide (Si/SiO_2), or silicon nitride/silicon dioxide (Si_3N_4/SiO_2) to observe the maximum resonance shift and sensitivity. It is observed from the simulation data analysis that $GaAs/SiO_2$ is the preferred PCW biosensor for the identification of *E. coli* and optimization is carried out to achieve highest sensitivity and quality factor by varying the ring slot width and radius of the design.

The proposed PCW biochemical sensor designs reveal that Si and GaAs materials are suitable as an active layer for sensing applications. By using effective refractive index phenomena, wavelength shift is observed due to change in refractive index. Finally, device optimization is achieved by introducing variations in geometry of the design.

THE THESIS INCLUDES FOLLOWING LIST OF SCI PUBLICATIONS

[1] B. Painam, R. S. Kaler and M. Kumar, “Photonic Crystal Waveguide Biochemical Sensor for the Approximation of Chemical Components Concentrations”, Plasmonics, DOI: 10.1007/s11468-016-0341-z, 2016 (I.F: 2.146)

[2] B. Painam, R. S. Kaler and M. Kumar, “On-Chip Oval Shaped Nanocavity Photonic Crystal Waveguide Biosensor for Detection of Foodborne Pathogens”, Plasmonics, DOI: 10.1007/s11468-017-0529-x, 2017 (I.F: 2.146)

[3] B. Painam, R. S. Kaler and M. Kumar, “Active layer identification of photonic crystal waveguide biosensor chip for the detection of Escherichia coli”, Optical Engineering, 55(7), 2016. (I.F: 0.984)

[4] B. Painam, R. S. Kaler and M. Kumar, “Label Free Chemical and Biochemical Sensing using Photonic Crystal Waveguide at Sodium-D Line”, Journal of Nanoelectronics and Optoelectronics, 12(1), pp.184-188, 2017. (I.F:0.675)

[5] B. Painam, R. S. Kaler and Mukesh Kumar “High Sensitive On-Chip Photonic Crystal Waveguide Biosensor with Ring Slot for Foodborne Pathogens Detection”. (Under Preparation)

CONFERENCE PUBLICATION

[1] B. Painam, P. K. Teotia, R. S. Kaler and M. Kumar, "Bio-Chemical Sensor Based on Photonic Crystal Waveguide for Estimation of Sulphuric Acid Concentration," in 12th International Conference on Fiber Optics and Photonics, OSA Technical Digest (online) (Optical Society of America, 2014), paper S5A.48.

LIST OF FIGURES

LIST OF TABLES

LIST OF ACRONYMS

1. One dimensional (1D)
2. Two dimensional (2D)
3. Three dimensional (3D)
4. Photonic crystal (PC/PhC)
5. Transverse Electric (TE)
6. Transverse Magnetic (TM)
7. Radio-Frequency Identification (RFID)
8. Optical Fiber Sensor (OFS)
9. Total Internal Reflection (TIR)
10. Photonic Crystal Waveguide (PCW)
11. Wireless and network sensors (WSNs)
12. Micro electro mechanical systems (MEMS)
13. Surface Plasmon Resonance (SPR)
14. Side-Polished (SP)
15. Mach-Zehnder Interferometer Sensors (MZIs)
16. Optical Path Difference (OPD)
17. Refractive Index (RI)
18. Optical Fiber Sagnac Interferometer Sensor (OFSIs)
19. Fabry-Perot Interferometer Sensor (FPIs)
20. Fiber Fabry-Perot Interferometer (FFPI)
21. Michelson Interferometer Sensors (MI)
22. Centre for Disease Control and Prevention (CDC)
23. Enzyme-Linked Immunosorbent Assays (ELISA)
24. Western Bolt Analysis (WBA)
25. Polymer Chain Reaction (PCR)
26. Photonic Crystal Fibers (PCF)
27. Photonic Crystal Waveguide (PCW)
28. Finite-Difference Time-Domain (FDTD)
29. Plane Wave Expansion Method (PWE)
30. Finite Element Method (FEM)
31. Terahertz (THz)
32. Omnidirectional Photonic Band Gap (OPBG)
33. Intelligent Polymerized Crystalline Colloidal Array (IPCCA)
34. Group Velocity Dispersion (GVD)
35. Silicon upon Sapphire (SOS)
36. Gallium Arsenide (GaAs)
37. Photonic Band Gap (PBG)
38. Phosphate-Buffered Saline (PBS)
39. Plane Wave Expansion (PWE)

40. Sulfuric Acid (H_2SO_4)
41. Hydrogen Peroxide (H_2O_2)
42. *Escherichia Coli* (*E. Coli*)
43. Silicon On Insulator (SOI)
44. Gallium Arsenide/Silicon Dioxide ($GaAs/Sio_2$)
45. Silicon/Silicon Dioxide (Si/Sio_2)
46. Silicon Nitride/Silicon Dioxide (Si_3N_4/Sio_2)
47. Polarization Maintenance Optical Fibers (PMFs)

CHAPTER 1. INTRODUCTION TO SENSORS

1.1 INTRODUCTION

This chapter introduces sensors and their working principle. Advancement in sensor technology is discussed along with the challenges faced by electrical sensors. Optical fiber sensors (OFS) are accessible due to their extensive advantages. The working of OFS and their reach into the communication, electrical field applications and approach in medical field are explained. It also describes the specifications, classifications and latest developments in sensor technology. Broad areas of OFS including photonic crystal waveguide sensors are covered along with their classification, principle of operation and applications.

1.2 SENSORS

A device which converts physical parameters to measurable electrical signals is known as sensor. In recent years, sensors usage is rapidly expanding in measurement and instrumentation fields. A new generation radio-frequency identification (RFID) based chip sensors are used in communications [1]. In most of the cases electromechanical sensors serve the purpose of all kind of requirements in industrial and domestic fields. Sometimes, electrical related sensors also experience difficult situations while performing their operations under challenging circumstances, for example the temperature of the sensor is affected by the external environment which in return effects on the performance of the sensor.

OFSs are similar to electrical sensors as they also convert physical parameters to optical signals. These optical signals are transmitted along the fiber from source to detector by the operational principle of total internal reflection (TIR). The major advantage of OFS over electrical sensor is its immune nature to electromagnetism. For this nature, OFS is extensively used in electrical related fields, eg. Substations, Communications, etc.

In communication networks, slow light phenomenon has promising and potential applications. Predominantly, PC materials are competent of carrying slow light transmission. The use of OFS has increased dramatically and commercialized in the past two decades and now it is expanding in the field of medical as well.

Optical biosensor has come up with solutions for all the existing problems of conventional test methods. Surface plasmon resonance and quartz crystal microbalance are two recent methods in optical biosensors and chemical sensing. Derived from the same optical biosensor family photonic crystal waveguide (PCW) sensor technology is quick, specific and does not require any kind of chemical deposition on the surface layer.

1.3 SENSOR SPECIFICATIONS

There are some specific features that must be taken into account while choosing the sensor. They are as follows:

- Accuracy – It is different from sensor resolution. It is a figure of merit - how accurately the sensor can measure unknown parameters. These parameters are measured at reference conditions excluding temperature effects. To calculate overall accuracy, temperature effect values are included where it can be compensated [2]. The noise factor limits the resolution of sensors which in turn effects the accuracy [3]. Accuracy is the combined effect of linearity, hysteresis, dead-band and repeatability errors.
- Limits – The physical quantity which is to be measured should have magnitude within the specified range of the sensor for accurate measurements [4]. If physical parameter measurements are above or below the sensor limits it may not give accurate results due to many factors involved in designing the sensor.
- Calibration – It helps both, the company and the buyer by providing important specification in sensor devices with continuous changes in the measuring values with time [5]. Calibration can be done by eliminating the structural errors from the design of sensor to improve its performance. The structural errors are defined

as the difference between expected outputs of the sensors to the measured output [6].

- Resolution – It is defined as the minimum detectable signal variation within the sensor device. Variations are temporal occurrences, the relation exists between the minimum measurand amplitude and timescale variations. The nature of measurand is included in defining the resolution. White spectral distribution creates noise in the sensor devices [5]. Quantifying the measurand concentration with accuracy and relating it to the error which is associated with the experimental measurement [7].
- Cost – Bundles of wires are connected to systems in traditional methods, so fault detection and correction are time consuming and expensive [4]. To overcome these issues, simple and low cost systems like sensors are developed in almost all the fields. Sensor devices are often specific to the application used. Based upon the specific application, suitable material, proper design and process has to be adopted to make low cost sensors [8].
- Stability – The maintenance of accuracy and a consistent output of a sensor is required for constant power supply. It is basically further categorized into two kinds that are (i) short–term and (ii) long–term stabilities. Ambient condition difference and low temperature coefficient leads to the short–term stability. Frequent calibration is done in the long–term calibration and measures within the 0.2^{o}C per year. Si has low temperature coefficient therefore, it is suitable in both the conditions [9].
- Repeatability – Sensors are able to produce the same results under repeated identical conditions. If the sensor is unable to produce the same results under specified conditions, it is known as repeatability error. Mathematically, it is shown as the output difference of two cycles. It is specified as percentage of full scale:

$$\delta_r = \frac{\Delta}{FULL\ SCALE} \times 100\%$$

Factors affecting the repeatability error may be the imbalance between positive and negative charges or Nyquist noise or type of material [10].

1.4 SENSORS CLASSIFICATION

Sensors can be classified depending upon power required by sensors, based on selected reference and applications [11].

Based on power supply:

- Active sensor: For these types of sensors external power supply is required. Example: Thermistor and strain gauges, etc.
- Passive sensor: These types of sensors do not require any external power supply rather they are capable of producing their own input power [5]. Example: Thermocouples and photodiodes etc.

Based on selected reference:

- Absolute sensor: It identifies a difference in reference to the actual measurement that is not dependent on the measurement condition. For example, electrical resistance of thermistor linearly depends on the actual scale of Kelvin temperature.
- Relative sensor: It generates a signal that relates to a special property. For example, thermocouple generates voltages which are the function of a thermocouple wires temperature gradient. Without knowing the reference line of a thermocouple, output signal do not come up with any particular value of temperature [10].

Based on applications:

- Industrial applications: In industries sensors' requirement is classified into three different fields, these are: visual monitoring, identifications of parts and adjusting repetitive. Most of the industries repetitive job operations are being replaced by robotic machines with sensors. Automation consists of robotics and sensors to perform specific task under the control of computers software programs [12]. But computer simulations indicate that, a unique phase exists [13].

- Non-industrial applications: Air turbulences cause route deviations of light weight aircrafts. To overcome this, very high resolution synthetic aperture radar sensors are used [14]. Medical ultrasounds consist sensors for imaging. Imaging cost depends upon the number of sensors used to sample the imaging aperture [15].

1.5 LATEST DEVELOPMENTS IN SENSOR TECHNOLOGY

Recently developed sensor technologies in various fields are shown below:

- Magnetic sensors: It is used for cancer treatment. A needle type giant magneto resistance sensor is employed to determine the weight density of magnetic fluid inside large tumors. It uses the magnetic loss property of magnetic nano particles due to external alternating current magnetic fields [16].
- Household appliances: It is one of the largest market for electronic products. Recently, modern sensors with intelligent control system are leading with distinguished features for example security alarms, fire detection alarms, dish washers and floor care equipments [17].
- Vision/image sensors: Present status of image sensors are much more improved compared to earlier. They have reached to the megapixels capacity. Foveated image sensors reduce image size and resolution to reduce data volume [18].
- Wireless and network sensors (WSNs): These network sensors are having wide variety of applications in almost all fields. It is very challenging research activity of wireless sensors in sensing distributed environmental monitoring [19].
- Humidity sensors: Due to its simplicity, low cost and ability to detect more number of gaseous metal oxides it became important for gas sensing materials [20].
- Gas sensors: By screen printing technique thick films are prepared which are used to determine the response of electrical resistance for different gases, like LPG, CO_2, O_2, NH_3, H_2S and CO at different temperatures [21].
- Micro electro mechanical systems (MEMS) thermal sensors: These are utilized in numerous fields, such as temperature sensing , human presence and medical thermograph [22].
- Surface acoustic wave sensors: Sensors are used for long term measurements at stable ambient conditions [18].

OFS can provide a solution when conventional sensors fail to perform [23]. Fiber technology was introduced mainly for telecommunication. But, due to increment in

quality and decrement in cost of optoelectronic components, their usages are extended towards sensing applications [24].

1.6 FIBER OPTIC SENSORS

Physical parameters measurements are converted into optical signals in optical fiber using optical fiber sensor [25]. Fiber optic sensor concept was introduced with the advancement, in the mid-1960s, of the "Fotonic" sensor, a device which detects and measures the physical parameters, particularly in automated industry [26]. Since past 25 years, optical fiber sensors are commercially successful in telecommunication field [27].

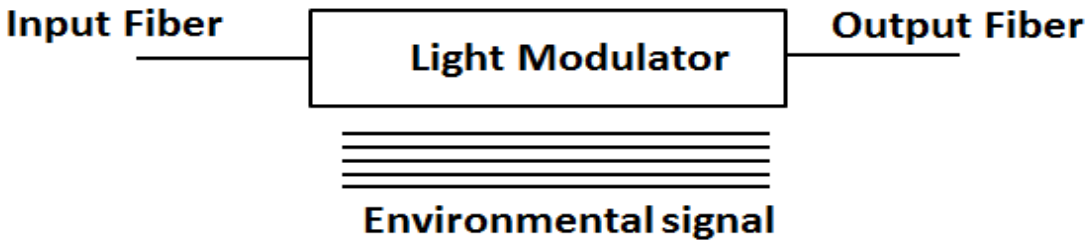

Fig. 1.1 Fiber optic sensor with optical fibers inserted into a "black box" to control and monitor the light transmission due to occurrence of an environmental effect.

Fiber optic sensors mass production has supported many industries. Improvements in the quality of sensors along with the reduction in cost has replaced the traditional sensors within the different field of applications. Along with the current trend, the requirement for the fiber optic sensor designers initiate to produce inexpensive and reliable products. The fiber optic sensor technology can be expected to achieve a leading position in the sensor market [28]. The most successful fiber optical sensor was the optical fiber gyroscope. Gyroscope was first reported in 1977 and later in 1990s, it evolved as a commercial instrument. Other fiber optic sensor devices gained importance in different field of applications such as temperature measurements, gas sensing, civil engineering, safety and security systems and biosensing applications [29]. The sensing abilities are improved by engineering the design structure of fiber optics by adding gratings, surface plasmon resonance (SPR) and fiber optic couplers [30]. In the following sections classifications and applications of fiber optic sensors are discussed.

1.6.1 CLASSIFICATION OF FIBER OPTIC SENSORS

Optical fiber sensors are classified on the basis of factors such as environment used, operating principle and point to point connections [31], which are discussed in the following sections.

1.6.1.1 INTRINSIC AND EXTRINSIC SENSORS

This classification is based upon the sensor location.

a) Intrinsic fiber optic sensor

Waveguide itself is the sensing element in intrinsic sensors [24]. Fiber plays an important role in sensing function when the modulation occurs inside the fiber medium. The above, sensors are further classified as - evanescent wave sensors, fiber grating sensors and interferometric sensors. Intrinsic sensors avoid dirt, dust, vibration and alignment problems by modulating the light while it is being transmitted within the fiber [32].

These sensors have completely dissimilar design. The alteration of the regulation of a measurand is done within the optical fiber. It is very difficult to develop these sensors but they show excellent performance. Sagnac gyro sensors were first one to be prospered for huge production. This type of gyros are diligently used these days for applications like transportation navigation, and satellite monitoring [33,34].

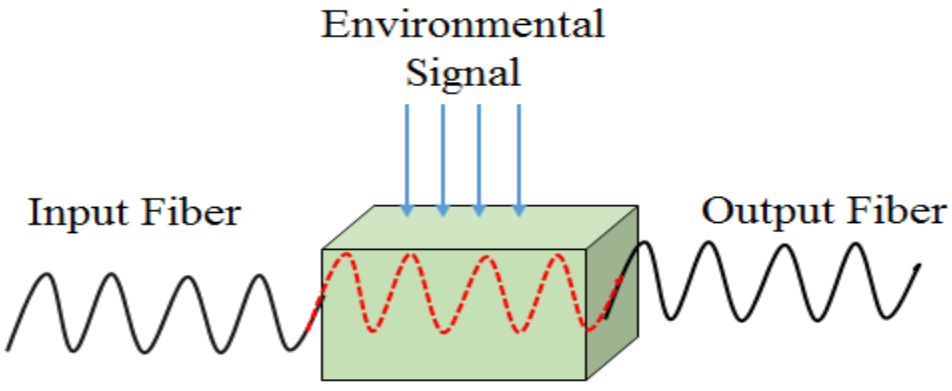

Fig. 1.2 Intrinsic fiber optic sensor.

b) Extrinsic fiber optic sensor

Detection takes place in the external region of optical fiber medium and the optical fiber performs as the channel waveguide for the input and output propagation of light till the area of sensing effectively [31]. In this, fiber is not used for sensing function [28]. It is further classified as direct spectroscopic based fiber optic sensor which covers absorption and florescence based techniques.

The optical fiber sensing element is controlling the light, in accordance with the physics phenomena (in this case a vibration). The light propagated through the fiber is guided through the device located at end point of fiber in order to convert regulated light into modulated electronic signal.

Various designs of optical fibers support these activities. And these are selected considering the necessity in applications. Fiber optic extrinsic sensors are usually not considered for the extraordinary level detections, rather they are appropriate only for desirable applications that require low cost and low resolution [33,34].

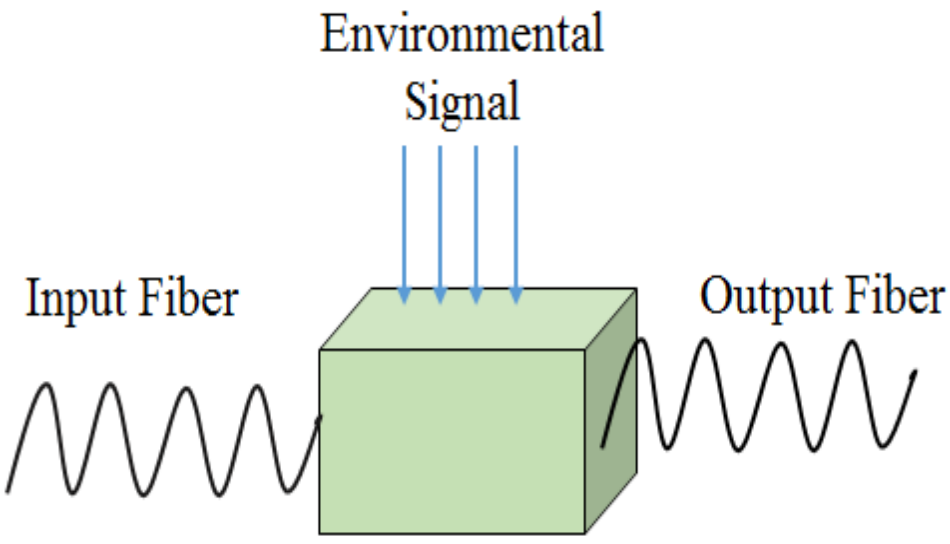

Fig. 1.3 Extrinsic fiber optic sensor.

1.6.1.2 MODULATION BASED FIBER OPTIC SENSOR

Depending upon the operating principle fiber optic sensors are classified into four types as shown below.

a) Fiber Optic Intensity-based Sensor

The extrinsic fiber optic sensor is based upon intensity regulation. Fig.1.4 represents the vibration sensor that has two tips of optical fibers held very closely. Light moves from one fiber to another depending upon their ability to come together. For example, these kind of optical fiber sensors are generally used for door applications.

Among sensors based on fiber optics, FOSs that are based on intensity are crucial because of their simplicity, low cost and since they were developed first, even today they are popular choice for numerous sensing applications. Because of their capability to compute a broad range of parameters, their usage of low cost sources of light and uncomplicated identifying schemes. They also have common advantages as of intrinsic sensors like minimum weight, tiny dimension, and immunity for electromagnetics. The optical fiber sensors require self-referencing feature to decrease the impact of aging in sources characteristics life span and are capable to handle the minute instabilities in optical fiber intensity at the input and output tip of the sensor [30].

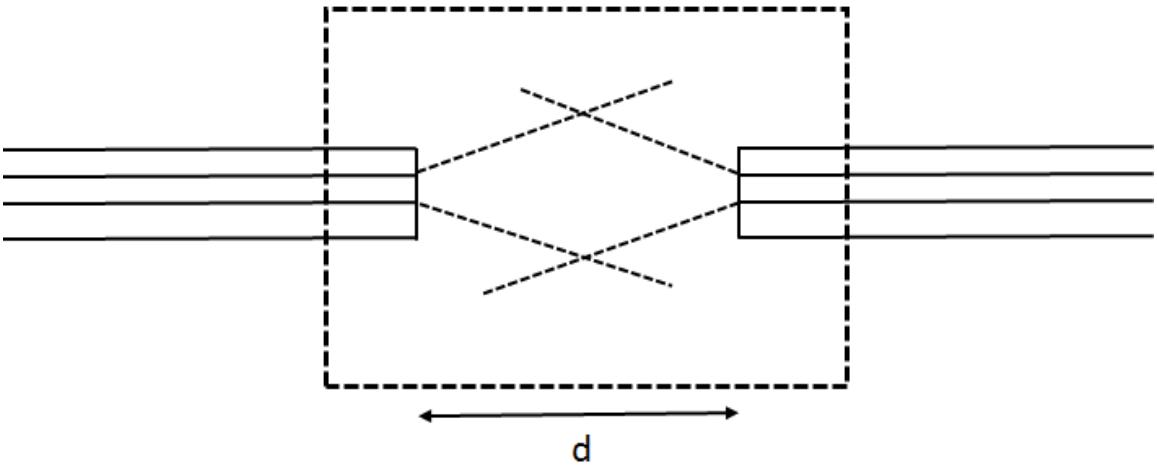

Fig. 1. 4 Intensity based fiber optic sensor.

b) Polarization-based Fiber Optic Sensor

Both the polarization devices and polarizers are crucial parts of sensor system and fiber optical communication. As shown in Fig. 1.5 D-shape optical fiber also called as Side-polished (SP) fiber optic polarizers are considered and operated as polarizer. Fundamental working operation of explained polarizer is to particularly attenuate the p-polarized or s-polarized mode of the optical waveguide that results in a p-polarized polarizer. Optical fiber sensor depends on polarization, mainly the sensing phenomena is functioned by the polarization feature [35, 36].

Glass is used to make optical fiber. The photo-elastic effect is created by the phenomena of variation in refractive index with implementation of strain and stress. Apart from this, in various situations, as the strain or stress in different directions are different and as the direction varies the induced refractive index also varies. This creates differences in phase between different polarization directions. Hence, depending upon variation in the polarization state at output, the detection of external perturbation takes place. These sensors are unaffected by environmental parameters, such as external surrounding temperature changes effects are null on the operation of sensors [31].

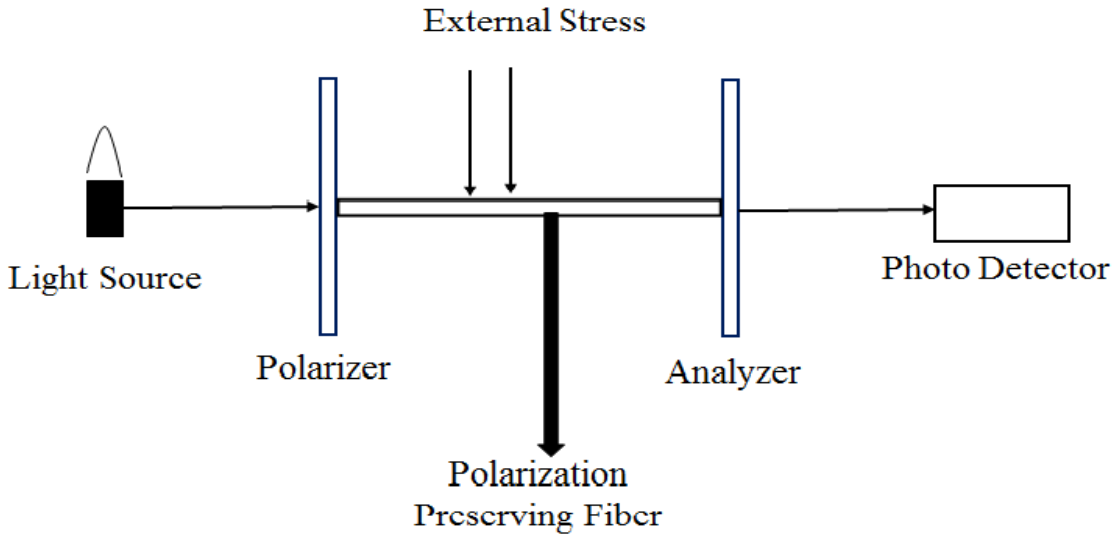

Fig. 1.5 Fiber optic polarization sensor.

c) Phase-based Fiber Optic Sensors

By applying external perturbations on optical fibers, phase of the light changes. Based on this principle fiber optic phase-based sensors are built. These sensors determines the corresponding phase delay initiated between light moving in two arms of an interferometer. To recover the information, the interference signal taken from the output of both arms either in the plane of a polarizer or at the surface of a detector is processed. Accordingly, this data can be retrieved only if the corresponding time lags between the transmission path which is less than the coherence time of each separate source [28].

d) Interferometer Fiber Optic Sensor

Interferometer fiber optic sensors need beam combining and beam splitting constituents in any arrangement, because they use interference between two rays which move via distinct fiber optical routes of one optical fiber or two distinct optical fibers. One of the optical path, is organized such that it can be easily disturbed by perturbations from outside. As the interferometer can give a lot of spectral and temporal data, one can measurably find the mesurand by various methods of determining changes in the wavelength, intensity, bandwidth, phase, frequency, etc. By utilizing sensing indicators, interferometer fiber optic sensors can provide extraordinary performance in exceptional dynamic range, optimum sensitivity and accuracy. Now a days, the size of fiber optic interferometers are scaled down in order to employ them in micro-scale applications. To facilitate the function of micro-scale sensors the old fashioned huge optic parts such as combiners, objective lenses and splitters are replaced by small sized fiber devices. In-line structures have undergone extensive investigation to check their ability to be implemented as fiber optic interferometers. The in-line architecture provides several benefits like simple alignment, huge coupling efficiency, and great stability [30].

i. Mach-Zehnder Interferometer Sensors (MZIs)

MZIs are often employed in different sensing applications due to their versatile design as shown in Fig. 1.6. Conventional MZIs have two non-dependent arms, like sensing arm and reference arm. Fiber coupler divides the incident light into two arms and later combines them. Interference component is present in recombined light in accordance with the optical path difference (OPD) between two arms.

For the sensing related applications, one arm is kept stable representing as a reference arm and another arm is used for sensing. The variation detected in the sensing arm is introduced due to refractive index (RI) changes the optical path difference of the MZI, temperature and strain are simply identified by studying the change in the interference signal [30].

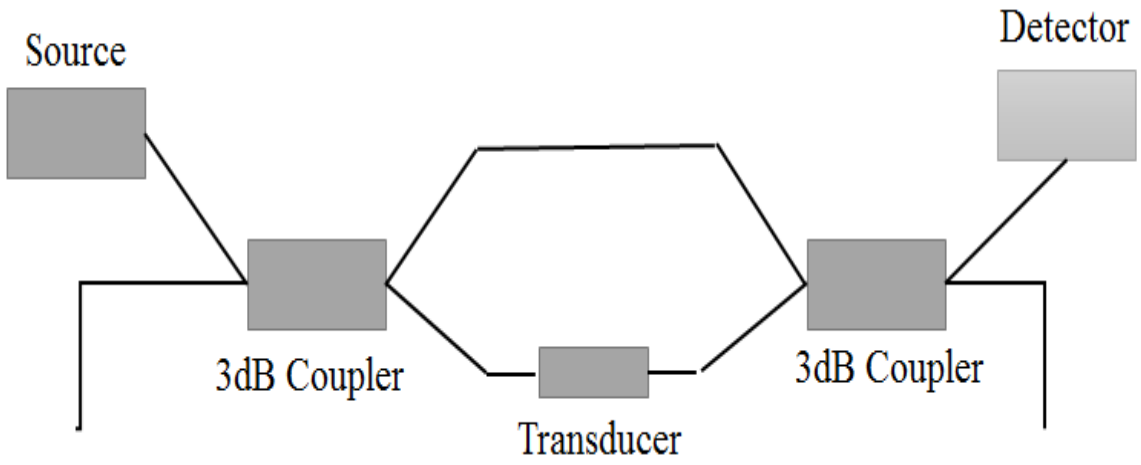

Fig. 1.6 Mach-Zehnder interferometer sensor.

ii. Optical Fiber Sagnac Interferometer Sensor (OFSIs)

OFSIs are extensively analyzed and employed in diverse applications of sensors for numerous years, such as gyroscopes etc. Few of those employed fibers that maintain polarization to initiate the difference in optical path and produce interference between the two oppositely moving waves in the Sagnac loop and are utilized as sensing elements. Panda and bow-tie Polarization Maintenance Optical Fibers (PMFs) have greater thermal expansion coefficient than the cladding due to the boron-doped stress-applying parts and their birefringence is very delicate to temperature as shown in Fig. 1.7 [37].

Sagnac interferometer has two famous arrangements, both in fiber optics and bulk, these two types are employed in many research applications to identify their maximum theoretical and practical sensibility, but the extensive studies has been carried out on interferometer in fiber optics than, interferometer in bulk optics, this is due to the principle proposed by Sagnac [38,39]. Theoretical study to build interferometer was available in previous centuries but technology to develop interferometer came when masers and lasers came into existence. After the first laser came into existence, the progress of interferometer in bulk optics was considered for academic presentation.

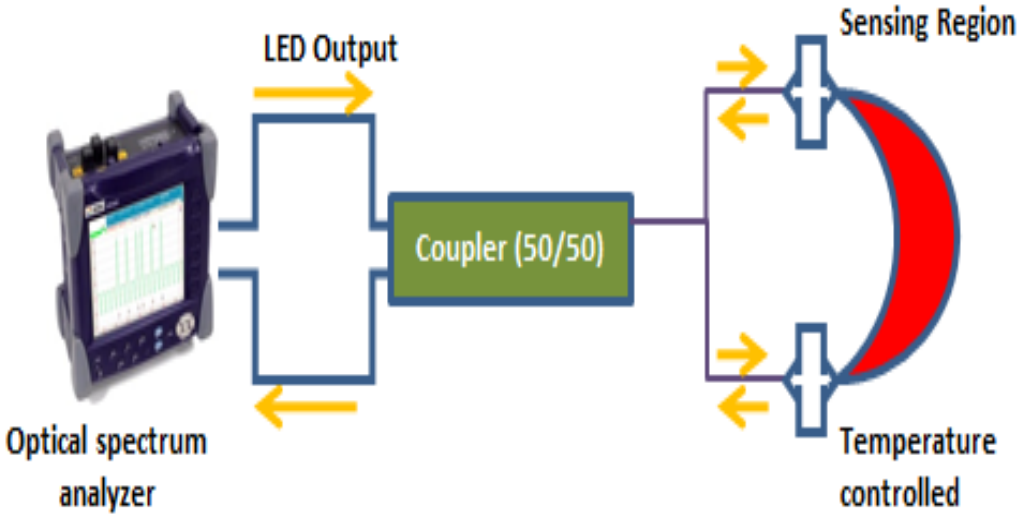

Fig. 1. 7 A conventional fiber Sagnac interferometer temperature system.

iii. Fabry-Perot Interferometer Sensor (FPIs)

Fiber-optic inline Fabry-Perot interferometers (FPI) are extensively considered in physical, biomedical, and chemical sensing applications because of their characteristics like miniature size, ability of concurrent multi-parameter detection with high sensitivity as shown in Fig. 1.8. Depending upon the geometrical structure, FPIs can be divided into two types as an open-cavity FPIs and sealed-cavity FPIs. Open cavity FPIs have less number of applications compared to sealed-cavity FPIs [40].

FBG sensor's new requirement is to improve its sensitivity in order to satisfy high-level needs, for example in the fields of monitoring in civil engineering, structural health diagnosis, etc. As familiar, a highly sensitive Fiber Fabry-Perot Interferometer (FFPI) is used in the most sensitive type of fiber sensor, as it has very narrowband transmission spectrum which allows extraordinary resolution sensing. The normal FFPIs use high reflectance as cavity reflector mirrors with dielectric thin film [41, 42].

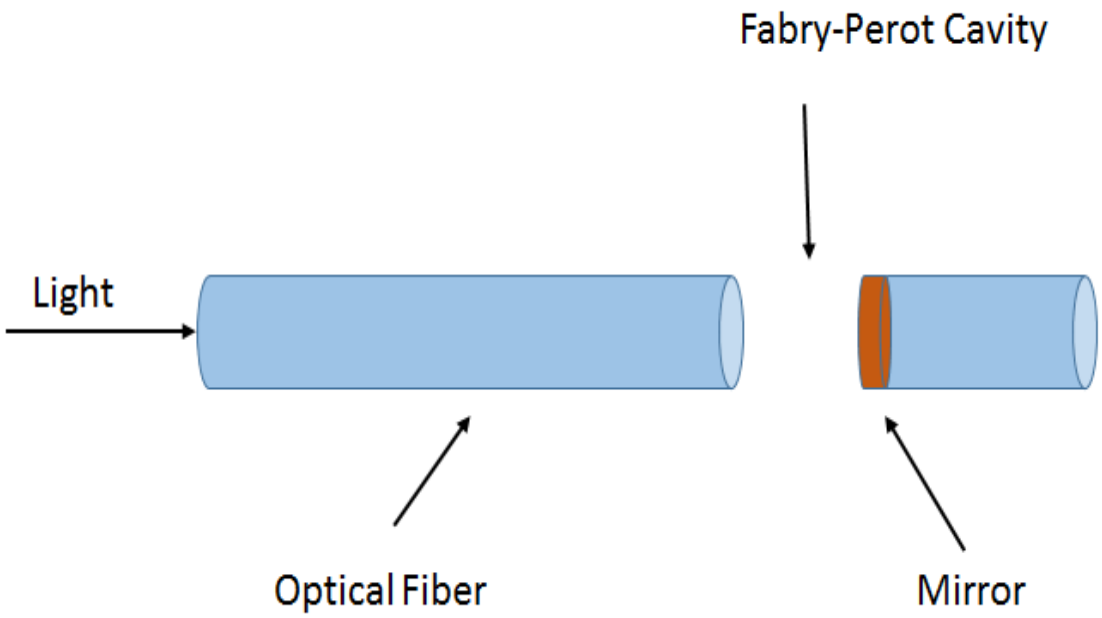

Fig. 1.8 Basic structure of a Fabry-Perot interferometer sensor.

iv. Michelson Interferometer Sensors (MI)

These sensors are based upon the concept of interference between the beams in two arms. As shown in Fig. 1.9 each beam is reflected at the end of each arm in MI. Moreover, MI is half similar to MZI in configuration. Hence, the assembly technique and the working procedure of MIs are quite similar to that of MZIs.

The important dissimilarity is reflectors. MIs are very convenient to use in practical situations and installation due to its reflection modes. One more advantageous point about MIs is their multiplexing capacity of many sensors with parallel connection. Anyways, it's necessary to tune between reference arm and sensing arm, fiber length difference should be within the light source coherence length. A fragment of the core mode beam is joined to the cladding mode(s) that is reflected along with the uncoupled core mode beam by the common reflector at the end of the fiber [30].

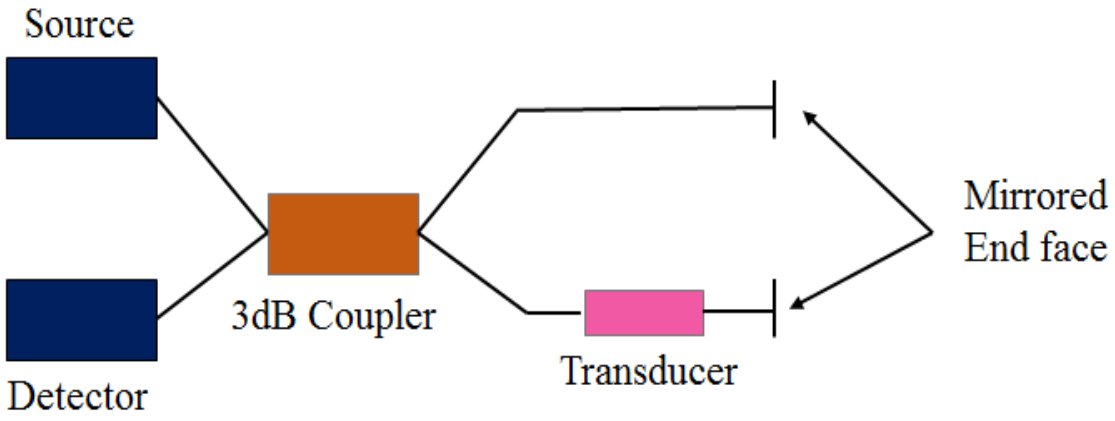

Fig. 1.9 Simple diagram of Michelson interferometer sensor.

1.6.1.3 MULTIPLEXED AND DISTRIBUTED SENSORS

The best advantage of fiber optic sensors is to sense at any point using one optical fiber. In response to measuring points fiber optic sensors are classified into three categories; point to point sensors, distributed sensors and multiplex sensors.

a) Distributed sensor

Sensing is allowed at any point throughout each fiber optic line as shown in Fig. 1.10 (a & b). The measurand field acting along the fiber length can be observed in both the temporal and spatial fields. It is very sensitive to measurand at any of its point. It is a replacement of 1000's of discrete sensors. Due to its low attenuation, distance upto 25 km can be monitored. So, distributed sensors are interest of choice when long distances are to be monitored. This distributed sensor is further categorized into two as shown below. While light is guiding through the fiber if measurand acts directly or indirectly it is called intrinsic sensors. If such intrinsic sensors are intrinsically distributed in nature then the measurand acts over a finite length of fiber. Quasi-distributed sensor consists of fiber sections joined into a long fiber at few intervals to provide localized difference in the loss, back-scatter intensity, polarization, fluorescence intensity, etc. [43].

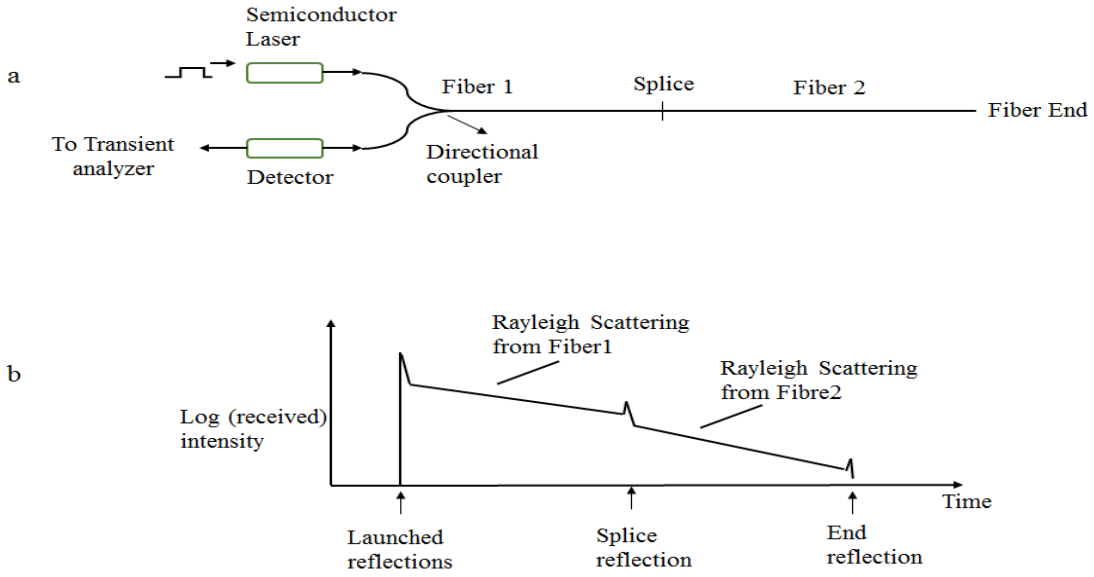

Fig. 1.10 Primary concepts of OTDR (a) Optical arrangement and (b) OTDR return.

b) Multiplexing sensor

Sensing is allowed at many points of a single fiber optic line. In some applications, multisensory systems are required to connect many sensors together in network configuration, individual sensors outputs are multiplexed. Multiplexing sensor uses methods like time, frequency and wavelength. Fig.1.11 demonstrates a system where a broadband light source (light-emitting diode), is joined to a sequence of fiber sensors that reflect signals over wavelength bands which are small parts in light source spectrum. To separate the signals from the sensors and detectors a dispersive element like grating or prism is used [28].

It is convenient to describe multiplexed sensors as those fabricated to accumulate information from numerous distinct regions and distributed sensors as those that work on a continuous length of fiber, additionally they are capable of finding the changes in parameter down the length of the fiber as a continuous function of distance [43].

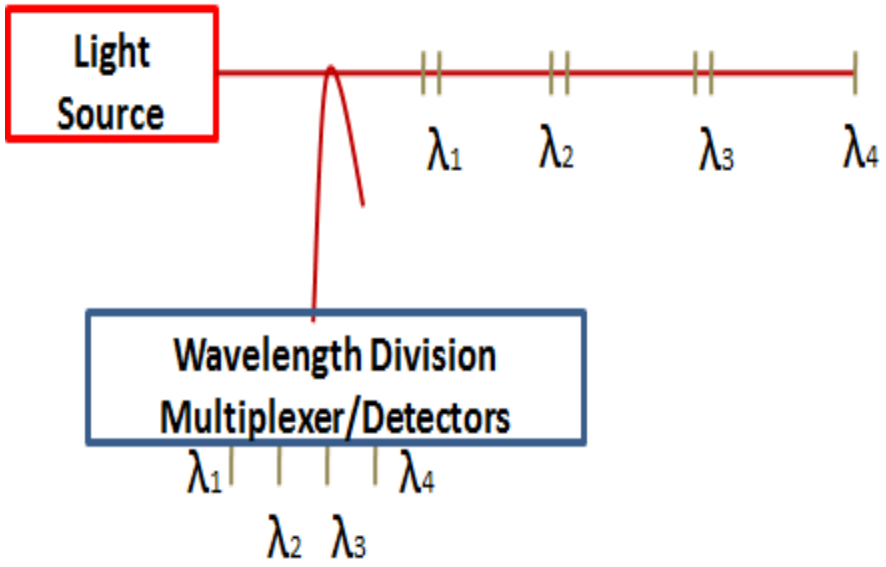

Fig. 1.11 A sequence of fiber sensors are arranged to be multiplexed in order to reflect in specific spectral band that is divided through dispersive element onto distinct detectors.

1.6.2 FIBER OPTIC SENSOR APPLICATION

Increase in number of physical parameters due to the automation requires proper monitoring with sensing devices. The greatest advantage of fiber optic sensors is multi-parameter sensing, which can sense many parameters like temperature, pressure, or refractive index etc. simultaneously [44].

Fiber Optic sensors are mainly used to serve the purpose of process control. Its main applications are communication and electrical generation, distribution and consumption fields. Recently, fiber optic sensors are manufactured for the medical diagnostics, biochemical sensing, and environmental monitoring. Over the electronic sensors, fiber optic sensors have greater advantages due to their immunity to electromagnetism, greater sensitivity, higher detection speed and low price. Moreover, fiber optic sensor materials are compatible for both bio and chemical sensing [28]. A fiber optic sensor as a biosensor or a chemical sensor consists of a membrane with biologically or chemically sensitive surface. Based on the concentration of specific species, optical signals are generated as shown in below Fig. 1.12 [45]. Applications are distinguished on the basis of analyte sensing as discussed in following sections.

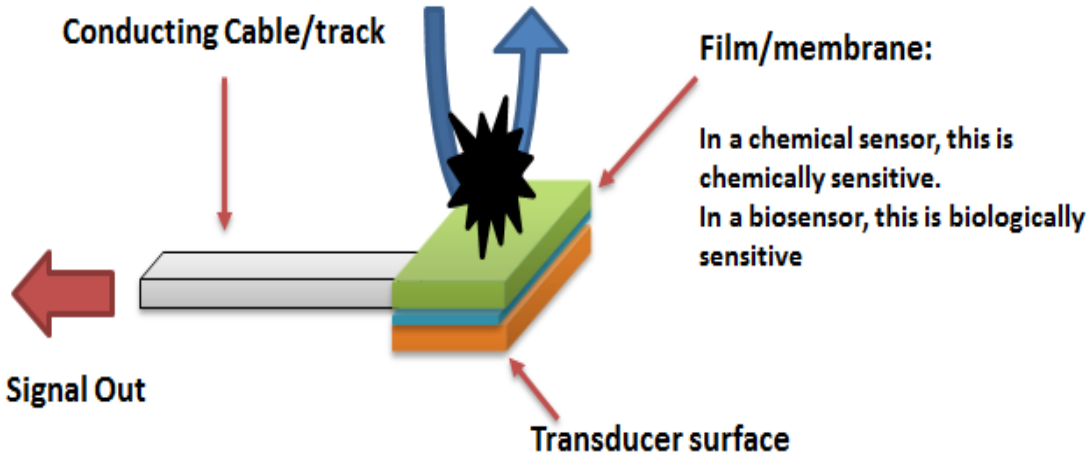

Fig. 1.12 Biochemical sensor prototype.

1.6.2.1 BIOSENSORS AND BIO-CHEMICAL SENSORS

Biosensors transform biological interactions into a measurable electrical or optical signals. The biosensors not only differentiate among species corresponding to the bio-recognition molecules that are accumulated on the surface, but also detects the analytes with lower concentrations. Biosensors have wide range of applications in medical and biological fields, such as, detection of foodborne pathogens and in medical diagnostics [46]. The major advantage of biosensors is that they are easy to use without any expertise and requires minimal sample treatment [47]. The concept of biosensors has grown immensely over the past few decades [45]. Different types of fiber optic sensors have been reported, such as Fabry-Perot interferometers, Michelson interferometers and Mach-Zehnder interferometers (MZIs). Among all the fiber optic sensors, MZIs exhibits many advantages [48], as discussed in the previous sections.

Detecting pathogens in food is a new fashion. The infections caused by foodborne pathogens have become a vital public health concern and a primary cause of death [49]. According to the 2015 reports by the Foodborne Diseases Active Surveillance Network (Food Net) of USA Centre for Disease Control and Prevention (CDC), foodborne diseases caused 20,107 confirmed cases, 4,531 hospitalizations, and 77 deaths [50]. Maximum number of deaths are caused by *Salmonella*, *Listeria*, *Escherichia coli (E. coli O157:H7) and Toxoplasma* [51], among them pathogenic *E. coli* is one of the most dangerous agent of foodborne diseases [52]. Several detection techniques are being in use for the detection of foodborne pathogens. Such as, biochemical kits [53], Enzyme-Linked Immunosorbent Assays (ELISA) [54], Western Bolt Analysis (WBA) [55], and Polymer Chain Reaction (PCR) [56]. These conventional detection methods often require extraction, isolation, enrichment, counting, etc., prior to measurement, and hence testing and resulting takes longer time to arrive at a quantitative conclusion [57].

1.6.2.2 CHEMICAL SENSING

Chemical and Bio-chemical sensing using fiber optics concept is among the most prominent applications. These fiber optic sensors are capable of sensing the chemical measurements even from remote locations. Fiber optic sensors in chemical and bio-chemical domain are less progressive. However, there is a possibility of new inventions in this field [29].

Expeditious advancement in chemical and biochemical applications with optical interfaces has created interest in always increasing demand for highly sensitive, accurate, and disposable biochemical sensors. An optical biochemical sensor, normally used for drug discovery, medical diagnosis, detection of harmful pathogens and others, is a device capable of converting biological or chemical data into effortlessly distinguishable optical signals [58].

Aqueous H_2SO_4 is the world's most commonly opted industrial chemical. Its uses are diversified in various sectors of science and technology and even in laboratories such as in resin production, ore and mineral dissolution and processing, production of fertilizer, storage batteries and catalytic processes [59]. H_2SO_4 gives a broad range of acidity values for different types of demands in industries and laboratories [60, 61]. Although useful, but because of its high density, oily and corrosive nature, it has to be diluted to definite concentration to get the required results. Similar to H_2SO_4, H_2O_2 also has an extraordinary importance as a chemical compound. It is used in large areas of research, industrial and manufacturing applications throughout the world. Because of its oxidizing capacity, it is utilized as bleaching agent in textiles, paper and mineral industries. Waste water treatment, removal of organic and inorganic contaminants are the most common applications [62]. A standard technique for chemical sensing is absorbance spectroscopy [63]. Recent technologies utilize surface plasmon resonance and micro-mechanical systems to reduce complexity but high sensitivity (S) and reduction in cost are also a major requirements of a measuring system which have to be fulfilled.

1.7 WHY PHOTONIC CRYSTAL WAVEGUIDE SENSORS?

Optical sensors have come up with possible solutions for all the existing problems related with conventional test methods. Surface plasmon resonance and quartz crystal microbalance are two recent methods in optical biosensors and chemical sensing. The two technologies render the benefits of biosensing with high sensitivity. Optical sensors are restricted with integration of factors that encompass cost of sensor, instrumentation problems and low-assay multiplexing throughput [64]. Derived from the same optical biosensor family PCW biosensor technology is quick, pathogen specific, and do not need chemical modification of the test sample. Current research focus is on controlling and manipulating the propagation of light in periodic structures [65]. In communication networks, slow light phenomenon has promising and potential applications. Predominantly, photonic crystal materials are competent of carrying slow light transmission.

The concept photonic crystal was first coined about 25 years ago. Photonic structures convey a distinct approach for guiding light and to manufacture integrated photonic devices [66]. Photonic band gap (PBG) is the basic concept behind the operation of PCW. Permittivity change as a function of position which leads to PBG. The variation of periodicity can be in 1D, 2D or 3D structures which can be operated by regulating the period of permittivity. Apart from these parameters, PCW operation also depends on the defect availability. The PCW with a defect (line or point) controls the electric field distribution within the waveguide [67]. By introducing a defect into the PCW, one can create low transmission loss waveguide [68]. PCW has a wide range of applications in the field of photonics [69]. Using PCW, light can be propagated in a minute scale which is in order of the wavelength of light [70]. It has the ability to identify the variation in refractive index (RI) with large sensitivity due to strong photon confinement [71, 72]. PCW slabs with a submicron scale periodic modulation of the refractive index forms a versatile platform to control the flow of light [73, 74]. Recently, nanocavity coupled PCW sensor platform is used to detect cancer with high sensitivity [75].

CHAPTER 2. THEORY AND LITERATURE REVIEW

2.1 INTRODUCTION

This chapter discusses the theory and literature review about the photonic crystal waveguide and its application as a biochemical sensor. Starting with the concept of electromagnetism using the Maxwell's equations, wave equation and band structures. Photonic crystal types, defects and mathematical tools are presented. Literature survey starts with theoretical analysis and later on covers the sensing applications. Problem formulation, current issues, objective, thesis contribution and thesis organization are discussed in the last section of this chapter.

2.2 ELECTROMAGNETISM

Light comprises of both magnetic and electric field with high rate of oscillations. Electromagnetic spectrum occupied by the optical frequencies from infrared through visible to the ultraviolet as shown in Fig. 2.1. Due to the shorter wavelength of light, optical wave transmitting and detecting techniques are different from techniques used for electromagnetic waves of longer wavelengths. In present scenario, optical devices miniaturization does not get affected due to these differences [76]. Ampere's and Faraday's law explains electromagnetic radiation. When the electric field in the space varies with time, it produces magnetic field in the same way as magnetic field in the space varies with time, it produces electric field [77].

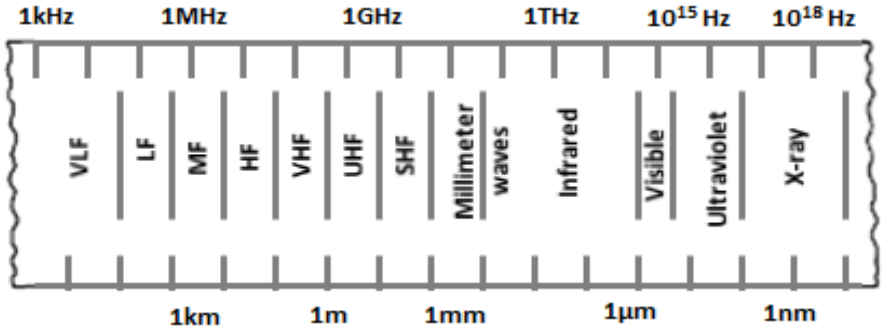

Fig. 2.1 Wavelength spectrum from visible to ultraviolet.

In 1864, James Clerk Maxwell presented equations for connections between the electric and magnetic field in his treatise, "A dynamic theory of the electromagnetic field" [78]. Electromagnetic wave propagation through any dielectric medium is described mathematically with a set of differential equations known as Maxwell's equations [79]. Maxwell's equations are cast as eigenvalue problem which brings the electromagnetic problems closer with Schrödinger equations, easy to demonstrate quantum mechanics, orthogonality of modes, variational theorem and perturbation theory. Due to the lack of fundamental scale in either spatial coordinate or in the potential strength, electromagnetics differs from quantum-mechanical case. This makes photonic crystals scalable than traditional crystals [80]. Electromagnetic waves propagation are controlled by periodic distribution of dielectric which is possible in photonic crystal [79].

2.2.1 MAXWELL'S EQUATIONS

Pulses in dielectric media are physical phenomena associated with the propagation of electromagnetic waves that consist of separate electric and magnetic fields and are required to satisfy the *Maxwell's equations* [81]. Materials carry electrons through it when electromagnetic wave travel through it, but in dielectric materials the case is different no electrons or charges exist [79]. The propagation of electromagnetic wave in a photonic crystal is governed by macroscopic Maxwell equations [80]. They are

$\nabla . \mathrm{D} = \rho,$ (Gauss's law) …….. (2.1)

$\nabla \times \mathrm{E} + \frac{\partial \mathrm{B}}{\partial \mathrm{t}} = 0,$ (Faraday's law of induction) ....…… (2.2)

$\nabla . \mathrm{B} = 0,$ (Gauss's law for magnetism) …….. (2.3)

$\nabla \times \mathrm{H} - \frac{\partial \mathrm{D}}{\partial \mathrm{t}} = \mathrm{J},$ (Ampere's circuital law) ……..…… (2.4)

here t denotes the time, ∇ is the nabla operator, "·" and "×" denotes scalar and vector products. In Cartesian coordinates, $\nabla = \mathrm{x}\frac{\partial}{\partial x} + \mathrm{y}\frac{\partial}{\partial y} + \mathrm{z}\frac{\partial}{\partial z}$,

where x,y,z are unit vectors, E is the macroscopic electric field measured in V/m, H is the macroscopic magnetic field in A/m, D is the electric field displacement in C/m^2, B is the

magnetic induction field in Tesla, ρ is the free charge in C/m^3 and J is the current densities measured in A/m^2. J and ρ are related to each other by the continuity equation, which is given by taking the divergence of (2.3) and using (2.4) and the relation $\nabla\cdot\nabla\times \mathrm{H} = 0, \nabla.\mathrm{J} = -\frac{\partial \rho}{\partial \mathrm{t}}$.

For nonconductive materials J=0 and ρ=0. In photonic crystals' theoretical treatment is focused on small field isotropic macroscopic systems so that the displacement field D can be represented linear to the electric field as shown below [82].

$$D = \varepsilon E, \qquad \text{……. (2.5)}$$

$$B = \mu H, \qquad \text{…….. (2.6)}$$

here ε is dielectric constant and μ is magnetic permeability of the material.

2.2.2 WAVE EQUATIONS

By assuming propagation of waves in non-dispersive, non-conducting, isotropic, homogeneous and linear materials, the ε and μ are real and constant numbers. Here, the inclusion of 2.5 and 2.6 equations into 2.1 to 2.4 equations, converts Maxwell's equations into:

$$\nabla.\mathrm{E} = 0, \qquad \text{…… (2.7)}$$

$$\nabla \times \mathrm{E} = -\mu\frac{\partial \mathrm{H}}{\partial \mathrm{t}}, \qquad \text{..…….. (2.8)}$$

$$\nabla.\mathrm{H} = 0, \qquad \text{…… (2.9)}$$

$$\nabla \times \mathrm{H} = \varepsilon\frac{\partial \mathrm{E}}{\partial \mathrm{t}}, \qquad \text{.....….. (2.10)}$$

Maxwell's equations 2.7 to 2.10 are merged to constitute an equation consisting of either electric field E or the magnetic field H [79]. This equation is known as *wave equations* and it explains the propagation property of electromagnetic waves in dielectric medium which are characterized by ε and μ.

Maxwell's equations from 2.1 to 2.4, explain the interdependence of E and H. In the process of determining D and B using equations 2.5 and 2.6, we focus to obtain E and H. To determine E and H we solve the equations from 2.7 to 2.10 [79].

By applying curl ($\nabla\times$) to the Maxwell's equation (2.8),

$$\nabla \times (\nabla \times \mathrm{E}) = -\nabla \times \left(\mu \frac{\partial H}{\partial t}\right) = -\mu \frac{\partial(\nabla \times \mathrm{H})}{\partial t} \quad \text{……. (2.11)}$$

After substituting the 2.10 in 2.11 the equation turns into

$$\nabla \times (\nabla \times \mathrm{E}) = -\mu\varepsilon \frac{\partial^2 E}{\partial t^2} \quad \text{……. (2.12)}$$

By substituting the vector identity $\nabla\times(\nabla\times\mathrm{E})=-\nabla^2\mathrm{E}+\nabla(\nabla.\mathrm{E})$, here ∇^2 is the Laplacian operator $\nabla^2=\partial^2/\partial x^2+\partial^2/\partial y^2+\partial^2/\partial z^2$, and nothing that $\nabla.\mathrm{E}=0$, we have

$$\nabla^2 E = \frac{1}{v^2} \frac{\partial^2 E}{\partial t^2} \quad \text{…….. (2.13)}$$

$v=1/\sqrt{\varepsilon\mu}$. …….. (2.14)

By applying the curl ($\nabla\times$) to the Maxwell's equation (2.10)

$$\nabla^2 H = \frac{1}{v^2} \frac{\partial^2 H}{\partial t^2} \quad \text{…… (2.15)}$$

Equations (2.13) and (2.14) of the electric field E and magnetic field H are also called as wave equations [79].

The velocity v is shown in equations (2.13) and (2.15). In case of electromagnetic wave propagating in vacuum, then $\varepsilon = \varepsilon_0 = 8.85\times10^{-12}\ s^2C^2m^{-3}kg^{-1}$ and $\mu=\mu_0=4\Pi\times10^{-7}mkgC^{-2}$. By considering the equation (2.14) the velocity of the wave is:

$v=1/\sqrt{\varepsilon\mu} \approx 3\times10^8\ ms^{-1}$.

2.2.3 BAND STRUCTURES

The first band gap of 1D periodic structures was displayed by Lord Rayleigh in 1887. It is also called as Bragg mirror. After many years band gap concept was extended to the 2D and 3D periodic structures by Eli Yablonovitch and Sajeev John in 1987, this structure is called as "photonic crystal" [79].

The general concepts behind the photonic crystals are photonic band gaps, eigen states and band structures. From the past evidences, the first band structures are presented of 3D photonic crystals with inverted opal, diamond lattices and FC cubic.

The information about the optical properties of photonic crystal is shown by the band structure. An Eigen state represents the band structure of an infinite periodic structure. Resonant frequency is the alternate name of the eigen-frequency. At media interface number of Fresnel reflections appear due to the infinite periodic structure of a photonic crystal. The transmission and reflection of waves are created by forward and backward motion of constructive and destructive interferences. The radiation wave vectors are represented as sets of eigen states. The band structures are signified in 2D plots, irrespective of the dimensionality of the photonic crystal waveguides. Fig. 2.2 illustrates the band structure of the 1D photonic crystal waveguide. Band structure signifies the radiation propagation through the optical domain [80-83].

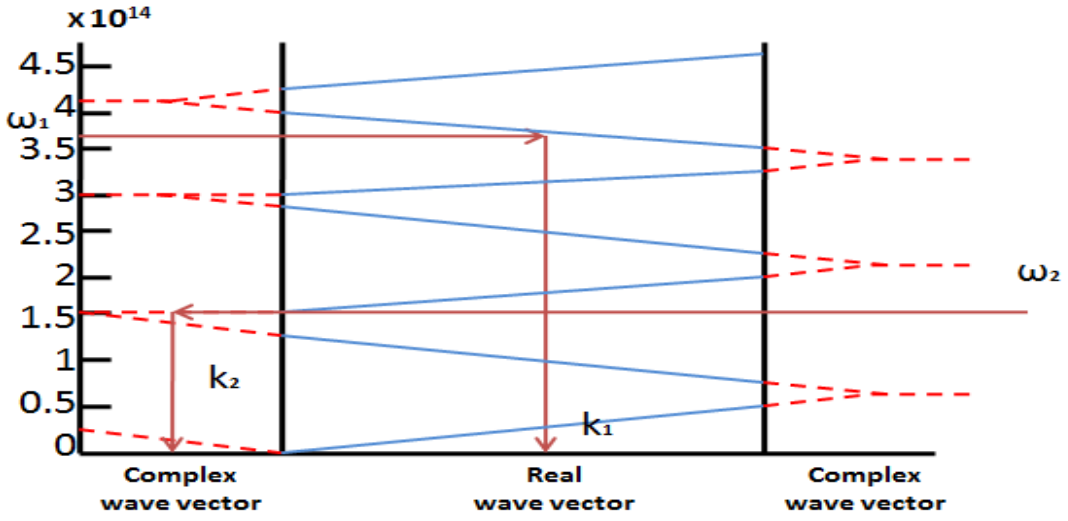

Fig. 2.2 Band gap structure of 1D photonic crystal.

In Fig.2.2 the wave vector is shown on horizontal axis and the resonance frequency is represented on vertical axis. The radiation frequency ω_1 acquires the wave vector same as structure to propagate through it. Band structures used to identify the values of wave vectors. From above Fig. 2.2, k_1 is the wave vector value matching with the ω_1 radiation frequency. In another situation ω_2 is the radiation frequency which falls in the complex wave vector k_2. The imaginary values of the wave vector corresponds to the radiation attenuation or gain. Here, in this case it relates to attenuation. So that in this exact frequency range, radiation will be reflected back from the structure in the region where radiations are reflected back and are recognized as photonic band gaps [83].

Fig. 2.3 explains that the photonic band diagram consists of three frequency ranges for different applications. The lower frequency range is also called as birefringence and the second one is mid-frequency range, this frequency range is for photonic band gap of reflection type especially for laser devices and the third higher frequency range is considered as superprism, anomorous dispersion specifically for transmission type devices [84].

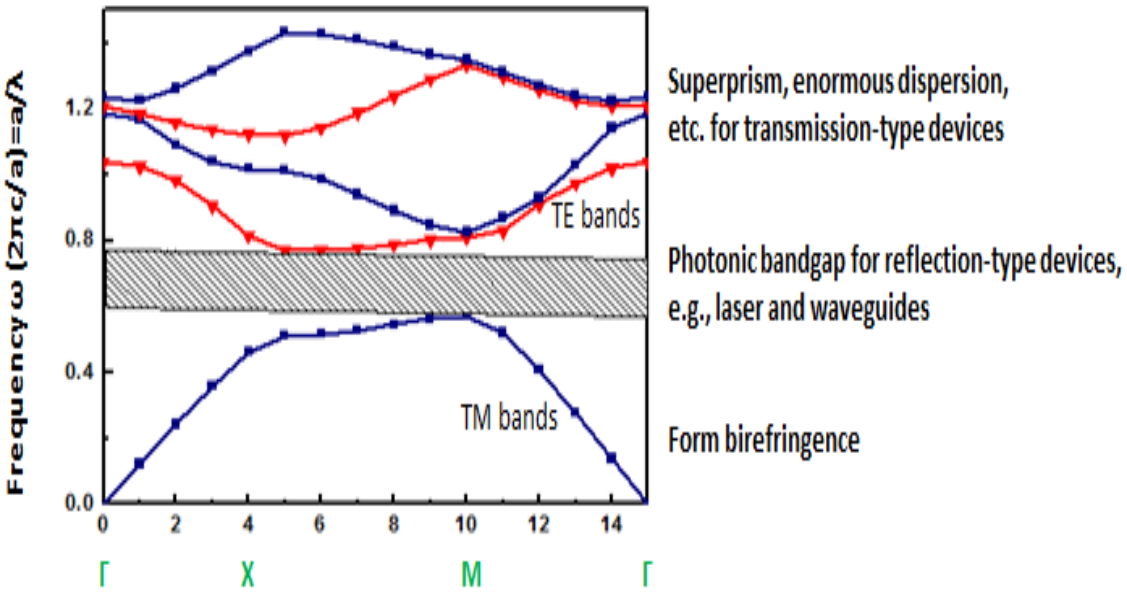

Fig. 2.3 Photonic crystal waveguide band diagram.

In Fig. 2.4, the plot ω_n (k) shows three different multilayer films. The left-hand plot is for a system in which all the layers have same dielectric constant; the medium is actually uniform in all three directions. The center plot is for a structure with alternating dielectric constants of 13 and 12, and the right-hand plot is for a structure with a much higher dielectric contrast of 13 and 1. The left-hand plot is for a homogeneous dielectric medium [80].

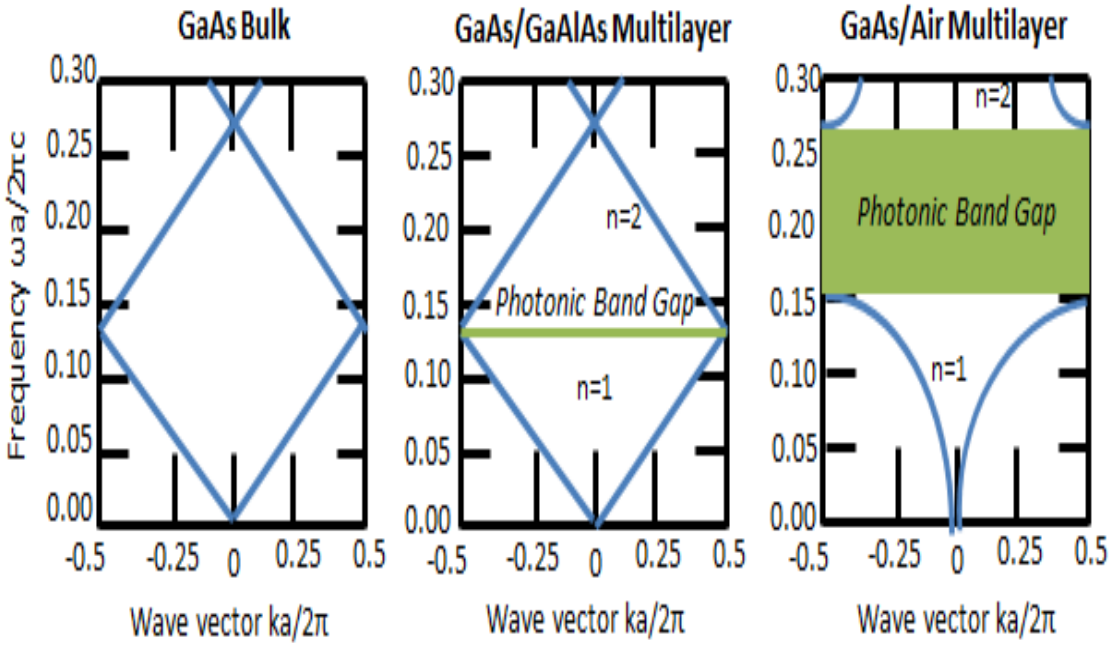

Fig. 2.4 Different band gaps based on dielectric variation .

2.3 PHOTONIC CRYSTALS

Over the past few years, optical fiber sensors have undergone into various technologies like distributed bragg reflectors, distributed feedback and fiber bragg grating devices. In recent technologies, new materials are used to design the sensors with a controllable optical response. In the field of biophotonics, nanostructured materials are introduced. Optoelectronics work on the principle of light matter interaction. Reflection or refraction occurs due to materials reaction with their dielectric constant.

The capability to modify structures at micro and nano-scale level, created a chance to inspect the relation between the light and matter structure. The light behavior in the photonic crystal is same as the electron in the crystal lattice. In the same way as periodic potential prohibit the propagation of electron, light is also prohibited in photonic band gap region [84]. Photonic crystals are basically designed to control the light propagation [85].

Photonic crystal materials are arranged with different refractive index materials in periodic manner [86]. The progress of photonic crystal research is evolved from the concept of photonic band. Photonic band represents the optical dispersion relation in a photonic crystal, between a given frequency and the corresponding wave vector, which is generated in analogy to the electron energy band. Plane wave expansion method (PWE) is to apply the periodic boundary conditions on the scalar approximated wave equations, to calculate the photonic band curves [87]. Photonic crystals types, defects and cavity are explained in the following sections.

2.3.1 PHOTONIC CRYSTALS TYPES

Electromagnetic wave propagation is controlled by photonic crystals periodic structures. Two different dielectric materials together constitute the periodic structures one with high dielectric constant ε_1 and another one with low dielectric constant ε_2. Photonic crystal waveguide exhibits a basic property of reflecting back of electromagnetic waves whatever wavelength falls under this range. These frequencies are called photonic band gaps [88].

The photonic band gaps originate from the wave propagation interaction at the interfaces of two different dielectric materials. To understand deeply about electromagnetic wave propagation phenomena in photonic crystals, constructive and destructive interference concepts need to be explained. Secondary waves are produced when the electromagnetic wave interacts with the interface between the two different dielectric materials. If the secondary waves interfere constructively the electromagnetic energy is reflected back so

that electromagnetic waves are not allowed to enter into the photonic crystal waveguide. In contrast, if the secondary waves interfere destructively the electromagnetic energy is transmitted and allowed to enter into the photonic crystal waveguide. The main advantage of photonic band gap is to control the electromagnetic waves.

On the other hand, if the electromagnetic wave is generated inside the photonic crystal (by emission from an internal source), its propagation (or existence) within the photonic crystal is absolutely prohibited. The wavelengths of the electromagnetic waves which are not allowed to propagate within photonic crystals are of the order of the spatial periodicity of the structure, which are determined by the thickness of the layers or by the distance between the cylinders.

The structure of a photonic crystal (PC) possesses spatial modulation of the refractive index with the period comparable to the wavelength of the interacting radiation. With respect to the character of the refractive index variation, photonic crystals may be divided into three basic classes; one-, two- and three-dimensional PCs as shown in Fig. 2.5.

i. 1D photonic crystal:

The simplest photonic crystal is a one-dimensional periodic structure made up of two different dielectric materials as shown in Fig. 2.5 (a) consisting of alternating homogeneous dielectric layers with dielectric constants ε_1 and ε_2 and magnetic permeabilities μ_1 and μ_2, the layers extend infinitely in one dimension.

ii. 2D photonic crystal:

As shown in Fig. 2.5 (b), an example of a two-dimensional photonic crystal consisting of cylinders with radius r arranged on a square lattice with lattice constant ‘a’ having different dielectric materials with dielectric constants ε_1 and ε_2, respectively. The dielectric constant $\varepsilon = \varepsilon(r)$ of the photonic crystal varies periodically in two dimensions.

iii. 3D photonic crystal:

Fig. 2.5 (c) shows, a three-dimensional photonic crystal consisting of spheres arranged on a simple cubic Bravais lattice with lattice constant ‘a’. The dielectric constant of the photonic crystal $\varepsilon = \varepsilon(r)$ varies periodically along any arbitrary direction in the three-dimensional space.

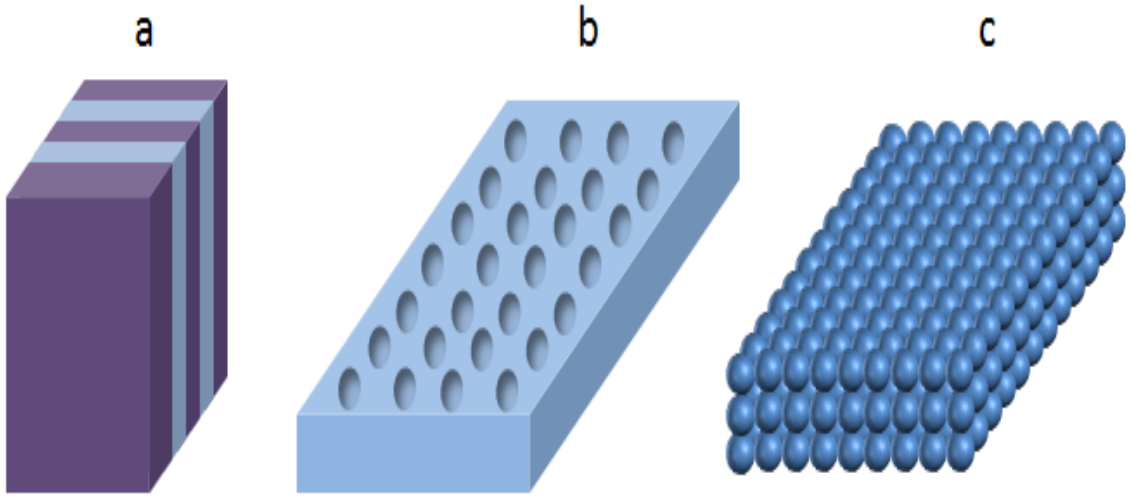

Fig. 2.5 Periodicity dielectric constant in 3 dimensions. (a) 1D PhC, (b) 2D PhC, (c) 3D PhC.

Photonic crystals can be designed as photonic crystal fibers (PCFs) and photonic crystal waveguides (PCWs). PCFs are particularly utilized in short range propagation and high sensitive interferometers. Whereas, PCWs are used in compact devices and photonic integrated circuits [83].

2.3.2 DEFECTS

Defects are introduced inside the photonic crystals to guide the desired wavelengths of light. The important property of photonic crystal is to create localized modes that may appear within the photonic band gaps, when the periodic structure is broken or modified locally by defects. There are two types of defects to introduce, first is point defect and second is line defect.

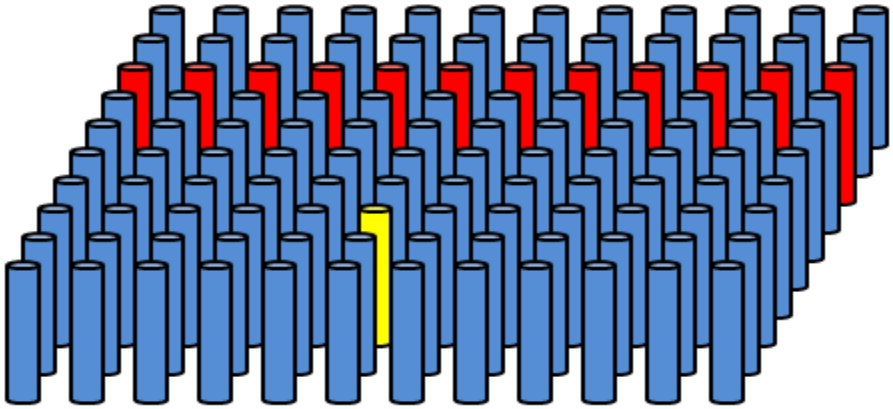

Fig. 2.6 Photonic crystal waveguide with a line (Red) and point defect (Yellow).

If one removes a single rod or change its properties in contrast to the rest of the lattice, the symmetry is not maintained. Contrarily, the symmetry of a 2-D photonic crystal can be broken by eliminating numerous rods. The impacts caused by breakage of symmetry in a 2-D photonic crystal are different than that by introduction of defects in periodic tubes. Thus, breaking has two effects. Light is trapped in the point defects of photonic crystal waveguides and light propagates from one point to another point is done by creating line defect. Same as the solid state crystal there are two important defects present in the photonic crystal waveguide, these are cavity defect and extended defect. Local disruptions create the cavities in the periodicity of the waveguide and electromagnetic modes are observed. Extended defects are similar to the dislocation of the crystal and resulted in the spectral region with transmission band. From the Fig. 2.6, by removing a single pillar or by changing the shape of the pillar, periodicity of the waveguide from its original structure is distrubed. By this, a cavity is created and light is confined in the middle of the waveguide [84].

2.3.3 PHOTONIC CRYSTAL CAVITY

Photonic crystal cavity design is governed by two parameters, first is Q factor and second is mode volume. Q factor is defined as the life of photon in the cavity before losing to the external world. Mode volume is characterized as the confinement of electromagnetic modes in all spatial directions. Cavities are open structures that might appear like leaky but balancing the bragg reflection and TIR, its design has high confinement properties. In photonic crystal cavity bandwidth of a bandpass filter is lower for higher Q factor. Cavities increase the light interaction with matters. High Q factor is very sensitive to the surrounding environment and is useful in biochemical or gas sensing applications. If the cavity has the proper size to support a mode in the band gap, then light cannot escape through the defect. By modifying the refractive index and changing size, defect is created [84].

2.4 COMPUTATIONAL STUDIES/MATHEMATICAL TOOLS

Computational studies applied for photonic crystal waveguide are broadly classified into two categories one is for transmission and reflection calculation and another is for the band structure calculation. Transmission and reflection calculation are performed using finite difference time domain or finite element method and for band structure calculation plane wave expansion method is used. Generally, these methods are implemented using formulas in terms of transmission, transfer and reflection matrices. To implement computational method, size along the vertical and horizontal direction must be finite, which further benefited by providing pseudo-periodicity properties [89]. Few mathematical tools are discussed in detail in the following sections.

2.4.1 FINITE DIFFERENCE TIME-DOMAIN (FDTD)

The Finite Difference Time-Domain (FDTD) method was originally proposed by Kane S.Yee in 1966. Yee proposed a discrete solution to Maxwell's equations based on central difference approximations of the spatial and temporal derivatives of the curl-equations. The novelty of Yee's approach was the staggering of the electric and magnetic fields in both space and time in order to obtain second-order accuracy. Yee derived a full three-dimensional formulation, and validated the method with two-dimensional problems. Yee's method went mostly un-noticed for nearly a decade. Finally, in 1975, Taflove and Brodwin applied Yee's method to simulate the scattering by dielectric cylinders and biological heating, and in 1977, Holland applied it to predict the currents induced on an aircraft by an electromagnetic pulse (EMP).

The number of companies offering FDTD software and consulting are continuing to grow. This trend will certainly continue as the application areas continue to expand. Although, there are plenty of search codes that have also been developed. The intention is to lay a foundation for the basic FDTD algorithm, including the central difference approximations, explicit time-domain solution methods, boundary conditions, stability, and sources of error, as well as to provide an introduction into more advanced concepts such as absorbing boundary conditions, subcell modeling techniques, and post processing methods [90].

The FDTD technique has emerged as a foremost numerical tool for the solution of the time-dependent Maxwell's equations in either differential or integral form. As computing facilities became faster and more widely accessible, its premises found tremendous applications and proved their superiority in radiation and scattering problems. Motivated by these advances, the scientific community introduced numerous enhancements to the initial idea that greatly broadened its applicability [91]. Hence, any reasonable problem would require a large amount of computer memory and time. Since 1990s, however, with the growth of computing power, the FDTD method has emerged [92].

2.4.2 PLANE WAVE EXPANSION METHOD (PWE)

Plane wave expansion method is a technique in resolving the band structures of photonic crystal waveguides. It is important to know the advantages, disadvantages and applications of this method. One of the most essential benefit is its high performance. Although, it takes several minutes even for basic structures, it is valid for computing both simple and complex structures such as infinite periodic structures and point defects, respectively. For easy designing of photonic crystal based active devices and investigating photonic crystal fibers calculation of eigen states can be carried out [93].

2.4.3 FINITE ELEMENT METHOD (FEM)

The finite element method (FEM) has become prominent in solving electromagnetic related problems. It is originated in the 1940s with the work of A. Hrennikoff and R. Courant. The finite element method (often known as Finite Element Analysis or FEA) was developed in the 1950s for airframe and structural analysis. Like the finite volume method, the finite element method divides the simulation space into small areas or volumes (in 2D and 3D, respectively) which can be arbitrarily shaped and oriented, for this reason, the finite element method is well suited for problems with complex geometry. Also similar to the finite volume method, while the small "subdomains" can have arbitrary shapes, triangles and tetrahedrons are most commonly used for their simplicity. Maxwell's equations are discretized and values of the fields are found which satisfy these equations. In the finite element method, however, the solution to Maxwell's equations is approximated over each subdomain with some functional forms, usually a low-order polynomial, which is known as a basic function. The solutions in each subdomain are then made to be continuous across their boundaries, and the solution must be made to fit the global boundary conditions enforced by any scattering structures. Finite Element Time Domain (FETD) is the state-of-the-art for time domain solutions of electromagnetic problems. Additionally, The Finite Volume Time Domain (FVTD) method became popular in modeling electromagnetic problems due to its flexibility in modeling irregular structures [92].

2.5 PHOTONIC CRYSTALS FOR BIO-CHEMCIAL SENSING APPLICATIONS

Chemical sensor converts chemical related parameters to the electrical/optical signals [94]. In analytical chemistry, different steps are required for determination of an analyte as shown in Fig. 2.7. Initially, as per problem description specimens are identified and collected. Further, valid method is used after taking the specimen to the laboratory. Samples are prepared for measurements. Finally, a comparison is made with the reference and quality control samples. The calculations of statistical parameters decide the performance and reliability of the analysis. Chemical sensors are suffering from various defects in detection , sensitivity and selectivity processes [95].

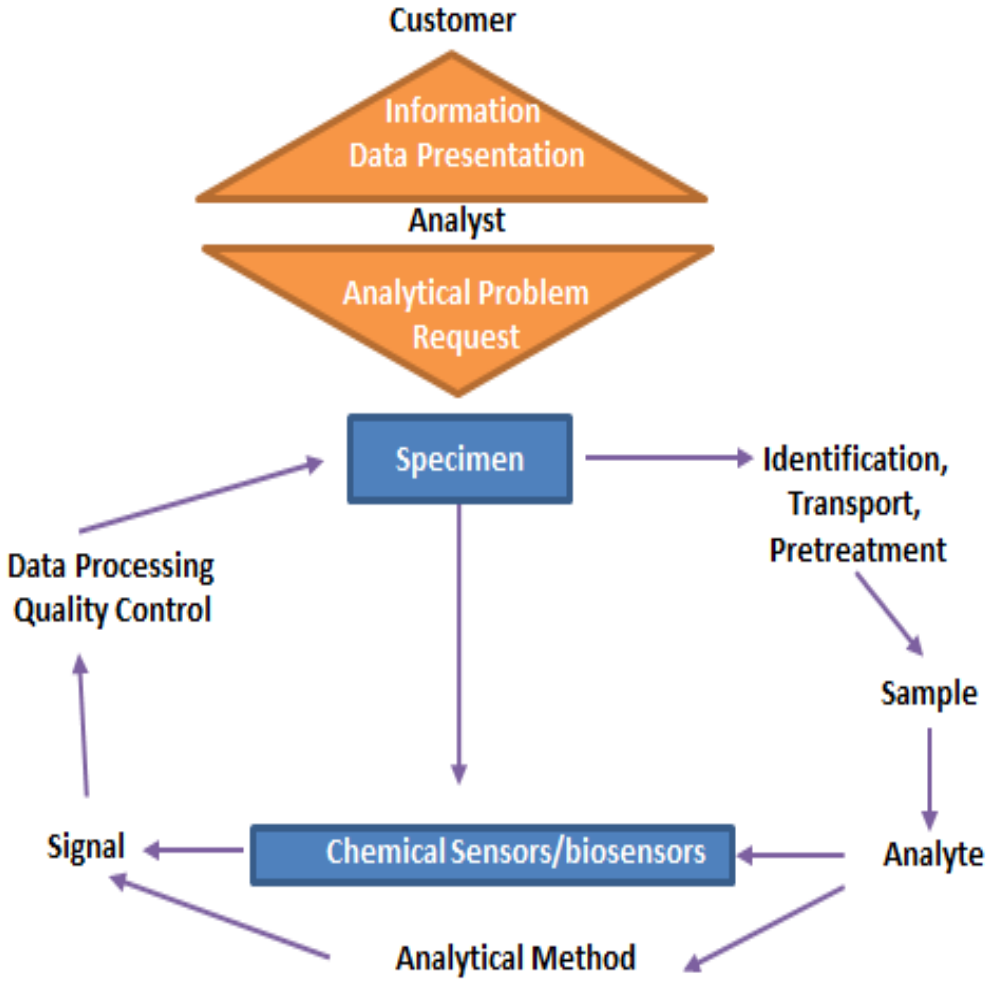

Fig. 2.7 Steps involved in analytical chemistry.

Optical fiber based sensors are small in size and flexible with the remote sensing ability, making them suitable for in-vivo experiments. Even more, due to the fact that these waveguides are electrically passive, they do not represent a risk for patients during medical exams, allowing real time and multi-parameter measurements. Wide ranges of optical sensors are developed for selective biomolecule detection. Most of them have reliability issues as they employ very fragile antibodies as sensing elements.

Photonic crystal waveguide offers a number of exceptional advantages for biochemical sensing applications. They have unique ability to accommodate biological and chemical samples in gaseous or liquid forms in the immediate vicinity of the fiber core and or inside the core, allowing simultaneously for fluidic channel role and light guidance with high light/sample overlap; the air holes can be functionalized with biorecognition layers that can bind and progressively accumulate target biomolecules, thus enhancing sensor sensitivity and specificity; and more importantly, the volume needed for sample analysis using photonic crystal fibers is of the order of hundreds of nanoliters to tens of microliters [96].

2.6 LITERATURE REVIEW

Literature review is carried out in two sections. First is for photonic crystal waveguide theoretical analysis of design and second is for photonic crystal waveguide as a bio-chemical sensor. Vast survey is carried out in both the areas and tables are presented with the specific time duration from 2007 to 2017.

2.6.1 PCW THEORETICAL ANALYSIS

Mekis *et al.* [97] proved transmissions have value greater than 95% over large frequency ranges like zero radius of curvature at 90^{o} bend, further for conventional dielectric waveguides highest transmission obtained was 98%. By using dynamic frequency-dependent a simple one dimensional scattering theory model was designed.

Similar to above Mekis *et al*. [98] designed the method in two-dimensional photonic crystal waveguides for appearance of bound states as against conventional guides. Further, it was revealed that frequency ranges were obtained with periodicity only where

no guide modes exist. The existence of these types of modes allow the creation of bound states whose appearance is solely dependent on lattice geometry.

Broeng *et al.* [99] stressed on the applications of photonic crystal fibers' high-index triangular core and even on bending losses' qualitative results and dispersive properties. The basic guiding properties which are different from today's all fibers were also investigated for the latest class of optical fibers. The outcomes depicted the initial efforts to present the potential and applications of these latest fibers.

Loncar *et al.* [100] used 3-D FDTD analysis to find the eigen modes of an optically thin slab perforated with 2-D lattice of holes, and single-line defects. It was depicted that both effective refractive index and photonic band gap effect guided modes are supported by single line defect.

Fan [101] analyzed the theory based and numerical simulations of waveguide branches in a photonic crystal. Identifying the structures with near-complete transmission and optimization in photonic crystals, numerical simulations of electromagnetic wave propagation were performed on the basis of perfect transmission and no reflection conditions.

Koshiba [102] designed and analyzed a two-channel MUX–DEMUX. The device dimensions were reduced drastically from scale of a few tens of micrometers to a few hundreds of micrometers in a MUX–DEMUX with a channel spacing of about 20 nm, required for wide-passband wavelength division multiplexing (WWDM) systems. The simulation results were obtained using a time-domain beam propagation method (BPM).

Lalanne [103] presented a theoretical study of the propagation of light in photonic crystal waveguides operating above the light cone. The waveguide geometries provided that the weakly confined systems are etched deeply into the substrate, attenuations of 10–30 dB/100 μm are predicted over the full band gap spectral region.

Boscolo *et al.* [104] studied the behavior of two straight photonic crystal waveguides. They showed that, the two guides considered as a single system realize an efficient wavelength selective directional coupler. In addition to it, by properly changing the

geometry of the dielectric region among the guide cores, the two waveguides can be decoupled.

Boscolo *et al*. [105] presented how to achieve wave propagation in two-dimensional (2-D) photonic crystal waveguides with finite length by borrowing simple concepts of propagation in transmission lines and combining them with other concepts.

Imada *et al*. [106] a channel drop filter was analyzed on the theory and experiment basis. They investigated that emitted wavelength from particular defect can be tuned by varying the radius of defect. By choosing proper radius of defect and location, high efficiency and emitted wavelength of good tuning can be obtained.

Sondergaard *et al*. [107] described three-dimensional (3-D) calculations for the dispersion relations and field profiles that are similar to 2-D. However, they found that being compared with 2-D calculations, the frequencies of the guided modes were shifted and the number of guided modes changed. Theoretically predicted frequency intervals were compared with an experimental measurement for propagation losses.

Soljacic *et al*. [108] explained that theoretical considerations showed all-optical devices using photonic crystal designs promised to be smaller than the wavelength of light, and operating with bandwidths that are very difficult to achieve electronically. By creating common materials, it consume only a few milliwatts and when combined with materials and systems that support electromagnetically induced transparency, operation at single-photon power levels could be feasible.

Notomi *et al.* [109] used time domain measurement to study loss mechanism in photonic band gap waveguides, and hence obtained minimal propagation loss (~1 dB/mm) with large group delay (>100 ps). After recognizing high Q factor in PC slabs with small sized volume resonators, concluded many types of coupled elements using resonant tunneling method in waveguides and resonators.

Patterson *et al.* [110] presented and analyzed light transmission measurements and frequency-delay reflectometry maps for GaAs photonic crystal membranes. Showing the transition from propagation with a well-defined group velocity to a regime completely dominated by disorder-induced coherent scattering. Experiments provided clear physical

insight into naturally occurring light localization and multiple coherent-scattering phenomena.

Panoiu *et al*. [111] presented a comprehensive theoretical description of the propagation of optical pulses in 1-D waveguides consisting of a line defect in a photonic crystal (PhC) slab waveguide made up of silicon. They demonstrated that both linear and nonlinear effects are stronger in the case of slow-light modes, with the nonlinear effects being more enhanced.

Long *et al*. [112] achieved a constant group velocity and small dispersion bandwidth (range 2.8 nm to 13.8 nm) by simply varying the radius of starting two rows of holes which were neighboring to the defect created. Therefore, they obtained a high performance application in a compact size. Further, analysis reveals sensitivity of modulation to be 0.386 nm/V, 0.8 ps/V and 0.37 bit/V, respectively.

Kocaman *et al*. [113] showed that optical beams propagating in path-averaged zero-index photonic crystal superlattices can have zero phase delay. The nanofabricated superlattices consist of alternating stacks of negative index photonic crystals and positive index homogeneous dielectric media, where the phase differences corresponding to consecutive primary unit cells are measured with integrated Mach-Zehnder interferometers.

Portalupi *et al*. [114] reported a study of photonic crystal nanocavities as a function of lattice disorder, using cross-polarized laser light scattering. They demonstrated that lattice disorder affects the cavity mode symmetry. They also quantified how the increase of lattice disorder leads to a reduction of the cavity Q factors and spread of resonance wavelengths. Interestingly, the disorder values derived from the variation of the Q factor are lower than those derived from the wavelength spread.

Lin *et al*. [115] proposed and theoretically examined a novel mid-infrared (mid-IR) photothermal spectroscopic sensing technique capable of detecting a single small molecule which attains such a high sensitivity by leveraging dramatically amplified photothermal effects at both mid-IR pump and near-IR probe wavelengths. Unlike conventional mid-IR spectroscopy, the technique eliminates the need for cryogenically

cooled mid-IR photodetectors, as optical detection is performed solely at the near-IR probe wavelength.

Fegadolli *et al*. [116] have developed a proof-of-concept for a new and entirely CMOS compatible tunable nanobeam cavity. A compact nanobeam cavity (~20 μm^2) with high Q-factor (~50,000) and integrated with a micro-heater atop, is able to tune the resonant wavelength up to 15 nm with low power consumption (0.35nm/mW), and attained high modulation depth.

Ishizaki *et al*. [117] explained three-dimensional photonic crystals which provide a fundamental building block for the realization of three-dimensional manipulation in silicon photonic crystals. They demonstrated clear optical guiding phenomena, in which light is incident on the crystal from one side which is bent vertically and horizontally, and is finally emitted from the other side of the crystal.

Radulaski *et al*. [118] showed details regarding the design, fabrication and characteristics of silicon carbide (SiC) which is grown on a silicon substrate having high quality factor (Q ~10^3) and negligible mode volume (V ~0.75 $(\lambda/n)^3$). With wavelength range (1.25 – 1.6 μm) cavity resonances are demonstrated in the telecommunication bands. Lastly, applications with different fields like interconnects, and quantum information science are discussed.

Minkov and Savona [119] contributed a lot for basic studies and applications in photonics with help of high Q-factor by simply combining with smallest modal volume. Further, by changing the location of some neighboring holes, they found the global maximum of Q-factor with employment of genetic algorithms. Investigated the effects it can have on the optimal designs.

Zhang *et al*. [120] studied a highly efficient adiabatic mode converter for coupling light into a silicon slot waveguide with a slot width as large as 320nm which was optimized to provide a measured insertion loss as low as 0.08dB. This mode converter was also used to couple light into and out of a 320nm slot photonic crystal waveguide, and it was experimentally shown to improve the coupling efficiency up to 3.5dB.

Savelev *et al*. [121] proposed and demonstrated experimentally an alternative approach for realizing subwavelength photonic structures, exploiting the waveguide properties of chains of high-index dielectric disks with both electric and magnetic dipole resonances.

Ofori-Okai *et al*. [122] described initially that within PhC slab, time resolving image having range in terahertz can be performed. Along a broad spectral range across the PBG for photonic lattices which have varying shapes and symmetries they utilized electro-optic impacts for recording THz fields.

Gonzalez-Tudela *et al*. [123] explained the quantum simulation with cold atoms in optical lattices to increase the energy and length scales in current set-ups. They explained how photons mediated in 2D photonic crystal waveguide with energy scales of several orders of magnitude larger than the exchange interactions in free space lattice and with capabilities to engineer strongly long range interactions.

Baker *et al*. [124] reported photonic crystal optical devices are able to respond to changes in the refractive index are an emerging class of label-free chemical- and bio-sensors. Therefore, the focus was on one class of photonic crystal, in which light is confined to a patterned planar material layer of sub-wavelength thickness. They defined characteristics and operation of two-dimensional photonic crystal sensors and reported detection results from chemical and biological sensing experiments.

Tavousi *et al.* [125] proposed two different optical channel add-drop filters (CDFs) based on rod-type two-dimensional square-lattice all-circular photonic crystal ring resonator. The photonic band gap and the WG-like modes of the PhC ring resonator were calculated using the PWE method, and the Q-factor of modes and the transmission spectra of CDFs were calculated using 2D-FDTD method.

Shen *et al*. [126] theoretically investigated a silicon-based hybrid nonlinear photonic device with a silicon nitride (Si_3N_4) film sandwiched between a graphene sheet and a silicon photonic crystal waveguide (PCW). It was presented that by properly designing, the structural improvement of four-wave mixing (FWM) process can be achieved. Numerical simulation results showed that up to 19.66 dB improvement of the FWM conversion efficiency can be obtained.

Gan *et al*. [127] had not only worked on photonic crystal (PhC) cavities but even on integrated optical devices. Methods for simulating PhC cavities using theoretical and numerical techniques were discussed. The cavity mode volume and Q-factor were showed as per the theory. A wide range of applications were shown which were designed and concluded in a group and provided solutions to few problems of integrated optics.

Hayran *et al*. [128] experimentally demonstrated a demultiplexer with point-defect resonators and a reflection feedback mechanism in a photonic crystal waveguide (PCW). The tapered PCW was chosen as the necessary reflector, which enhances the drop efficiency further with varied width of the tapered PCW. Spatial alteration of the effective refractive index can be achieved. This phenomenon is used to reflect back the forward propagating wave which was then coupled again via resonators.

Liu *et al*. [129] A high efficiency all-optical diode based on photonic crystal (PC) waveguide investigated by finite-difference time-domain (FDTD) method. Because of interference between two cavities, Fano peak and F–P peak can both appear in transmission spectra. This design has many advantages, including high maximum transmittance (>90%), high transmittance contrast ratio, low power threshold, short response time (picosecond level), and ease of integration.

Zaytsev *et al*. [130] demonstrated an ability for highly efficient terahertz (THz) waveguiding in multichannel sapphire shaped crystals. The edge-defined film-fed growth (EFG) technique of shaped crystal growth is implemented to manufacture the THz photonic crystalline (PC) waveguide. These results demonstrated the capabilities of combining the EFG technique advantages with unique properties of sapphire.

Lavdas and Panoiu [131] presented computational study of four-wave mixing (FWM) of optical pulses co-propagating in one-dimensional silicon photonic crystal waveguides (Si-PhCWGs). Theoretical analysis described a setup of the interacting optical pulses, generally nondegenerate FWM in a configuration where at each frequency exists a superposition of guiding modes. Numerical simulations revealed differences between the characteristics of FWM in the slow- and fast-light regimes.

Liu and Houck [132] demonstrated that hybridization can create localized cavity modes that live within the photonic band gap, whose localization and spectral properties they explored in detail. Then they demonstrated that the coloured vacuum of the photonic crystal can be employed for efficient dissipative state preparation.

Xue *et al*. [133] reported an omnidirectional photonic band gap (OPBG) in one-dimensional (1D) plasma photonic crystals (plasma-PCs) with Pell quasi-periodic structures, which consists of plasma and two isotropic dielectrics were theoretically calculated by the transfer matrix method. The calculated results demonstrate that the 1D plasma-PCs with Pell quasi-periodic can not only obtain a larger bandwidth of OPBG but also have a shorter length in realizing devices.

Table 1 Progress in design and development of PCW, reported between 2007 & 2017.

Reference	**Design parameters**	**Wavelength**	**Material**	**Techniques**	**Purpose**
A Massaro *et al*. [2007] [134]	r=0.11µm w_1= 5.94µm w_2= 0.22µm	1.31µm	GaAs & AlGaAs	HPM, FEM, FDTD & Fabrication	Tapered waveguide coupling analysis with low computational cost.
C Lee *et al*. [2008] [135]	r = 0.36*a l = 6.4µm w = 4.8µm t= 200nm	3.621 & 3.843µm	Si & SOI	FEM & PWE	Strain & Force detection.
S Haxha *et al*. [2009] [136]	r = 0.48*a w = 1.05µm h = 1.5µm	1.55µm	SOI	FDTD	To design photonic integrated circuit.
H Ling-Juan *et al*. [2010] [137]	r = 0.32*a	1.31µm 1.49µm 1.55µm	Si	FDTD	PCW as Triplexer for application in FTTH systems.
K Ustun & H Kurt [2011] [138]	r = 0.2*a l = 10*a	1.55µm	Si/GaAs	FDTD	Efficient input and output power coupling.
L Gan & Z Li [2012] [139]	r = 0.279*a t = 235nm	1.5 to 1.64 µm	SOI	FDTD & Fabrication	PCW designed as a transport channel for infrared light.
W Shimizu *et*	r ~ 0.3*a	1.55µm	GaAs	FDTD &	Achieved large

al. [2013] [140]	t = 204nm			Fabrication	optomechanical coupling factor
P T Lin *et al*. [2014] [141]	r = 0.33*a w = 500nm t = 250nm	1.543µm	SOI	FEM	PCW design to trap and detect 50nm radius polystyrene particle
H Liu *et al*. [2015] [142]	r = 0.2*a	1.50µm	Si	FDTD	Stress sensing device
L Athanasekos *et al*. [2016] [143]	r = 0.19*a w = 400nm t = 200nm	0.8 µm	Si_3N_4, Si & SiO_2	FEM & Fabrication	Biological and environmental applications
S Feng *et al*. [2017] [144]	r = 0.4 to 0.15*a w = 10*a	1.55µm	SOI	FDTD & PWE	Light beam splitting and intensity adjustment using hole size

2.6.2 PCW BIO-CHEMICAL SENOSR

Chow *et al.* [145] demonstrated a 2D photonic crystal microcavity based biochemical sensor. Resonant wavelength for the microcavity designed on a silicon-on-insulator was nearly 1.5 µm. Sensor's transmission spectrum was calculated with varied range of ambient refractive indices from n = 1.0 to n = 1.5. A variation in refractive index of $\Delta n = 0.002$ was evident by observing shift in resonant wavelength.

Jensen *et al*. [146] reported detection of biomolecules (Flurophore-labeled) present in aqueous solutions that are placed in airholes of PC fiber's microstuctured portion. The silica structures that are suspended in air and are positioned between three adjacent air holes in cladding crystal, tour the light such that good fraction of the optical field penetrating into sample. The performance was excellent even in the visible range. The important benefit of this detection technique based sensor was the probability of achieving good efficient interaction areas when using sample volumes of submicroliter.

Sharma *et al*. [147] demonstrated a sensor to detect creatinine. Intelligent polymerized crystalline colloidal array (IPCCA) sensor sensed with physiologically having detection limit of 6μM. It can also be fabricated for any kind of species.

Konorov *et al*. [148] compared the two procedures of optical sensing that are designed with the same photonic-crystal fiber. In procedure one, diode laser radiation to the sample was sent using central core that has few micrometers diameter of double cladding PCF, and fiber cladding having greater diameter was responsible to collect the sample generated fluroscent response and sent it to a detector in opposite direction. In the next procedure, sample (liquid) was assembled by micropillary array present in fiber cladding and was tested by laser radiated passed through the fiber mode.

Walker and Sanford [149] developed colloidal array of polymerized crystalline (generally termed as PCCA) which was a PC sensing material used in sensing ultra-trace concentrations of parathion, an organophosphorus compound in aqueous solutions. Colloidal particle's periodic array was arranged in array of hydrogel that had lattice spacing so as to diffract visible light in Bragg fashion. The enzyme acetylcholinesterase (AChE), acts as a molecular recognition agent of the sensor, to create an anionic phosphonyl species molecular recognition agent that binds organophosphorus compounds irreversibly. Donnan potential was created by the charged particles, that increases the size of hydrogel network and also increases the lattice spacing of embedded particle array and enables a red-shift in the wavelength of light diffracted. Diffraction of red shift obtained was correspond to the size of bound parathion.

Kurt and Citrin *et al.* [150] computationally investigated the effects of injecting tiny amounts of molecules, like deoxyribonucleic acid into chosen air holes for sensor applications by the propagation of terahertz waves in 2D PCW.

Rindorf *et al.* [151] presented experimental outcomes of biochemical sensors that use long-period gratings in PCF. One biomolecule layer was inactivated on the sides of holes of PCF, the thickness measurement of the layer was possible by noticing the alteration in the resonant wavelength of long period grating. The CO_2 laser was employed to inscribe long-period gratings in grater-mode area silica PCF. This device was used to measure the thickness of single layer of poly-L-lysine and double stranded DNA. According to this

the sensitivity obtained for grating was nearly 1.4nm/1nm in terms of shift in resonance wavelength (nm) observed per nm thickness of biomolecule layer.

Block *et al*. [152] greatly increased the PC optical biosensors sensitivity by introducing the porous dielectric material having small refractive index into the device structure. The 1D photonic crystal biosensor's reflectance spectra and sensitivity performance were predicted using computer models. In the case of detection of proteins, polymer layers, and bulk liquids, the porous glass biosensors exhibited up to a four-fold sensitivity increase when compared with sensors having non-porous polymer material.

Schwartz *et al*. [153] investigated the physiological changes in primary rat hepatocytes using photonic crystal waveguide sensor. Treated cells were accumulated on the surface of the sensor and observed the change in optical resonance in the spectrometer. They also demonstrated the potential of the technique as a complementary tool for cell viability studies.

Nishijima et al. [154] reported a optical sensing technique named inverse silica opals attractive systems that has simple optical detection setup for sensing, less energy consuming fabrication process. Inverse silica opal photonic crystal structures were fabricated from direct polystyrene micro sphere opals utilizing sol-gel infiltration of silica having low temperature.

Sun *et al*. [155] demonstrated a photonic band gap fibers that is mainly used for biomedical sensing. In accordance with the analytical prediction the reported photonic band gap fiber has a shift of 280 nm in the wavelength that falls in the photonic band gap edge, in this case the ambient refractive indices inside the holey region vary from 1.333 to 1.39

Mathias *et al*. [156] demonstrated a biomolecule detection using two different sensing models that use 2D PC surface with distinct period in every lateral direction. Both sensing methods use same technique of generating resonant reflection peak at any one particular wavelength that is based on PC incident light polarization. One of the two polarization gives reflection peak in visible spectrum so as to match the fluorophores

excitation wavelength, where the other polarization gives reflection peak in infrared wavelength that can be employed in adsorbed biomolecule's label-free detection.

Wu *et al*. [157] presented the concept of refractive index sensing in a microfluidic channel utilizing 3D photonic crystals. These sensors have 3D void channel photonic crystal which are fabricated by femtosecond laser writing in a polymer substrate.

Buswell *et al*. [158] demonstrated the use of planar photonic crystal waveguides for protein detection. An immobilized biotin was used as a probe to catch streptavidin making the waveguide mode cut-off to red-shift. They also explained the design of an enhanced PC waveguide sensor that has 40% boosted bulk refractive index response.

Rindorf *et al*. [159] studied the sensitivity of fiber grating sensors in the applications of strain, temperature, internal label-free biosensing, and internal refractive index sensing to derive novel valid analytical equations for sensitivity of photonic crystal. They also introduced the idea of quality factor Q to distinguish long period grating sensors.

Hsiao and Chengkuo [160] investigated the possibility of biosensing for a novel 2D PC which was based on nano-ring resonator. The PC consisted of silicon plate with normal hexagonal array of holes which was placed in the middle of two silicon PC waveguides. This was kept in a channel of fluid, and the analytes flowing through a sensing hole were caught. Because of the incorporated analytes in a specific hole down the hexagonal ring, the output resonant peak wavelength moved to longer wavelength region

Slatanovic *et al*. [161] demonstrated a PC microcavity sensor of complete area 50 μm^2 with an operative area of detection of 0.272 μm^2 for time-resolved label-free observation of protein binding in a physiological buffer. This ultra-compact sensor was used to observe biotinylated-bovine serum albumin (b-BSA) and anti-biotin binding, in order to measure an affinity constant of $6.94 \times 10^7\ M^{-1}$. The drawback of sensor is noise and this was demonstrated based on results obtained by comparing experimental data to theoretical data.

Pineda *et al*. [64] made an analysis for the direct detection of complete feasible rota viruses and the results of this research indicated that PC biosensors can be useful to keep

track of virus to avoid contamination of water resources. Detection sensitivity of 36 virus focus forming units was obtained in partially processed water sample after assessing it for 30 min and this was done without using any external reagents.

Dahdah *et al*. [162] presented a PC cavity depending upon a single hole defect filled with a sensitive absorbent layer for sensing applications. An introductory study completed with the plane wave expansion method showed that the resonance peak of the cavity mode is 0.5 nm that is moved for a 1 nm thickness difference of the sensitive layer. Using the planned geometry, they found that a variation in the refractive index of 10^{-7} leads to a variation in the transmittivity of 23% at the resonance peak.

Hsiao and Lee [163] theoretically investigated the properties of biochemical sensors that were based on PCs nano-ring resonators. By removing holes of a hexagon from a 2D silicon PC slab in hexagonal lattice the nano-ring resonators were obtained. They reported resonant peak having quality factor of around 3000. At the output side wavelength shift of resonant peak was obtained when biomolecules such as DNAs were captured in hole which was made functional using molecule probes.

Guo *et al*. [164] reported the enhancements in highly sensitive PC biosensor for label-free, actual-time biomolecular binding analysis. They explained working of a biosensor based on regular streptavidin-biotin binding system.

Scullion *et al*. [165] demonstrated the utilization of functionalized slotted photonic crystal cavities that use integrated microfluidics to detect dissolved avidin concentrations as small as 15 nM or 1 μg/ml. Surface mass density values of order 60 pg/mm^2 whose bound mass values are nearly 100 ag are detected using 2.2 μm^2 surface area for cavity sensing. Here, slotted waveguide cavity geometry creates a powerful modal overlap, this leads to high sensitivity values in small areas. The overlap also leads to an altered cavity peak wavelength.

Sun *et al*. [166] demonstrated a PCF RI sensor uses particular resonant coupling between traditional solid core and a microstructure core. Incorporated microstuctured core was made by stuffing the air-hole present in the core with analyte having low refractive index.

They demonstrated a detection limit (DL) of 2.02×10^{-6} and a sensitivity of 8500 nm/RIU can be obtained for analyte with refractive index of 1.33.

Junhua *et al*. [167] designed an air-bridged PC microcavity with enhanced sensitivity and a greater quality factor. Finite difference time-domain method was used to enhance the structure parameter of micro-cavity. They also made comparisons between the performance of silicon-on-insulator PC microcavity and an air-bridged PhC microcavity and also analyzed the consequences on the performance air-bridged PhC microcavity of slab thickness and defect hole's radius.

Liu and Salemink [168] demonstrated a sensor depending upon a 2D PC cavity structure. The working of this device, theoretical simulations, experiments and fabrication were also discussed. Sensor's sensitivity was obtained by noticing the change in resonant wavelength of the photonic crystal cavity according to the refractive index alteration of the analyte. It is established that all optical sensor gains a sensitivity of 460nm/RIU when water and ethanol solutions are mixed through elastomeric micro-fluidic channel.

Bougriou *et al*. [169] PC sensors have grabbed attention due to the characteristics like compactness, greater sensitivity and biocompatibility. The design of highly sensitive infiltrated liquid sensors based on a 2D PC slab waveguide is established by growing the radii of air holes confined on each side of the line defect and stuffing with unvaried de-ionized water ($n_c = 1.33$) is analyzed. Finite difference time domain method is used to obtain transmission spectrum of sensor. For sensitivity greater than 818 nm, upper band edge shifts to 270nm wavelength is observed per refractive index unit.

Lim *et al*. [170] demonstrated a cascaded fiber device from a photonic crystal fiber (PCF) interferometers for sensing refractive index (RI). These kind of interferometers have microbubbles on two sides of splice region, they play a role of diverging lens and spread light for enhanced excitation of greater order cladding modes and disturbance of the core modes in transmitted spectrum. The RI sensitivities obtained by monitoring three resonance wavelengths are as follows 252, 187, and 207 nm/refractive index unit (RIU).

Quan *et al*. [171] reported a detection of single particle that uses PC nano beam cavities that are fabricated in silicon-on-insulator platform, and implanted into microfluidic channels fabricated in polydimethylsiloxane (PDMS). This system works in wavelength band of telecommunication, hence using the extensively available, adjustable and tough laser sources. Using this proposal, they showed the detection of polystyrene nano-particles with dimensions down to 12.5nm radius.

Liang *et al*. [172] designed and demonstrated PC sensor chips with which proteins can be detected with high sensitivity and can be manufactured in bulk with extendable deep-UV lithography. They produced the detection of carcinoembryonic antigen from pg/mL to μg/mL, with increased quality factor PC nano beam cavities.

Xu *et al*. [173] demonstrated the design, fabrication and characterization of high-Q slotted 1D PC cavities with measured Q-factors of approximately 10^4 and parabolic-width stack. Maximum of optical field was distributed in the slotted area having low-index, interaction of light and matter was also developed. For solutions of different NaCl concentrations sensitivities nearly 410 are given with RI sensing measurement. They have greater Q- factor and sensitivity values than 2D slotted PC cavities. Dimensions of the sensing part were as low as $16.8 \times 2.5\ \mu m^2$.

Zou *et al*. [174] presented a biosensing system formed by collaborating PCW with both sub wavelength grating coupling and high sensitivity PC microcavity side coupled. Resultant sensors have greater sensitivity and yield. Quality of transmission spectrum was enhanced by using sub wavelength grating coupling. When optical loss rate from cavity to waveguide is engineered, 1 pM (67 pg/ml) and 50 femto-molar (3.35 pg/ml) detected avidin concentration binded to biotin in phosphate buffered saline for L21 and L55 PC microcavities.

Zhao *et al*. [175] reviewed chemical sensors based on PCF surface Plasmon resonance. Various fiber structures like microstructured optical fiber, Bragg fiber with various structures were applied, including fuse-tapered fiber structure, D-type fiber structure and cladding-off fiber structure were applied to SPR sensors.

Guo and Guo *et al.* [176] demonstrated a hybrid plasmonic optical resonance spectrometer which uses hybrid metal i.e., nano fabricated- dielectric nano hole array photonic crystal gratings. Unlike, the conventional method where optical resonance is measured from transmission this spectrometer optical resonance is measured from first order diffraction.

Eftekhari *et al*. [177] reported revolutionary fluorescence development with a novel structure of multilayer three-dimensional colloidal photonic crystals that are self-assembled from polystyrene spheres. Dual heterostucture employed in this technique contains a top layer and bottom layers designed with periodicity so as to overlap the emitter's excitation wavelength (E), the middle layer designed has periodicity equivalent to fluorescence wavelength (F) and thickness to maintain the constructive interference for the excitation wavelength.

Rifat *et al*. [178] proposed a hexagonal lattice photonic crystal fiber biosensor that uses surface plasmon resonance phenomenon. The fabrication process is very simple since the active plasmonics gold layer and sample are positioned on the outer side of fiber structure. Due to the birefringent behavior of sensor the sensitivity is enhanced. Finite element method was used to numerically investigate the sensing performance and guiding properties. Highest sensitivity of 4000 nm/RIU and 320 RIU^{-1} can be achieved using amplitude and wavelength interrogation techniques, where the resolutions of the sensors should be 3.125×10^{-5} RIU and 2.5×10^{-5}.

Yang *et al*. [179] presented a novel 2D silicon PC α-H0-slot micro-cavity with enhanced Q-factor and sensitivity. Developed design of photonic crystal integrated sensors array (PC-ISA) on monolithic silicon on insulator (SOI) was shown based on α-H0-Slot micro-cavities. Simulation results obtained by using FDTD method showed that at telecom wavelength high sensitivity of 200 nm/RIU and large Q-factor $>10^4$ were simultaneously obtained. Sensor's figure of merit (FOM)>7000 was greater in magnitude than 2D PC sensors array. Presented sensor property where each sensor exhibited to independently shift its resonance wavelength as a result of variations in RI and does not disturb others, makes it an ideal sensor for fabricating ultra-compact lab-on-a-chip applications with dense arrays of functionalized spots for multiplexed sensing.

Men *et al*. [180] demonstrated a visualized optical sensors that were based on responsive PC built by periodic 2D or 3D PCs and responsive material hosts. Optical diffraction color of this type of sensors was set reversibly by stimuli from outside. For example pH, biomolecules, and metal ions increasing their scope of applications.

Wang *et al*. [58] introduced design of a polyatomic photonic crystal ring resonator (PCRR). Unlike the traditional sensors, this PCRR has two distinguished branching waveguides (WG), placed in the similar lattice direction, and with varied optical propagation properties due to the binary nature of the diatomic square lattice. An on-chip biochemical sensor was presented based on this technique. For sensing performance various techniques like Electromagnetic analysis, PWE and FDTD were used. According to results, sensor can effectively detect minute variations in RI inside sensing area.

Hameed *et al*. [181] presented a self-calibrated biosensor design with high sensitivity and based on surface plasmon photonic crystal fiber. Analysis of sensor was carried out by full-vectorial finite element method. Changes were made to geometrical parameters of sensor to obtain greater sensitivity for two polarized modes. Numerical results showed that resonant peaks of two polarized beams were very sensitive to change the analyte refractive index. Hence, optimum refractive index sensitivity of nearly 6700 nm/refractive index unit (RIU) and 10000 nm/RIU, resolution being 1.49×10^{-5} and 1.0×10^{-5} RIU was achieved in accordance to the quasi-transverse magnetic (TM) and quasi-transverse electric (TE) modes.

Peng *et al.* [182] demonstrated a higher-order PC based nanofluidic sensor, that performed at 532nm. A detailed method for fabricating a PC at a required peak wavelength value and required materials were illuminated. Higher mode was employed to design PC based nanofluidic sensor for the first time and refractive index (RI) sensitivity of the sensor was confirmed by FDTD simulation software. The enhanced electrical field of higher order mode structure was mostly confined in the channel area, where the enhance field was wholly interacting with the analytes in the channels. The comparison of RI sensitivity between fundamental mode and higher order mode showed that the RI variation of higher order mode is 124.5 nm/RIU which is much larger than the

fundamental mode. The proposed PC based nanofluidic structure pioneered a novel style for future optofluidic design.

Table 2 Few reports are presented based on PCW as a sensor between 2007 & 2017

Reference	**Type of device**	**Target**	**Sensitivity**	**Quality factor**	**Detection Limit**
M R Lee & P M Fauchet [2007] [183]	Si 2D PhC	Protein	Not given	~2000	Not given
D F Dorfner *et al*. [2008] [184]	Si PhC naostructures	RI sensing	155±6 & 63±9	4000&3000	0.018&0.006
A D Falco *et al*. [2009] [185]	SPhC cavities	Chemicals	1538nm/RIU	4000	$\approx 7.8\times10^{-6}$ RIU
J Jagerska *et al*. [2010] [186]	ASPhC nanocavity	RI sensing	510nm/RIU	$\sim 2.6\times10^{4}$	$>1\times10^{-5}$RIU
W C Lai *et al*. [2011] [187]	PCSW absorption spectrometer	Xylene extraction from water	Not given	Not given	100 ppb (parts per billion) (86 µg/l)
W C Wong *et al*. [2012] [188]	Polyvinyl alcohol coated PCF sensor	Humidity measurement	0.04 nm/%RH, 0.15 nm/%RH & 0.60 nm/%RH	Not given	0.5%RH, 0.14%RH & 0.04%RH
C Nicolaou *et al*. [2013] [189]	2D PCS RI sensor	Detection enhancement	>800 nm/RIU	10600	1.6×10^{-7} RIU 4.9×10^{-7} RIU
D Yang *et al*. [2014] [190]	NPQC	Streptavidin	451nm/RIU	>7000	~10zM
Y Tan *et al*. [2015] [191]	PCEF	Surface-based microspot fluorescent assay	2–10 pg/mL	Not given	80 fM
X Zhang *et al*. [2016] [192]	SPCNC	RI sensing	58 & 139 nm/RIU	Not given	1.8×10^{-4} & 4.1×10^{-6} RIU
S Arafa et al. [2017] [193]	IPCC	Biological analytes	462nm/RIU	1.11×10^{5}	3.03×10^{-6} RIU

2.7 PROBLEMS FOR FORMULATION

- In the literature, there is complexity in designing photonic structures of PCW with point / cavity or line defect with minimized dispersion and scattering loss.
- Various factors have come into existence to challenge the size reduction phenomenon.
- Geometrical parameters like radius and lattice constant sizes affect the slow light propagation in waveguides.
- Difficulty arises while increasing the hole radius of photonic crystal waveguide sensitivity improves, but at the same time quality factor declines.
- Light transmission efficiency and sensitivity are the major issues associated with PCWs.

2.8 CURRENT ISSUES

- Due to bulkiness and problem to scale down, fiber optic temperature sensors are less in use.
- Size reduction will penalize the optical sensitivity in an inversely proportional manner.
- Photonic crystal waveguide requires precise control of technological procedures to adopt while designing and fabricating.
- In the photonic crystal waveguide the optical signal is significantly distorted by the large group velocity dispersion (GVD) at the band edge.
- To design photonic crystal waveguide with novel slow light structures for high group index transmission with wide bandwidth and low dispersion is an important aspect of PCW research.
- Throughput efficiency is poor in a photonic crystal waveguide due to back reflections at the transition between different sections.
- Complexity of the device is increased by cascading design, thus it leads to complicated fabrication and testing process.

- The refractive index is smaller for biomolecules compared to other analytes, due to light confinement in high refractive index region optical waveguide posses challenges in detection.

2.9 OBJECTIVES

1) To analyze the effect of changes in geometry and material on the guiding properties of photonic crystal waveguide for sensing applications.
2) To design photonic crystal waveguide with improved modal and propagation characteristics.
3) To enhance the performance of proposed photonic crystal waveguide for bio-chemical applications.

2.10 THESIS CONTRIBUTION

The research work started with analyzing the various parameters of PCW like waveguide materials, thickness of waveguide, lattice constant, radius of holes, radius of nanocavity, change of position of holes, etch depth of holes, holes shape and transmission wavelength which influence the sensitivity of PCW biosensor. This work proposed few designs using plane wave expansion method (PWE) and simulated using finite difference time domain (FDTD) technique to analyze the sensing properties.

The proposed PCW biochemical sensor waveguide combinations are identified by calculating the optical power efficiencies with reduced optical loss and light confinement. The experiments are performed on two samples, firstly on chemical components to identify the refractive index and secondly, on *E.coli* for morphology and refractive index identification. Further, validation of the PCW sensors as biochemical sensor was done by determining the chemical component concentrations and detection of pathogens. Finally, the PCW sensor performance enhancement is carried out using FDTD software.

2.11 THESIS ORGANIZATION

The thesis has been organized into seven chapters. The content of each chapter is briefly described below:

Chapter 1 introduces sensors along with specifications, classification and latest development in sensor technology. In this chapter, we will discuss the broad areas of optical sensors, principle of operation, types of optical sensors, photonic crystal waveguide sensors and its applications.

Chapter 2 mainly focuses on photonic crystal waveguide geometry. Discussion is made on band structures, types, defects and its applications. It also includes theory and literature review, gaps in present study, problem formulation, objectives, contribution of thesis and thesis organization in support of research work carried out.

Chapter 3 discusses first objective which is analyzing the effect of changes in geometry and material of PCW. Different parameter effects on the design of PCW sensors for various applications are reviewed. This chapter also explains the experimental analysis on culturing of *E.coli* pathogen for identification of refractive index and morphology using SEM image. High to low refractive index materials are considered for the suitability of the PCW design.

Chapter 4 covers the design of PCW with improved modal and propagation characteristics, which represents the second objective of thesis work. Experiment is performed to identify the refractive indices of H_2SO_4 and H_2O_2 chemical components using refractometer and a design of photonic crystal waveguide is proposed to identify the chemical components concentrations by means of standard deviation and coefficient of determination. Device optimization is carried out by varying the radius of center cavity to achieve maximum resonance shift.

Chapter 5 discusses the proposed design of photonic crystal waveguide sensor for chemical sensing in sodium doublet line (Sodium-D-line) wavelength. This chapter support of second objective. The principle of measurement is based on variation in refractive index of sample that causes change in effective refractive index (ERI) for guided mode leading to blue shift. Experimental results of refractive indices are used in

sensing analysis. Proposed design is capable of allowing Sodium-D-line wavelength through structure to work as chemical and biochemical sensor. Better results are achieved after optimizing the device geometry.

Chapter 6 highlights the design and performance enhancement of PCW used in biochemical applications which accomplishes the final objective of the thesis. In this design three different waveguide combinations along with different input wavelengths are chosen to test the suitability for sensing applications through resonance shift and sensitivity. Performance enhancement is carried out by introducing the slotted ring shape design around the test sample. Sensitivity and quality factors are the measuring quantities for validation.

Chapter 7 comprises of conclusion, recommendations and future scope of the work.

CHAPTER 3. IMPACT OF GEOMETRY AND MATERIALS ON PCW FOR SENSING APPLICATIONS

3.1 INTRODUCTION

In this chapter, first objective is addressed to analyze the effect of changes in geometry and material of PCW. Furthermore, the chapter entails the parameters' effects on PCW design which have been reviewed based upon the literature survey in support of proposed work. This chapter also covers the experiment on culturing of *E.coli* pathogen for identification of refractive index using refractometer and morphology using SEM image. High to low refractive index materials are considered for the suitability of the PCW design. A PCW bio-chemical sensor is designed for detection of foodborne pathogens. After designing, detection technique is carried using simulation software.

3.1.1 LATTICE CONSTANT AND RADIUS EFFECTS ON PCW SENSOR DESIGN

It is a fact that wavelength should be analogous to the periodicity of the lattice to ensure that particle interact with its periodic environment. Typically, the range of lattice constant of photonic crystals should be 100 nm to 1 μm. These lattice constant dimensions are suitable for the conventional self-assembly and nanofabrication techniques [194]. Photonic crystal fabrication mainly depends upon the size of the lattice constant. Photonic crystal designs for far-infrared and microwave regions are easy to fabricate. Whereas, photonic crystals working in visible regions are little bit difficult due to their smaller lattice constant size. However, numerous technologies are introduced within a decade to resolve this problem of size. No matter, how small the lattice constant size is recent technologies are capable of fabricating PCW [86]. Though, photonic crystal idea is exciting but the practical realization is not that easy. Wavelength and lattice constant are arranged by the rule of thumb that is photonic crystal lattice constant is in-between one half to one third of its wavelength. For example, if the selected input wavelength is about 1.5 μm then lattice constant should be in between 0.5 to 0.8 μm. Fabrication inside the waveguide is much smaller than outer (0.25 to 0.4 μm) [195-199].

3.1.2 THICKNESS EFFECTS ON PCW SENSOR DESIGN

Thickness is one of the most important parameter and plays a key role in defining the photonic band gap as well as light confinement within the photonic crystal waveguide slab. Consequently, thickness is the parameter which requires repeated study in the designing part of photonic crystal waveguides.

Photonic crystal slab waveguides are similar to the 2D crystals apart from usage of third dimension for index confinement. There is also another type of photonic crystal waveguide that is photonic crystal fiber which is a two dimensional periodic structure with infinite thickness in principle. Wave propagation takes place at right angle to the plane of periodicity, in contrary wave propagation in PCW slab is in parallel to the plane of periodicity.

Here, defect is studied for two types of photonic crystal waveguide slabs one is photonic crystal waveguide slab with square lattice dielectric rods and another one is photonic crystal waveguide with triangular lattice air holes in dielectric slab as shown in Fig 3.1.

Rods and slab are sandwiched by “extruded” substrate which is having the identical cross section of rods and slab with lesser refractive index. This arrangement is made to make the design as a mirror symmetry to provide the band gap [200, 201].

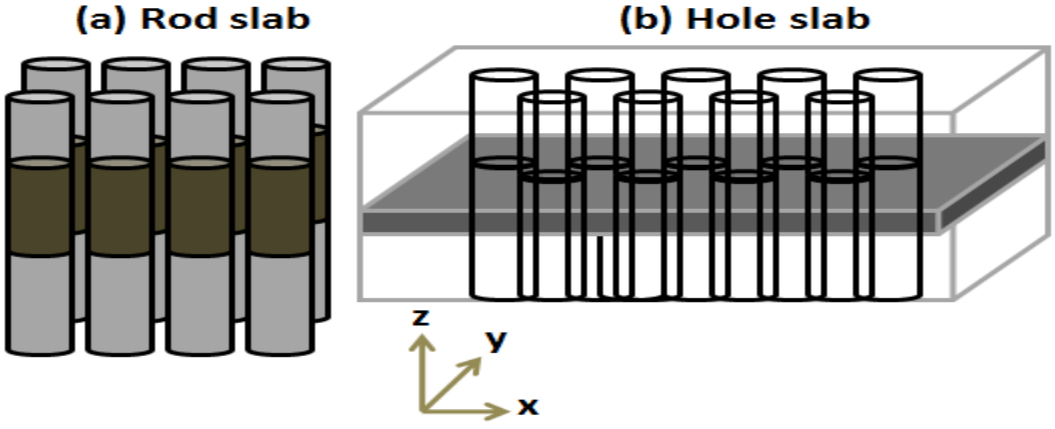

Fig. 3.1 Photonic crystal waveguide slabs with (a) square lattice of dielectric rods in air and (b) triangular lattice of air holes in dielectric slab.

The effective refractive index method can analyze the effect of slab thickness. By using the finite difference time domain method (FDTD) one can identify the band number and eigen frequencies of a photonic crystal waveguide slab with a finite thickness. For both photonic crystal waveguide slab with square and triangular lattice, eigenmodes are identical.

Two conditions are important such as smaller band gaps are created due to the smaller value of slab thickness and band gap is vanished for the thickness less than 1.0a. TE and TM modes agree with the differences in the slab thickness [202].

The study of modal propagation of TE and TM modes have taken greater interest in the modern optoelectronics field. To accomplish the propagation of TE and TM modes, optimization technique is adopted to measure the thickness of photonic crystal waveguides. By using FDTD software, thickness of the slab is identified. The measures are taken to ensure the thickness of slab to provide guiding of TE and TM modes [203-205].

3.1.3 EFFECT OF MATERIALS ON PCW SENSOR DESIGN

From group IV elements, silicon (Si) and germanium (Ge) are extensively used in fabricating optoelectronic devices. Generally, silicon photonic devices are operated in near infrared regions but in recent years it's been shifting towards mid and long wave infrared regions. Dispersion is the key parameter to consider the operating wavelength [206]. At present, very less research is going on in the photonic field using group IV elements in mid and long wave infrared region. Silicon photonics has greater potential application in the mid infrared region for example chemical and biosensing.

Medical sensing, bio-agent and trace gas detection are possible applications including, industrial process control and environmental monitoring. To attract the growing number of researchers and industries in this field, group IV photonic devices needs to be developed with low cost and miniature sensors.

Fig. 3.2 demonstrates the infrared region transmission 'windows' of waveguide materials of core such as germanium, silicon and $Ge_{0.9}Sn_{0.1}$, as well as the waveguide materials of cladding such as SiO_2, Si_3N_4 and Al_2O_3. At 4.5 μm remarkable development was made on single-mode TE_0 silicon-on-sapphire strips. Extensive simulations of SOI waveguides and silicon channel clad with porous silicon were performed at 3.4 μm [207].

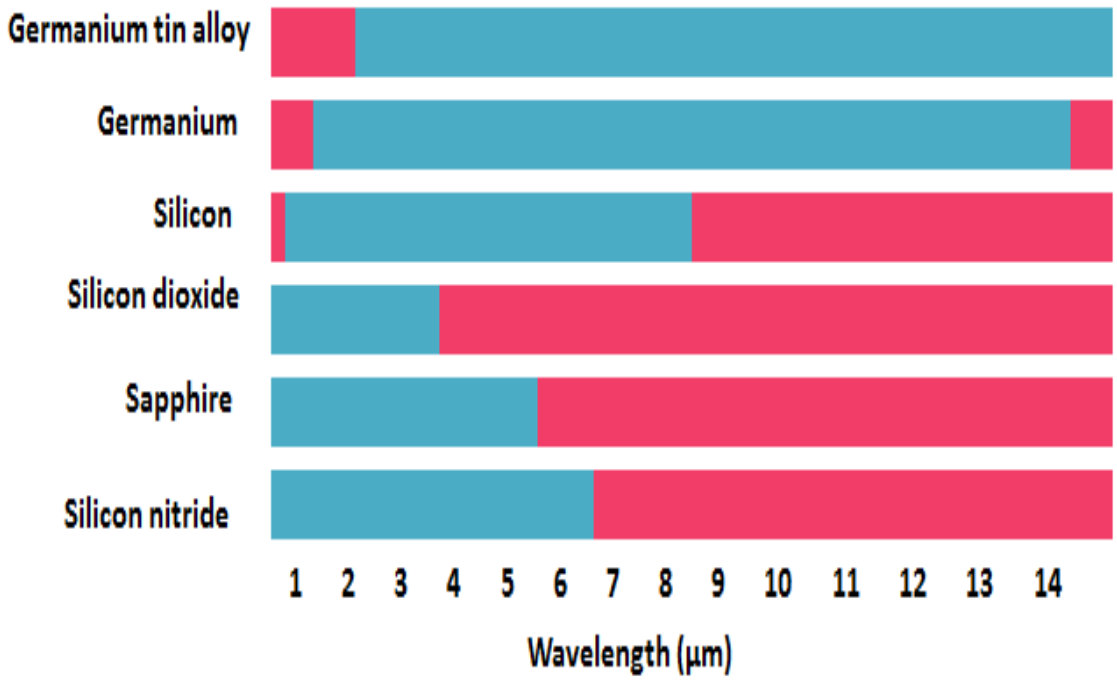

Fig.3.2 Wavelength propagation in different materials, optical transparency is presented as blue area and high loss signified by red areas.

Silicon core structures are considered first among Si based waveguides for experiment. The standard waveguide considered for any kind of optoelectronics device related fabrications are silicon-on-insulator (SOI) wafers. Additional types of waveguides are SiGeC/Si, SiGe upon Si and SiGeSn/Si (and other hetrostructures from group IV alloys), nanocrystalline amorphous Si upon SiO_2/Si, Si upon sapphire (SOS) and high-density porous Si upon low-density porous Si which are integral on a Si wafer. There is also Si/SiC waveguide in which a Si rib is fashioned upon a buried layer of $CoSi_2$ [208].

Same as Silicon, Gallium Arsenide (GaAs) has also reached for high Q values, namely, Q>700,000. Due to this, it is evident that group III–V material combinations resulted in attractive properties of PhCs. [209].

Graphite lattice substrate has GaAs pillars on it, a plane was cut at right angle to the GaAs pillars. Graphite lattice based GaAs pillars in air obtained two dimensional PBG model. The operating wavelength of this waveguide is 1550 nm for simulation and the relative permittivity of GaAs is ε_r=12.18. The applied stress on GaAs pillars may show effect on site but not on the PBG caused by elasto optical effect of the medium [210].

At visible and near-infrared wavelengths silicon nitride (Si_3N_4) with low loss and high index makes it suitable for designing photonic crystal slab devices. Furthermore, mechanical properties of Si_3N_4 are excellent. Deposition of silicon nitride on surfaces are possible using plasma-enhanced chemical vapor deposition or by chemical vapor deposition. In integrated circuits silicon nitride films are used as passivation layers [211].

Geometry and material selection are the major parameters of photonic crystal nanostructures to gain high quality factor. Upper bound of the attainable quality factor is set by the material and by optimizing the structure scattering, non-uniformities and surface roughness are reduced for the periodic structure. Silicon slab wafer deposited with Si_3N_4 layer gives high quality factor in visible wavelength range [212].

Because of its amazing optical properties Chalcogenide glasses have been studied since the 1950s. Its applications have already occupied imaging applications and electronics industry. Due to its unique mid-infrared properties and optical nonlinearities it has gained interest in these materials. Chalcogenides with nonlinearity united with dispersion engineered and confinement make waveguides ultrafast devices.

In recent years, Chalcogenide photonics have attracted both technological and scientific fields in solving challenges in technology and electronic bottleneck in optical communications. Light matter interaction in metamaterial structures and in nanostructures are investigated using Chalcogenide platform. The flexibility in altering the structure, unique optical property and fabrication methodology makes the Chalcogenides convincing in the field of photonics [213, 214].

3.2 EXPERIMENT OF *ESCHERICHIA COLI* CULTURE PREPARATION

Nutrient broth is prepared in aqueous medium. About 0.65 g of broth is added to 50 ml of distilled water (dH_2O). Flask is closed with cotton plug and autoclaved at 121^o C temperature for 30 minutes at a pressure of 15 psf. The liquid mixture (Nutrient broth and *E.coli*) is then cooled at room temperature and a smear is prepared on glass slide using inoculation loop. Fixation of cells is done using 2.5% glutaraldehyde solution. To remove excess glutaraldehyde, washing is done with phosphate-buffered saline (PBS). Dehydration is done using ethanol with 30%, 50%, 60%, 70%, 80%, 90% and 95% and the smear is dried at room temperature. Finally, the morphology of *E.coli* is obtained using SEM images which are taken using instrument (JEOL-JSM, Japan).

By the above preparation methodology, we came across different lengths and diameters of *E. coli*. Therefore, we considered the values of length and diameter as 2.192 µm and 0.57 µm respectively for simulation. SEM instrument and image of *E.coli* shown in Fig. 3.3 (a&b).

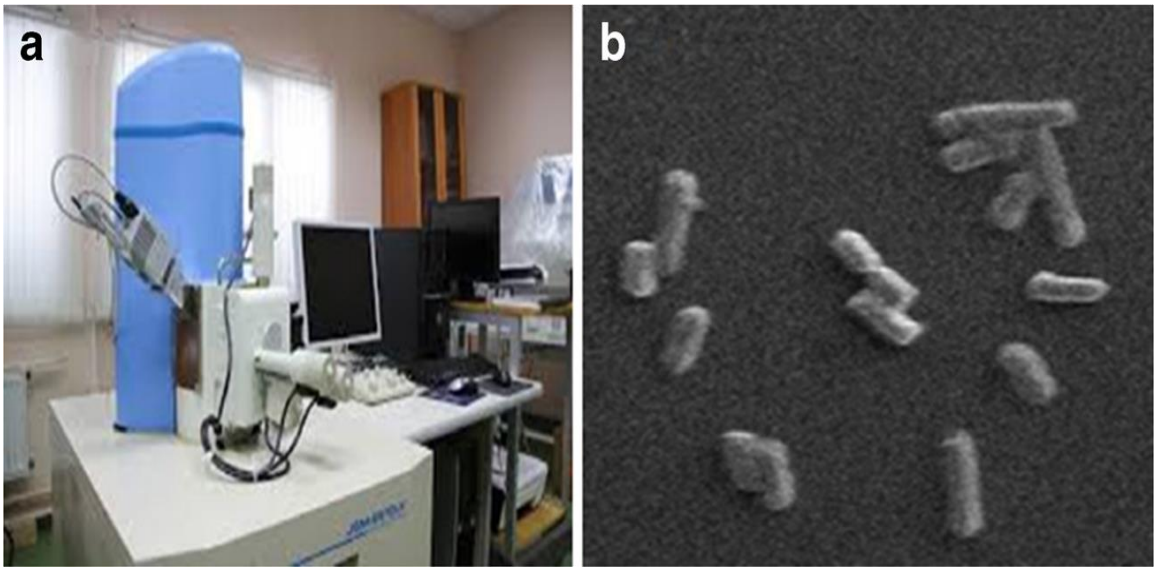

Fig. 3.3 (a) SEM instrument, (b) SEM image of *E. coli* strain

3.3 MATERIAL SELECTION FOR SENSING APPLICATIONS

For the selection of suitable material as a sensing platform, high to low refractive index materials with insulator (Si, GaAs, Si_3N_4, and SiO_2) are considered. Silicon (Si) substrates have emerged as low-cost optical biosensors due to its ease of fabrication, large internal surface area, and compatibility with much surface chemistry. They show a unique stability and are easy to regenerate by a short rinsing step for multiple biosensing analysis. The near-infrared wavelength range transmitted through the gallium arsenide (GaAs) based device is ideally suited for biological sensing applications. Silicon nitride (Si_3N_4) waveguide represented as sensors and hybrid photonic devices at various wavelengths ranged from visible to mid-infrared wavelength regions. Due to its low loss and stress property, it is promising for photonic integration applications. Silicon dioxide (SiO_2) is used for sensing application due to the presence of free hydroxyl groups on its surface.

We have proposed a design along with a suitable sensing waveguide to detect foodborne pathogen using a compact PCW biosensor. It consists of two inverted J-shaped defects surrounding the *E. coli* shaped cavity. An optical setup consists of a tunable light source ranging from 250 to 2700 nm, PCW waveguide, and an optical spectrum analyzer ranging from 192 to 11,000 nm as shown in Fig. 3.4.

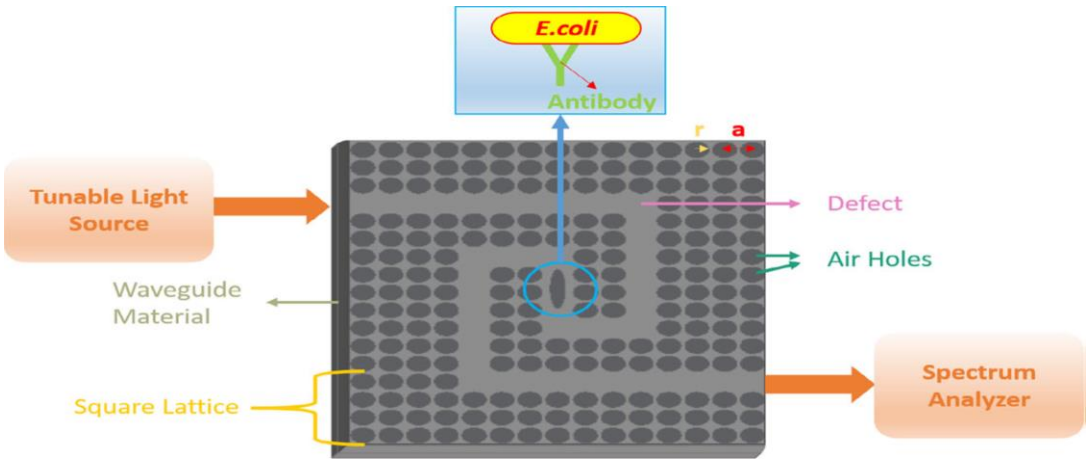

Fig. 3.4 Optical setup for transmission measurements. Light transmitted from a tunable light source through waveguide and detected by an optical spectrum analyzer.

3.4 DESIGN CONSIDERATIONS OF PCW

Photonic crystal structure is patterned on different waveguide materials such as Si, GaAs, Si_3N_4, and SiO_2. The pattern of circular air holes is arranged in a square lattice with lattice constant (a = 1 μm). Plane wave expansion (PWE) method is carried out to observe band gaps of Si, GaAs, Si_3N_4, and SiO_2 waveguides. We achieved considerable band gaps for Si and GaAs based PCW biosensors. Due to a very less difference in refractive indices between air holes and Si_3N_4 and SiO_2 waveguide slabs, band gap observed is very less. For GaAs based PCW, we obtained band gaps between 0.984 and 0.991 μm^{-1}, at air hole radius (r) of 0.3952 μm and band gaps between 0.6435 and 0.6459 μm^{-1} at r of 0.465 μm respectively. The corresponding wavelengths are from 1 to 1.02 μm and from 1.548 to 1.554 μm. For Si-based PCW, band gaps are obtained between 0.645 and 0.651 μm^{-1} and at 0.925 and 0.927 μm^{-1} at r of 0.48 μm. The corresponding wavelengths are from 1.53 to 1.55 μm and from 1.0787 to 1.081 μm.

Engineering is carried out to create two inverted J-shaped defects with a central cavity of oval shape in the middle of the waveguide structure of diameter 0.57 μm and length of 2.192 μm. By introducing defect, input wavelength of 1 μm for r of 0.3952 μm design and 1.55 μm input wavelength for r of 0.465 μm design are able to propagate through GaAs waveguide. For Si-based PCW, 1 and 1.55 μm input wavelengths are able to propagate through r of 0.48 μm design by introducing defect. The center cavity is designed exactly with the matching length and diameter of *E. coli* as shown in Fig. 3.5 (a). *E. coli* refractive index is used in sensing region and transmission of light through it as shown in Fig. 3.5(b).

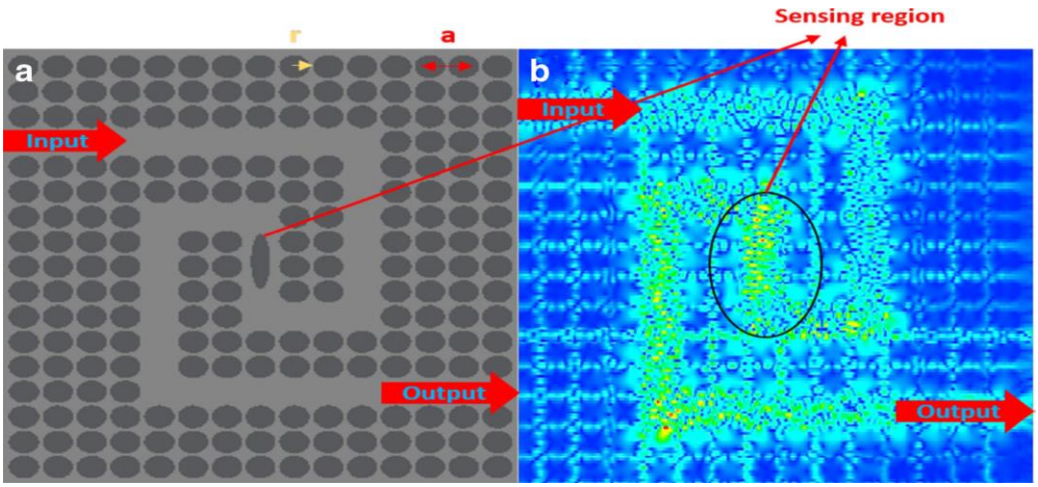

Fig. 3.5 (a) Inverted J-shaped defects with oval-shaped defects in the center of PCW biosensor. (b) light propagation through sample.

3.5 ANALYZING THE MATERIALS FOR SENSING PLATFORM OF PCW

This design uses the refractive index of *E. coli* as n = 1.39 refractive index unit (RIU) obtained using a refractometer (Atago, Japan), and this value resembles with that of study done by Xin et al,. We hypothesized that *E. coli* is positioned in the waveguide's central cavity with n = 1.39 RIU for simulation. Here, air hole refractive index is considered as n = 1 RIU. For simulation analysis, particular wavelength of 1 μm through r of 0.3952 and 1.55 μm wavelength transmitted through r of 0.465 μm of GaAs based PCW design. Input wavelength of 1 and 1.55 μm wavelengths transmit through r of 0.48 μm of Si-based PCW design. These input wavelengths are transmitted through the waveguide by band gap engineering. For GaAs-based PCW, before assuming the *E. coli* refractive index in the middle of the waveguide, a resonance peak of 999.597201 nm is observed and considered as reference. After assuming *E. coli* refractive index, the resonance peak shifted to 998.98445 nm with the shift difference of 0.612753 nm for the input wavelength of 1 μm. In GaAs based wavguide for input wavelength of 1.55 μm with and without *E. coli* refractive index, a resonance peak shift difference is observed as 0.59764 nm. For Si-based PCW, with and without *E. coli* refractive index, the resonance peak shift difference is 0.1991 nm for input wavelength of 1 μm and for input wavelength of 1.55 μm, the shift observed is 3.45701 nm.

Table 3 Resonance wavelength shift with and without *E. coli* for 1000 and 1550 nm input wavelengths

S.no	PCW	Without *E. coli* in nm	With *E. coli* in nm	Resonance wavelength shift in nm	Without *E. coli* in nm	With *E. coli* in nm	Resonance wavelength shift in nm
1	GaAs	998.371697	998.98445	0.612753	1549.43524	1550.0329	0.59764
2	Si	999.384581	999.58365	0.199067	1547.60609	1551.0631	3.45701

Table 3 shows how GaAs and Si based PCW resonance wavelengths are shifting with and without *E. coli* in the center cavity over two operating wavelengths (1000 and 1550 nm). It clearly represents that the two wavelength resonances are shifting towards higher wavelengths (i.e., red shift) in the presence of *E. coli*. According to the table 3, GaAs PCW is showing a larger resonance wavelength shift of 0.612753 nm at input wavelength of 1000 nm because the operating wavelength is nearer to the band-edge of gallium arsenide. Si-based PCW shows a less resonance wavelength shift at input wavelength of 1000 nm, caused by a high absorption coefficient. It is observed that greater resonance wavelength shift of 3.45 nm at operating wavelength of 1550 nm is achieved as a result of the input wavelength corresponding to a photon energy below the silicon band gap, and absorption is very low.

Table 4 PCW sensitivities at 1000 and 1550 nm input wavelengths

Sensitivity in nm/RIU			
S.no	PCW	1000 nm	1550 nm
1	GaAs	1.551823	1.55353
2	Si	0.51043	8.8641

Table 5 PCW quality factor at 1000 and 1550 nm input wavelengths

Quality factor			
S.no	PCW	1000 nm	1550 nm
1	GaAs	339	416.022
2	Si	338.869	394.871

Tables 4 and 5 illustrate GaAs and Si based PCW sensitivities and quality factors at operating wavelengths of 1000 and 1550 nm. From the table 4 and table 5, with operating wavelength at 1000 nm, both the sensitivity and quality factors are shown less than the 1550 nm input wavelength. Therefore, GaAs and Si based PCWs at an operating wavelength of 1550 nm are best suited for detection of foodborne pathogens.

We further, validated the response of GaAs and Si based PCW designs with bulk refractive indices from 1.39 to 1.44 with an increment of 0.01 RIU. The variation in effective refractive index at center position causes shift in resonance due to light matter interaction. Sensitivity is calculated from change in resonance shift to the change in refractive index, and quality factor is calculated from resonance peak to the half-width full maximum. Sensitivity plot against refractive indices is shown in Fig. 3.6.

The Fig. 3.6 shows the sensitivity distribution of GaAs and Si based PCWs over the refractive index between 1.39 and 1.44 RIU. From the Fig. 3.6, bar chart GaAs and Si sensitivities are steadily decreasing with the increase in refractive index. GaAs shown with the lowest sensitivity with an average sensitivity variation of 0.01 nm/RIU for every 0.01 RIU increment in refractive index. Si represents the highest sensitivity with an average sensitivity variation of 0.14 nm/RIU for every 0.01 RIU increment in refractive index. Overall, it is observed that Si-based PCW is displaying higher sensitivity variation than that of GaAs based PCW.

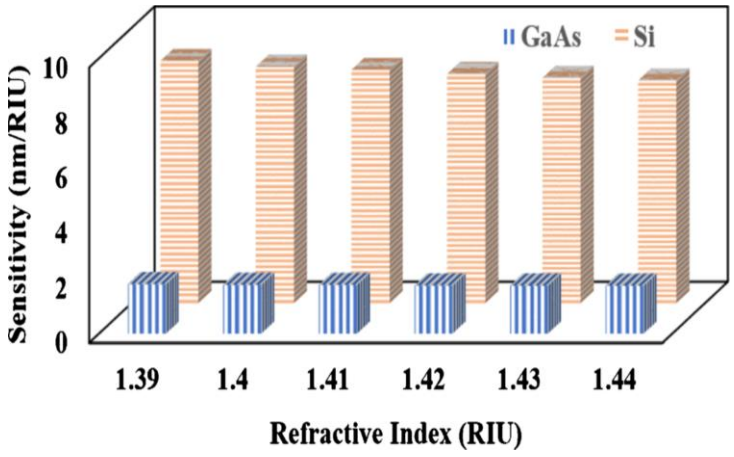

Fig. 3.6 Variations in sensitivity due to change in refractive index.

The Fig. 3.7 demonstrates the variation in quality factor with change in refractive index. GaAs and Si quality factor distributions are represented along with linear fittings. It is witnessed from the graph that both PCW quality factors are steadily increasing. For GaAs-based PCW, average quality factor variation of 1.326 for every 0.01 RIU variation in refractive index and for Si-based PCW, average quality factor of 4.19 for each 0.01 RIU variation in refractive index are observed. Moreover, GaAs-based PCW seems to be heading towards saturation but Si-based PCW have a chance of further improving the quality factor.

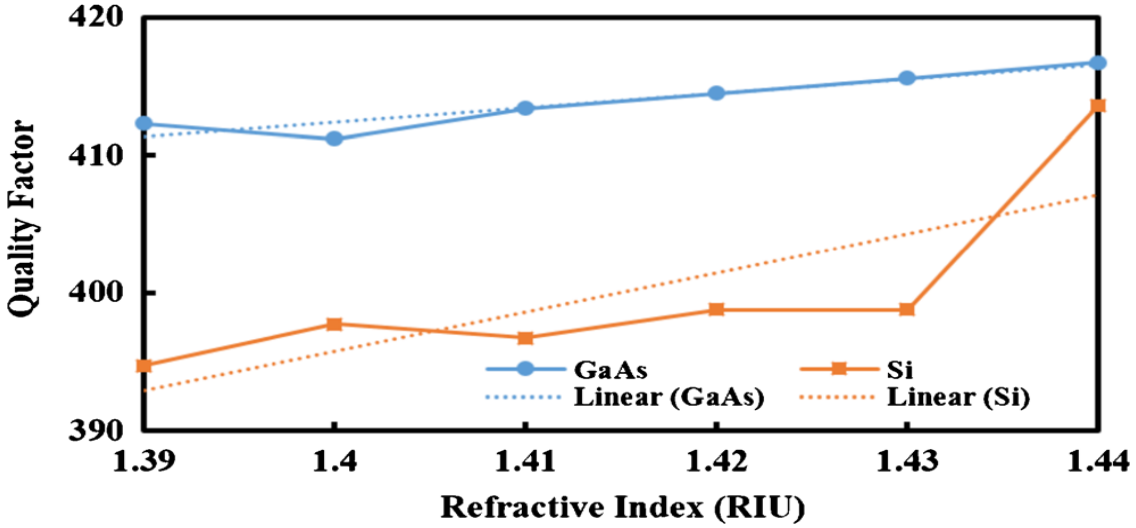

Fig. 3.7 Change in quality factor due to variation in refractive index with linear fitting.

3.6 OUTCOME

Effect of geometrical parameters on PCW senor design is analyzed from review. An on-chip platform based on a 2D PCW biosensor is designed for the detection of foodborne pathogens using different materials. We prepared *Escherichia coli* (*E. coli*) culture to verify the length and diameter of pathogens ranging to fit in the middle of the waveguide. Two inverted J-shaped defects are introduced to transmit input wavelengths 1 and 1.55 μm. The results show that Si is best fit with the highest sensitivity and quality factor to build a label-free on-chip platform for optical detection of foodborne pathogens.

CHAPTER 4. PCW BIO-CHEMICAL SENSOR DESIGN FOR DETECTION OF CHEMICAL COMPONENTS CONCENTRAIONS

4.1 INTRODUCTION OF PCW SENSOR DESIGN FOR CHEMICAL SENSING

This chapter addresses the design of PCW with improved modal and propagation characteristics, which represents the second objective of thesis work. The experiment is performed to identify the refractive indices of H_2SO_4 and H_2O_2 chemical components using refractometer and a design of photonic crystal waveguide is proposed to identify the chemical components concentrations by means of standard deviation and coefficient of determination. Device optimization is carried out by varying the radius of center cavity to achieve maximum resonance shift.

4.2 EXPERIMENT OF REFRACTIVE INDEX ON H_2SO_4 AND H_2O_2

The experimental results of H_2SO_4 and H_2O_2 refractive indices are obtained using refractometer instrument (ATAGO, Japan) at 18 ^{0}C. The RIs are represented in the form of bar chart as shown in Fig. 4.1. With the increase in concentration, there is a significant increment in RI values of H_2SO_4 and H_2O_2. It is observed that H_2SO_4 has higher RI than H_2O_2 [215].

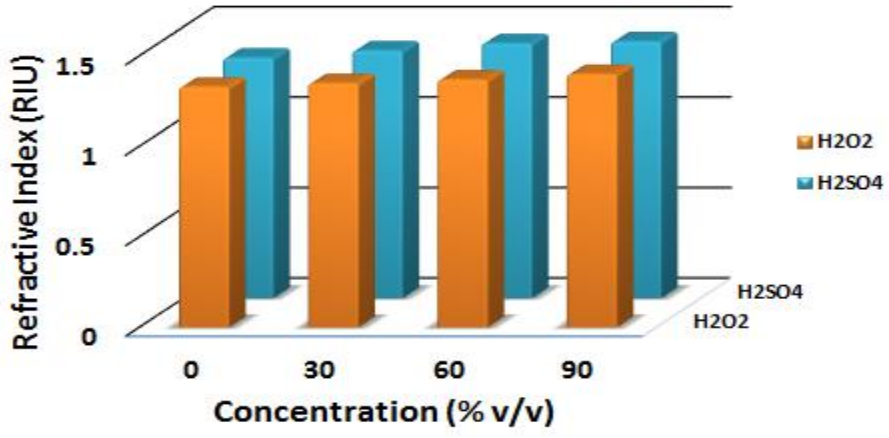

Fig. 4.1 Bar chart representation of refractive index variation with H_2SO_4 and H_2O_2 concentrations.

Fig. 4.1 summarizes the RI values for both H_2SO_4 and H_2O_2 against different concentration percentages which are used for further analysis. By depositing the cavity with different concentrations of chemical solutions, we detect the changes in resonance wavelength shift of the PCW. Source and detector are positioned in such a way that maximum light should pass through the cavity and examine the variations caused by sample refractive indices in the transmission spectra. In this investigation, H_2SO_4 and H_2O_2 concentrations are determined at 1550 nm wavelength.

4.3 PROPOSED PCW SENSOR DESIGN FOR CHEMICAL COMPONENT CONCENTRATION DETECTION

The proposed PCW bio-chemical sensor is designed using hexagonal lattice of air hole on SOI wafer as shown in Fig. 4.2. Helmholtz equation is used to compute the electric field distribution in the PCW biosensor. Helmholtz equation is independent of time functions. Transmission, reflection, electric field distribution and Eigen-frequencies are computed from Helmholtz equation [83].

$$\frac{1}{\varepsilon(r)}\nabla \times \{\nabla \times E(r)\} = \frac{\omega^2}{c^2} E(r), \quad \ldots\ldots\ldots (4.1)$$

where ε is permittivity of material and r is a vector in coordinate space. Electric field component represented in the form of Bloch function is shown in equation 4.2 [83].

$$E(r) = E_{k,n}(r).e^{j.k.r}, \quad \ldots\ldots\ldots (4.2)$$

Where $E_{k,n}$ is a periodic function with periodicity same as that of the lattice. Every wave vector k and Eigen state n indicates different periodic functions for different indices. To satisfy the following condition, functions need to be periodic [83].

$$E_{k,n}(r + R) = E_{k,n}(r), \quad \ldots\ldots\ldots (4.3)$$

Where R is the lattice vector.

The sensitivity is obtained by the ratio of wavelength shift in response to the change in surrounding refractive index change. Sensitivity units are nm/RIU and it should be as high as possible. Sensitivity analysis of PCW is made using equation 4.4 [216].

$$S = \frac{\Delta\lambda}{\Delta n}, \qquad \text{……. (4.4)}$$

where Δλ is the change in resonance wavelength and Δn is the change in refractive index of the sample. The photonic crystal waveguide bio-chemical sensor has a hexagonal structure with a lattice constant (***a***) = 450 nm. It is designed by periodic deposition of cylindrical air holes of radius r = 200 nm on silicon layer which is the top layer of SOI wafer. The radius to lattice constant ratio (r/a) is 0.44. The PCW bio-chemical sensor is a semiconductor based platform in which the line defect is introduced by eliminating the middle row of holes and creating a cavity (sensing region) in the center of the waveguide where the sample has to be placed. The optical source is positioned to the left side of the waveguide structure as shown in Fig. 4.2. Light transmits through the structure to analyze the sample concentrations. Light propagated from polarization controller is directed through the line defect and cavity region of the waveguide.

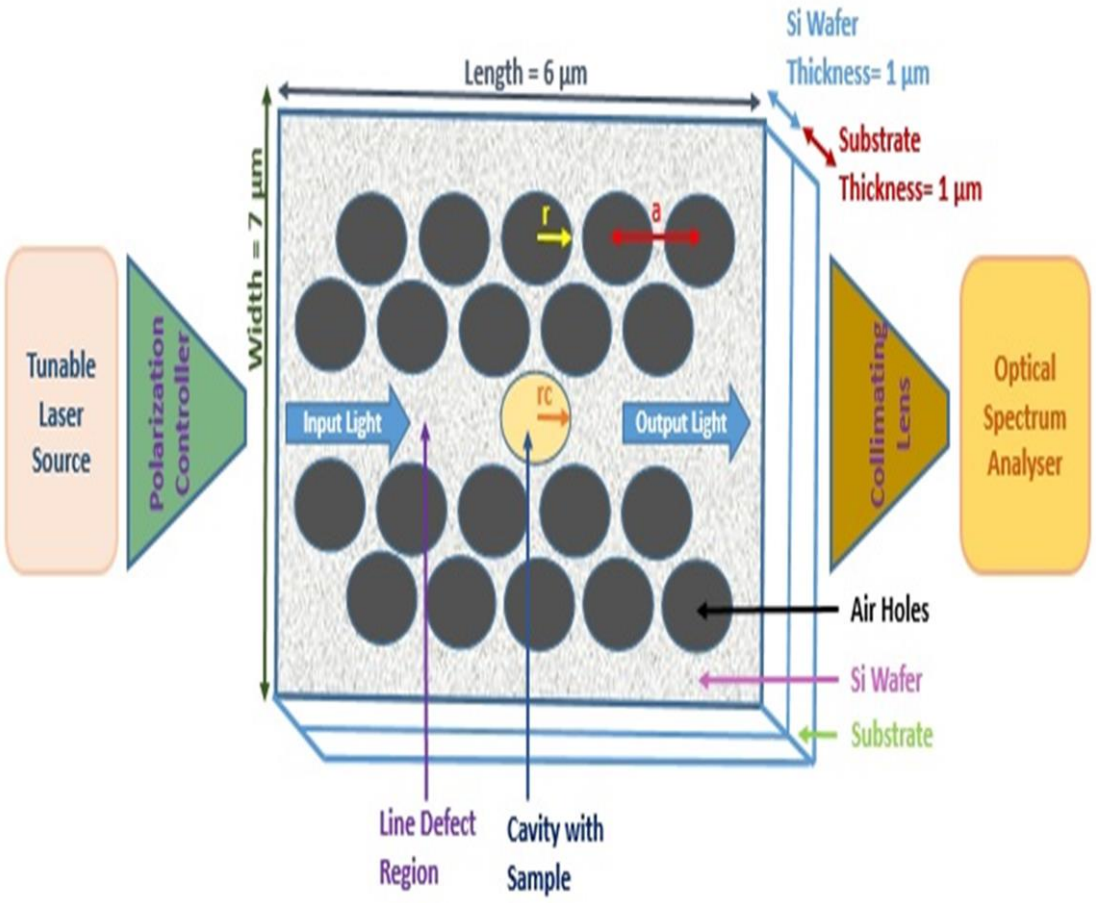

Fig. 4.2 Illustration of the photonic crystal waveguide bio-chemical sensor detection setup.

The measurements are analyzed at the right side of the waveguide using an optical spectrum analyzer as shown in Fig. 4.2. Before finalizing the structural parameters of the device, PWE simulation method is carried out to verify if the selected transmission wavelength could transmit through the device. We obtain the band structure of PCW bio-chemical sensor without defect by using PWE simulation as shown in the Fig. 4.3.

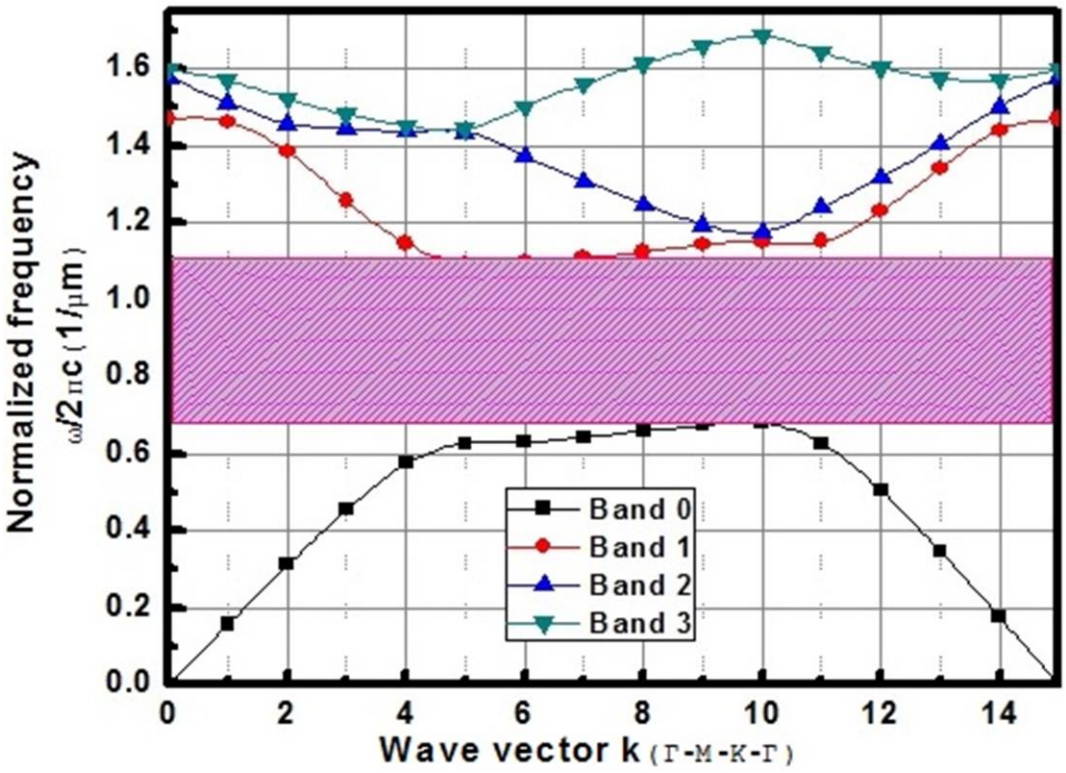

Fig. 4.3 Band diagram of designed PCW.

The band gap is found in TM mode between frequencies 0.66 and 1.08 1/μm, which covers the wavelengths between 0.92 μm and 1.51 μm, while our desired frequency falls near to the stop band region as shown in Fig. 4.3. By creating line defect in the middle of the PCW along with the cavity, we are able to allow the desired frequency mode at 0.66 1/μm.

4.4 APPROXIMATION OF CHEMICAL COMPONENTS CONCENTRATIONS

Fig. 4.4 illustrates the optical power propagation through the cavity (sample) along the line defect region. The light transmission is adjusted to propagate the maximum light through the center cavity holding the sample and an optical spectrum analyzer is used to analyze the transmitted light. Light matter interaction experiences the change in effective refractive index of the waveguide.

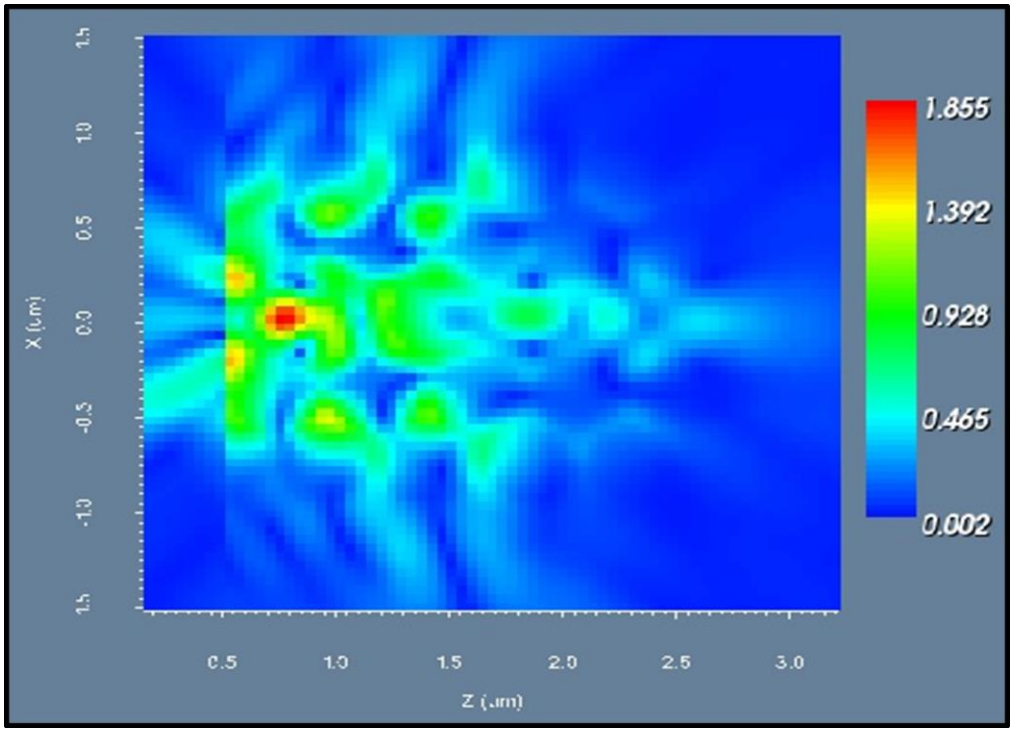

Fig. 4.4 Light propagation through samples.

Fig. 4.5 (a&b) shows how the light is sensitive to the RI variation of the sample corresponding to the concentrations. Fig. 4.5 (a) gives information about the light propagation through the PCW due to the presence of H_2SO_4 samples with refractive indices (n) 1.33, 1.37, 1.41 and 1.42 RIU corresponding to different concentrations in the center cavity. The graph represents a significant rise in intensities along with an increase in refractive indices of the sample within a particular range of wavelengths (1475 nm to 1550 nm). The resonance wavelength shifts towards right (towards higher wavelengths or red shift) with the increase in refractive indices of H_2SO_4. Fig. 4.5 (b) illustrates resonance wavelength shift for different refractive indices of H_2SO_4. The refractive index of deionized water is considered as a reference. Refractive index variation of the sample from 1.33 to 1.37 RIU causes resonance wavelength shift of 1.2 nm and sensitivity obtained is 31 nm/RIU, from 1.33 to 1.41 RIU variation in RI of sample causes resonance wavelength shift of 2.5 nm and sensitivity obtained is 32 nm/RIU, from 1.33 to 1.42 RIU change in RI causes resonance wavelength shift of 3.7 nm and sensitivity obtained is 42 nm/RIU with average device sensitivity of 35 nm/RIU and standard deviation of 6.2. The coefficient of determination obtained a high value of 95.21% as seen in Fig. 4.5 (b).

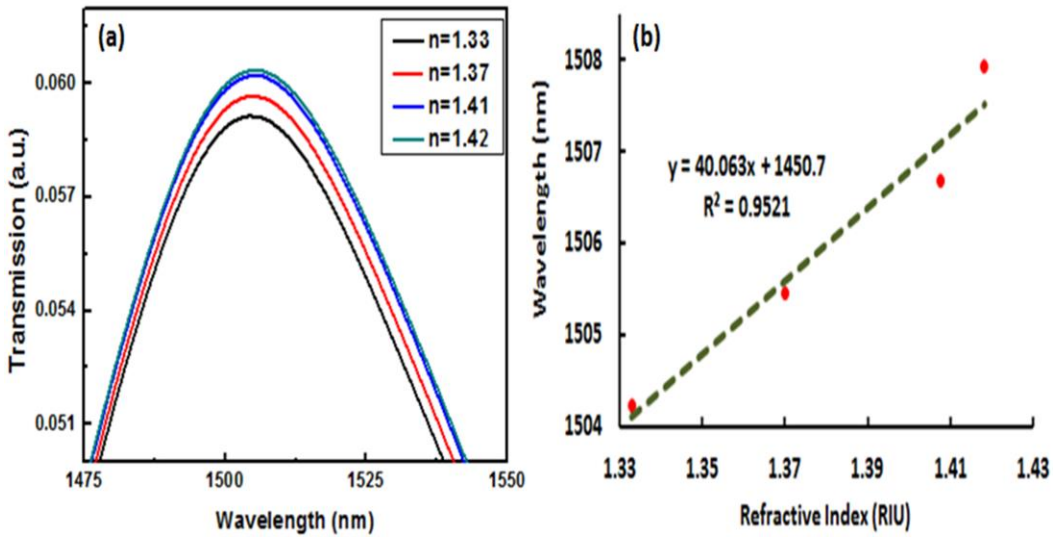

Fig. 4.5 (a) H_2SO_4 transmission spectra of the designed bio-chemical sensor for different RI values and (b) the wavelength shift as a function of variation in refractive indices.

Dependence of light propagation on sample RI variation of H_2O_2 is signified in Fig. 4.6 (a&b). Fig. 4.6 (a) graph provides information about the light transmission through the PCW due to the presence of H_2O_2 samples with refractive indices (n) 1.33, 1.35, 1.37 and 1.4 RIU corresponding to different concentrations in the center cavity. The graph represents a substantial rise in intensities along with an increase in refractive indices of the sample within a particular range of wavelengths (1485 nm to 1525 nm). The resonance wavelength shifts towards the right with the increase in refractive indices of the H_2O_2 sample. Fig. 4.6 (b) demonstrates the resonance wavelength shift for different refractive indices of H_2O_2. The refractive index of deionized water is considered as a reference. Refractive index variation of the sample from 1.33 to 1.35 RIU causes resonance wavelength shift of 0.2 nm and sensitivity obtained is 10 nm/RIU, from 1.33 to 1.37 RIU variation in RI of sample causes resonance wavelength shift of 0.4 nm and sensitivity obtained is 9.5 nm/RIU, from 1.33 to 1.4 RIU change in RI causes resonance wavelength shift of 0.6 nm and sensitivity obtained is 8.7 nm/RIU with average device sensitivity of 9.4 nm/RIU and standard deviation of 0.62. From Fig. 4.6 (b) the coefficient of determination is attained with a high value of 99.59%.

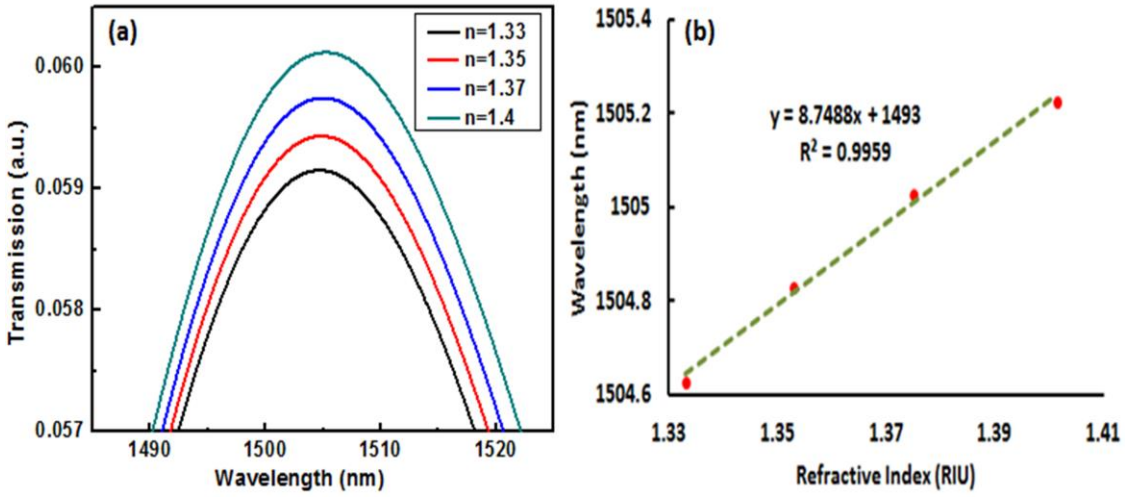

Fig. 4.6 (a) H_2O_2 transmission spectra of the designed bio-chemical sensor for different RI values and (b) the wavelength shift as a function of variation in refractive indices.

4.5 DEVICE OPTIMIZATION

Optimization of the device is performed to achieve greater sensitivity for different cavity radius (**rc**) values ranging from 0.17 µm to 0.23 µm. Fig. 4.7 (a) illustrates the resonance wavelength shifts at different cavity radius filled with H_2SO_4 solution. In this bar chart deionized water with refractive index n=1.33 RIU is considered as a reference.

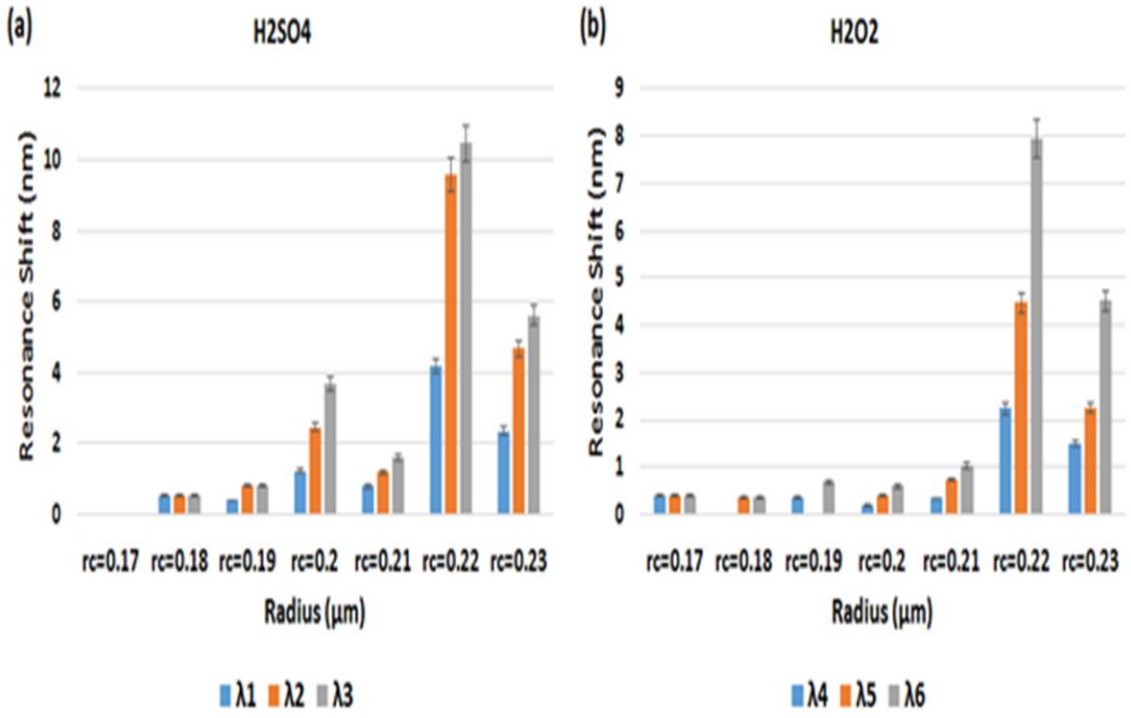

Fig.4.7 Bar chart representation of resonance shifts for different cavity radius (**rc**) at different refractive indices for (a) H_2SO_4 (b) H_2O_2.

We assume λ_1 as the difference in resonance wavelength shift for variation in sample refractive indices from n = 1.33 to 1.37 RIU, λ_2 (from n = 1.33 to 1.41 RIU) and λ_3 (from n = 1.33 to 1.42 RIU). From Fig. 4.7 (a) it is evident that the radius (**rc)** from 0.2 to 0.23 µm are of suitable sizes due to significant variation in resonance wavelength shifts but by taking the sensitivity and standard deviation into consideration **rc =** 0.2 µm shows good performance with an average sensitivity of 35 nm/RIU and standard deviation of 6.2. In Fig. 4.7(b) bar chart illustrates the resonance wavelength shifts at different cavity radius filled with H_2O_2 solution. We consider n = 1.33 RIU as a reference and λ_4, λ_5 & λ_6 are

resonance shifts from n = 1.33 to 1.35, 1.37 & 1.4 RIU respectively. From H_2O_2 bar chart, **rc** = 0.2 µm and above shows a substantial shift in resonance wavelength.

Radius **rc** = 0.23 proves to be the best with average sensitivity 64.98 nm/RIU and standard deviation of 10.87. In addition, the limit of detection (DL) represents the smallest change in sample RI that can accurately be measured in refractometric sensing. The DL is obtained using sensitivity (S) and sensor resolution (R) of proposed sensor as DL = R/S [217]. We calculated R and DL as 1.2 nm and 4×10^{-2} RIU for H_2SO_4 solution and 0.2 nm and 2×10^{-2} RIU for H_2O_2 solution.

4.6 OUTCOME

In this work, for detecting chemical concentrations a PCW bio-chemical sensor is designed which transmits the required wavelength (1550 nm). Initially, concentrations of both H_2SO_4 and H_2O_2 are measured in terms of resonance wavelength shift. The average sensitivity is calculated as 35 nm/RIU for H_2SO_4 against 9.4 nm/RIU for H_2O_2 and standard deviation of 6.2 and 0.62 respectively. Further, very high coefficients of determination are obtained. Later, both components reach their optimum values with average sensitivities of 35 nm/RIU and 64.98 nm/RIU and standard deviation of 6.2 and 10.87 respectively, when optimization technique is adopted. Resolution and limit of detection are also calculated for H_2SO_4 solution and H_2O_2 solution. This is helpful in obtaining exact values for biochemical detection.

CHAPTER 5. DESIGN OF PCW AT SODIUM-D LINE WAVELENGTH

5.1 INTRODUCTION OF PCW DESIGN AT SODIUM-D LINE WAVELENGTH

We proposed a design of photonic crystal waveguide sensor for chemical sensing in Sodium-D Line wavelength. This chapter also supports the second objective of thesis, i.e., designing of PCW with improved modal and propagation characteristics. The principle of measurement is based on variation in refractive index of sample that causes change in effective refractive index (ERI) in guided mode leading to blue shift. Experimental results of refractive index are used in sensing analysis. Proposed design is capable of allowing sodium doublet line (Sodium-D line) wavelength through structure to work as chemical and biochemical sensor. Better results are achieved after optimizing the device geometry.

5.2 DESIGN AND BAND STRUCTURE ANALYSIS

The PCW chemical sensor is designed with periodic deposition of air hole (n=1) of radius r =157 nm in the silicon on insulator (SOI) wafer. Air holes are arranged in hexagonal structure with ‘a’ as the lattice constant of 450 nm. Air hole radius to lattice constant ratio (r/a) is calculated as 0.35. To transmit desired wavelength through the PCW biosensor a line defect with center cavity is introduced by removing air holes along the line and creating center cavity by varying the radius. Center cavity acts as a sensing region to accommodate the sample. By introducing line defect along with point defect input wavelength of 589 nm is able to propagate through waveguide. Optical setup is arranged as shown in Fig. 5.1 (a). Tunable light source with 589 nm wavelength is positioned in left side of the waveguide and optical spectrum analyzer is placed on right side of the waveguide to analyze the sample concentration. Plane wave expansion (PWE) method is adopted to identify the band gap and wavelength that can be transmitted through the

waveguide. Using the above method, PCW obtains 7 band gaps but we are interested in 5th band gap which is achieved between 1.697 (1/μm) and 1.706 (1/μm) frequencies, and covers the wavelengths from 586 nm to 589 nm. The 5th band structure obtained is shown in Fig. 5.1 (b) for the photonic crystal waveguide on silicon on insulator (SOI) wafer. By creating a line with a point defect in the middle of the waveguide, a desired wavelength of 589 nm is transmitted.

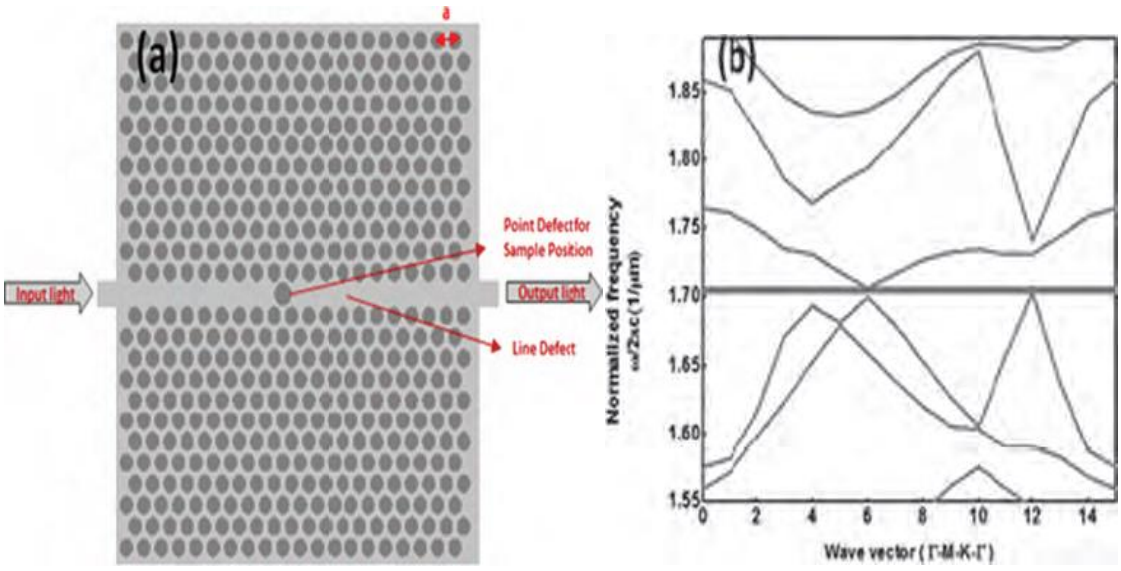

Fig. 5.1 (a) Design of photonic crystal waveguide sensor setup and (b) band gap structure.

5.3 OBSERVATION AND ANALYSIS

Fig. 5.2 depicts the light transmission through sample. The Light source is used to transmit Sodium D-Line wavelength (589 nm) as input and optical spectrum analyzer is used to analyze the spectral response of light transmitted through the sample. The sample is placed in the middle of the waveguide so that maximum light can pass through it as shown in Fig. 5.2. Light interaction with sample leads to the effective refractive index variation which further leads to shift in wavelength.

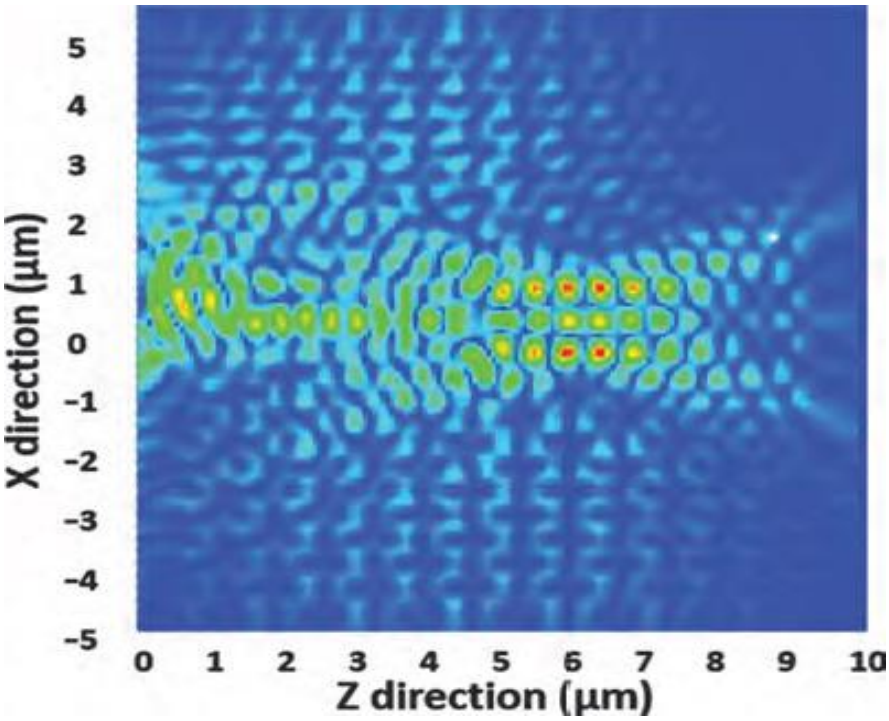

Fig.5.2 Sodium D-line wavelength transmission through samples.

Fig. 5.3 (a) represents the refractive index variation which leads to shift in wavelength for H_2SO_4 sample. From the graph it is observed that as the refractive index increases, the wavelength shifts towards lower wavelengths. Wavelength shift shows that light is sensitive to the variation in refractive index. This wavelength shift is also known as blue shift. From Fig. 5.3 (b) it is observed that 0.03, 0.07 and 0.08 increments in RIs cause wavelength shift of 1 nm, 1.9 nm and 2.2 nm wavelength towards left. Device average sensitivity is calculated as 29.32 nm/RIU and standard deviation as 2.84. The Fig. 5.4 (a & b) illustrates the strong dependence of light interaction with sample is similar as shown in Fig. 5.3 (a & b).

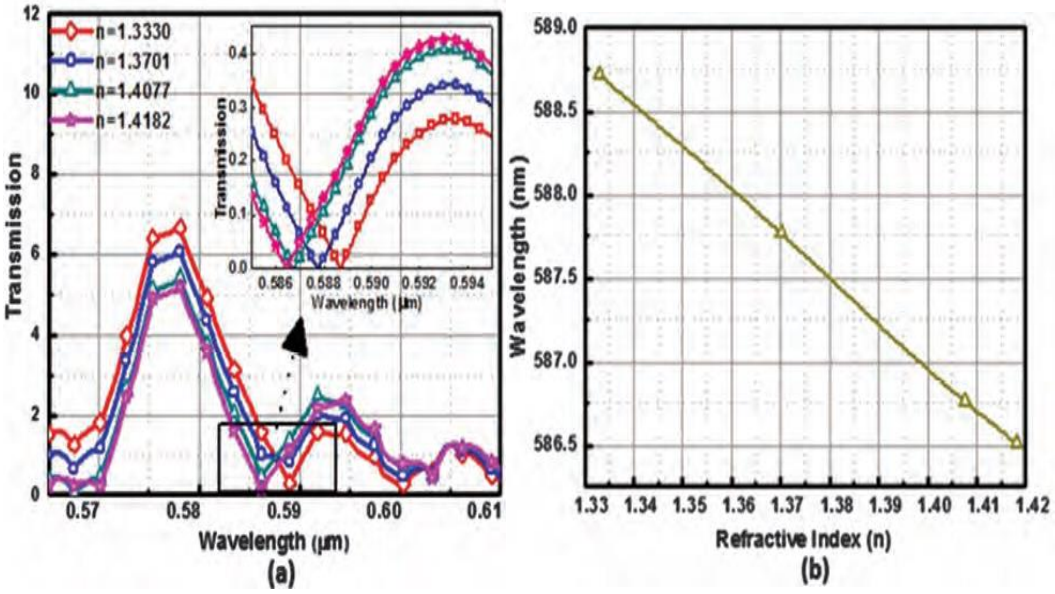

Fig. 5.3 (a) Transmission spectrum of H_2SO_4 (b) wavelength shift dependence on variation of refractive indices.

From Fig. 5.4 (a), it is observed that 0.02, 0.04 and 0.06 increment in RI causes wavelength shift of 0.5 nm, 1 nm and 2 nm respectively towards lower wavelengths (blue shift). Average sensitivity of 27.78 nm/RIU and 3.93 standard deviation is obtained.

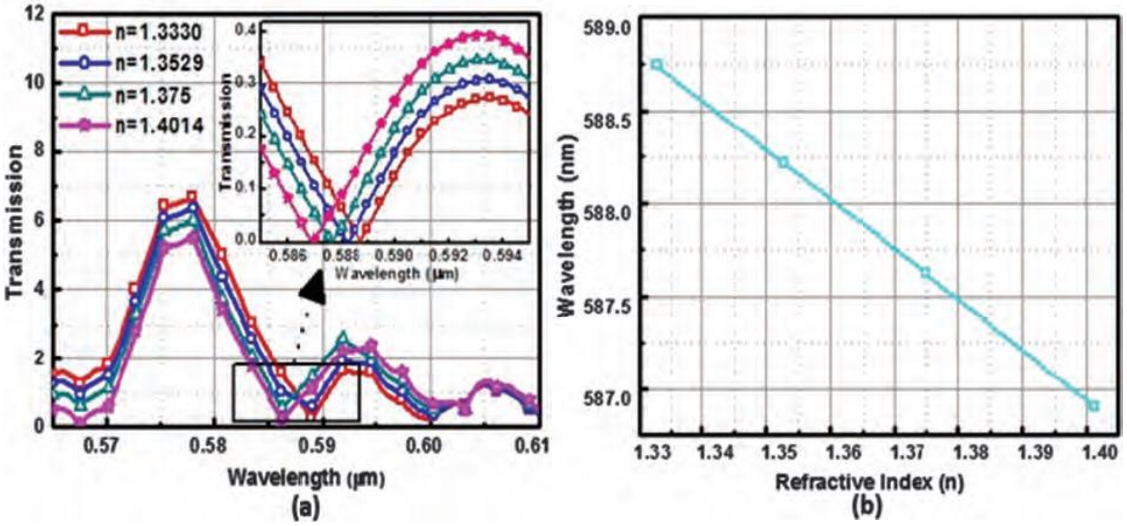

Fig. 5.4 (a) Transmission spectrum of H_2O_2 (b) wavelength shift dependence on variation of refractive indices.

5.4 STRUCTURAL OPTIMIZATION

The optimization technique is adopted to attain higher sensitivities by varying the center cavity radius (rc) from 0.17 µm to 0.23µm. The below bar chart, Fig. 5.5 (a & b) explains how wavelength shifts are obtained due to change in refractive indices for different center cavity radius. Refractive index n = 1.333 is considered as a reference and a wavelength shift for this particular refractive index is 0 nm for both the chemicals. Using Fig. 5.5 (a) sensitivities for all the center cavity radius (rc) ranging from 0.17 µm to 0.23 µm are calculated and at rc = 0.21µm sensitivity increases. Device sensitivity at rc = 0.21µm is equal to 41.06 nm/RIU for the refractive index difference of n=1.33 to 1.37, 35.34 nm/RIU for n= 1.33 to 1.4077 and 34.33 nm/RIU for n = 1.33 to 1.4182. For H_2SO_4, rc = 0.21µm is most suitable with average device sensitivity of 36.91 nm/RIU and standard deviation of 2.96. From the above calculations, it is evident that center cavity radius (rc) 0.21µm is an appropriate size for measuring the H_2SO_4 concentration. Fig. 5.5 (b) illustrates the wavelength shift for H_2O_2. Similar to H_2SO_4, H_2O_2 refractive index at n=1.333 is considered as reference and its wavelength shifts is 0 nm. Excluding 0.19µm center cavity radius, all other wavelength shifts increase but at rc = 0.21µm it increase dramatically. However, at center cavity radius rc = 0.21µm, device achieves maximum average sensitivity as 43.48 nm/RIU and standard deviation as 5.59.

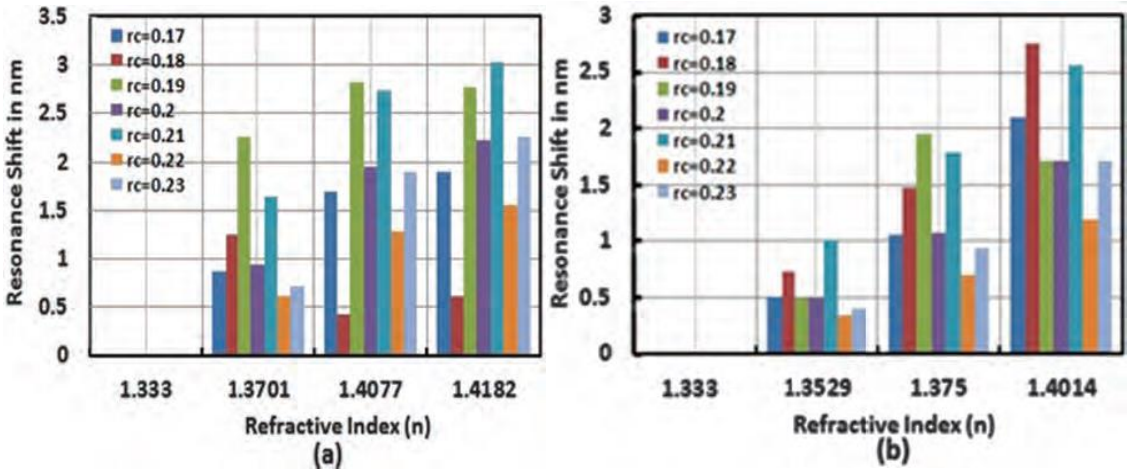

Fig. 5.5 Resonance wavelength shifts against refractive index for different cavity radius (rc = 0.17 to 0.23) (a) H_2SO_4, (b) H_2O_2.

5.5 OUTCOME

A PCW bio-chemical sensor is designed for the detection of chemical concentrations at an operating wavelength of 589 nm. Detection of chemical components' concentration is determined in terms of wavelength shift. At cavity radius of 0.2µm, H_2SO_4 and H_2O_2 average device sensitivities are calculated less comparatively with optimized geometry. Enhanced values of resonance shift and sensitivities are achieved by varying center radius from 0.17 µm to 0.23 µm. From 0.17 µm to 0.23 µm of center cavity, at radius 0.21 µm, it attains optimum average sensitivities of 36.91 nm/RIU and 43.48 nm/RIU and standard deviation of 2.96 and 5.59 for H_2SO_4 and H_2O_2 respectively. Further, improvement in sensor sensitivity is achieved by changing the geometry and thickness of waveguide pattern.

CHAPTER 6. PCW BIO-CHEMICAL SENSOR DESIGN FOR DETECTION OF FOODBORNE PATHOGENS

6.1 INTRODUCTION OF PCW SENSOR DESIGN FOR FOODBORNE PATHOGENS SENSING

This chapter highlights the design and performance enhancement of PCW used in biochemical applications which accomplishes the final objective of the thesis. In this design, three different waveguide combinations along with different input wavelengths are chosen to test the suitability for sensing applications by resonance shift and sensitivity. Performance enhancement is carried out by introducing the slotted ring shaped design around the test sample. Sensitivity and quality factor are considered for validation.

6.2 PROPOSED PCW SENSOR DESIGN FOR DETECTION OF FOODBORNE PATHOGENS

Waveguide structure is designed on semiconductor wafer material consisting of GaAs, Si, or Si_3N_4 as active layers with thickness of 0.57 µm (i.e. average diameter of *E. coli*) and oxide layer as base with a thickness of 1 µm. Circular air holes with lattice constant (a=1 µm) and diameter 0.9 µm are arranged in a hexagonal lattice. For these three materials, we obtain three different band gap regions which are further used in identification of transmitting wavelength by creating defect.

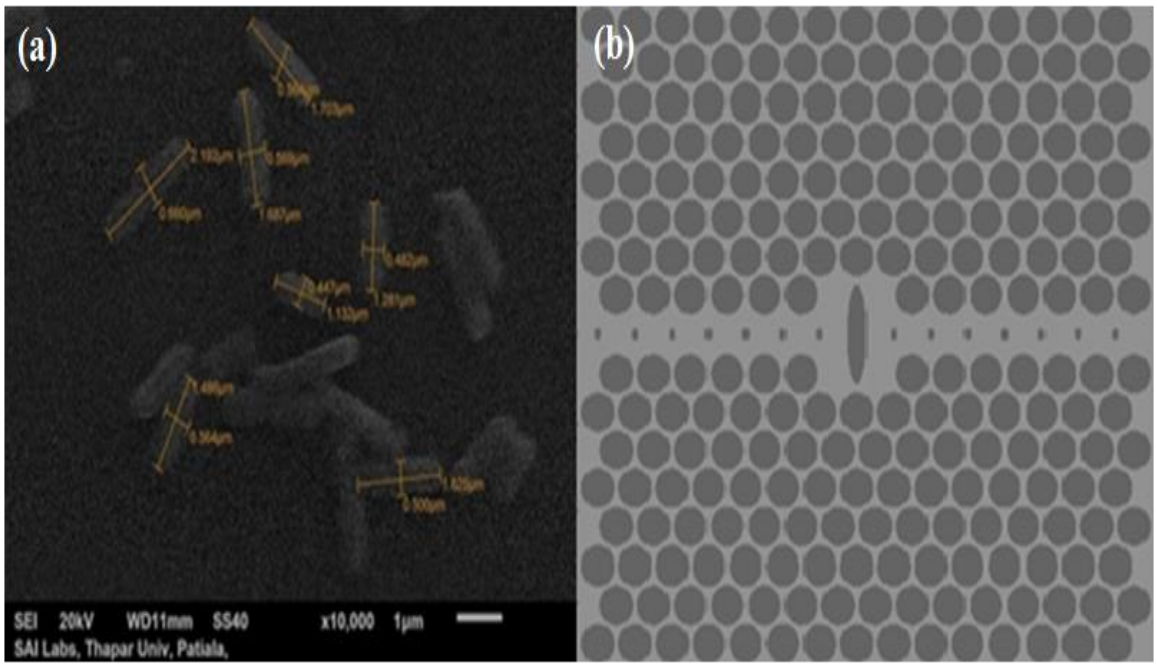

Fig. 6.1 (a) SEM image of *E. coli* and (b) line with point defect in PCW biosensor.

To observe the band gaps in waveguide, plane wave expansion (PWE) method is applied. Band gaps obtained for GaAs/SiO_2, Si/SiO_2 and Si_3N_4/SiO_2 waveguides are between 0.303828 to 0.391145 μm^{-1}, 0.296381 to 0.389746 μm^{-1} and 0.40848 to 0.40970 μm^{-1}. The corresponding wavelengths for the above frequencies are between 2.5566 and 3.29133 μm, 2.56577 and 3.37403 μm and 2.4408 and 2.4481 μm.

Engineering is carried out to create line defect with point defect in the middle of the waveguide structure in horizontal direction with small cavities of radius 0.1 μm and a bigger size cavity (*E. coli* as mentioned above) positioned in the center with average length 1.096 μm and diameter 0.57 μm as shown in Fig. 6.1 (a & b). By creating a defect state within a PC lattice, the prohibited modes from internal propagation may be confined within the defect [218]. Introducing defects, λ_1 = 2.55 μm, λ_2 = 2.6 μm and λ_3 = 2.44 μm, wavelengths are able to propagate through GaAs / SiO_2, Si / SiO_2 and Si_3N_4 / SiO_2 PCW biosensors.

6.3 DETECTION OF FOODBORNE PATHOGENS

Refractive indices of nutrient broth and *E. coli* are obtained using refractometer (Atago, Japan). When PCW is dipped in the nutrient broth (n=1.33) solution, all the holes including cavities are filled with refractive index of 1.33. We then transmit particular wavelengths (λ_1, λ_2 & λ_3) through the GaAs/SiO_2, Si/SiO_2 and Si_3N_4/SiO_2 waveguides. Resonance is obtained at 2.5003 µm, 2.6005 µm and 2.445 µm. By applying the bio-recognition molecule (antibodies) on sensing surface (center cavity), it will allow the detection of specific foodborne pathogens and viral species of ubiquitous cylindrical shape *E. coli* (n=1.39). Resonance shifts to 2.5002 µm, 2.5999 µm and 2.445 µm for the three different waveguides. Resonance shifts from nutrient broth to *E. coli* take place in a very minute level as 1×10^{-4} µm, 6×10^{-4} µm and 6.06×10^{-8} µm. Sensitivities are calculated for all the three PCW biosensors from resonance shifts and it is observed that Si/SiO_2 PCW has obtained highest sensitivity of 10.10438 nm/RIU, GaAs/SiO_2 PCW showed a medium sensitivity of 2.02 nm/RIU whereas Si_3N_4/SiO_2 PCW showed lowest sensitivity of 0.001 nm/RIU.

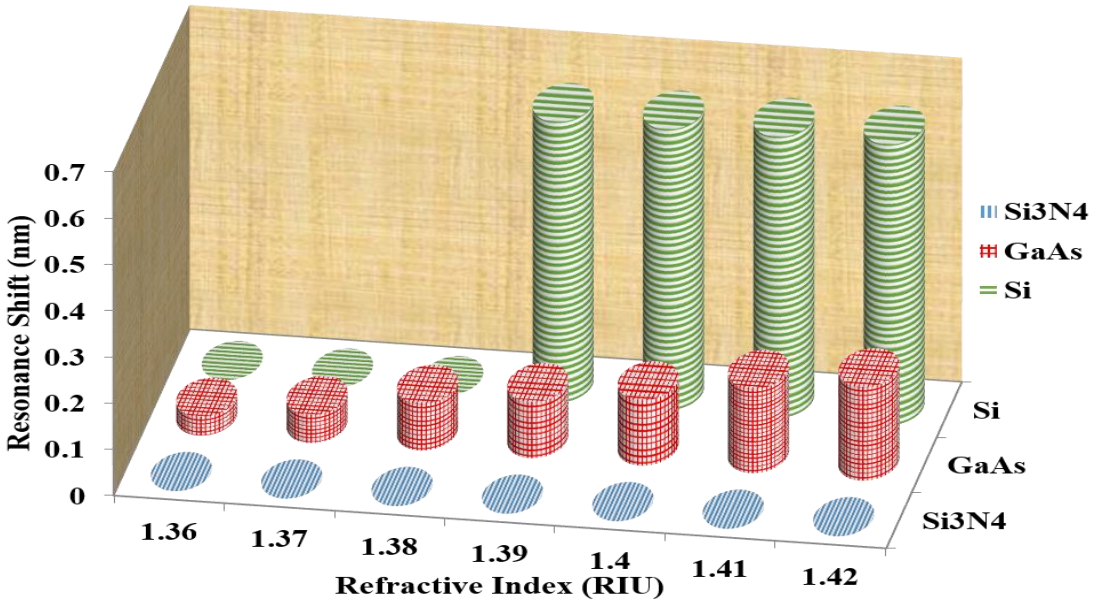

Fig. 6.2 Variations in resonance shift due to change in refractive index.

It is observed that increase in *E. coli* concentration leads to decrease in refractive index [52]. The size and refractive index of bacteria vary as per their growth rate and culture conditions. We validated the response of GaAs / SiO_2, Si / SiO_2 and Si_3N_4 / SiO_2 PCW design with bulk refractive indices from 1.36 to 1.42 with an increment of 0.01 RIU. The variation in effective refractive index at center position causes a shift in resonance. Sensitivity is calculated from the ratio of change in resonance shift to the change in refractive index. Resonance shifts and sensitivities are plotted against refractive indices as shown in Fig. 6.2 and 6.3.

From Fig. 6.2 it is observed that Si / SiO_2 PCW biosensor has a resonance shift of 0 nm for refractive index from 1.36 to 1.38 RIU and at 1.39 RIU it suddenly increases to 0.6 nm and remains same till 1.42 RIU. GaAs shows a significant increase in resonance shift of 0.02 nm for every 0.01 RIU change in refractive index. Si_3N_4 has a resonance shift of almost 0 nm for all refractive indices.

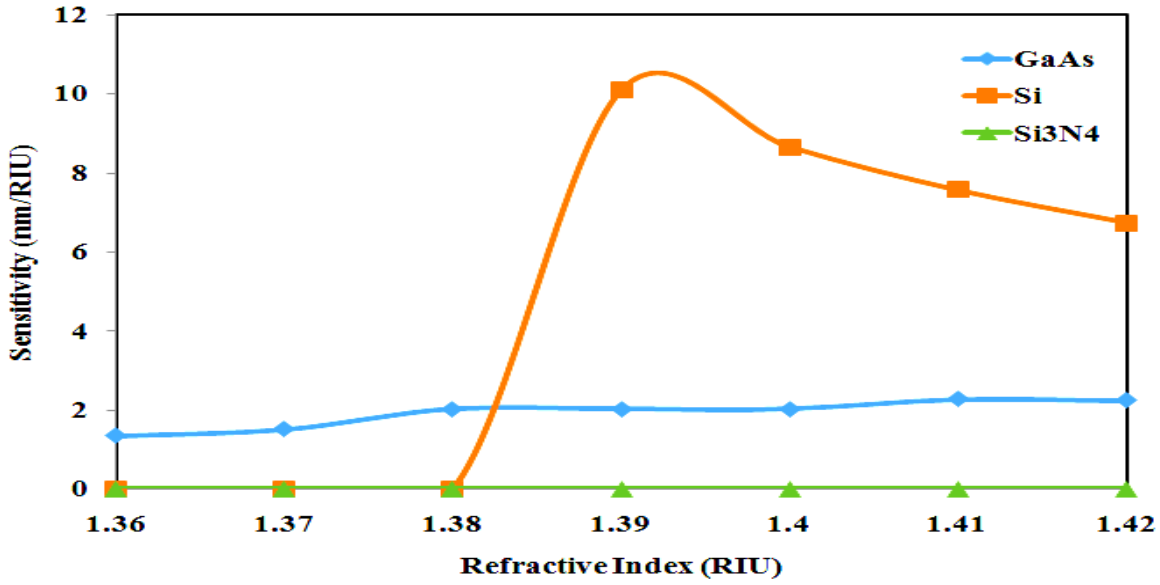

Fig. 6.3 Variations in sensitivity due to changes in refractive index.

From Fig. 6.3, we observe that Si / SiO_2 obtains highest average sensitivity of 4.725 nm / RIU. From 1.36 to 1.38 RIU, its sensitivity remains 0 nm/RIU and from 1.38 to 1.39 RIU it increases to 10.104 nm / RIU and then again decreases to 6.736nm/RIU at 1.42 RIU. GaAs / SiO_2 has a moderate average sensitivity of 1.92 nm / RIU with a consistent

increment in sensitivity and refractive index distribution. Si_3N_4/SiO_2 obtains the lowest average sensitivity of 0.002832 nm/RIU.

Although Si / SiO_2 PCW obtains highest average sensitivity as shown in Fig. 6.3 but it is not preferred because of its inconsistency in sensitivity distribution. As shown in Fig. 6.2, for first three refractive indices (from 1.36 to 1.38 RIU), resonance shift is 0 nm, thus the calculated sensitivity obtained as 0 nm/RIU and for remaining four refractive indices (from 1.39 to 1.42 RIU), all resonance wavelength shifts reach to 0.6 nm, which leads to a sudden increase in sensitivity up to 10.10 nm/RIU and then gradually decreased to 6.73 nm/RIU. Si_3N_4/SiO_2 PCW is also not preferred as it has very low average sensitivity. Therefore, GaAs / SiO_2 PCW is preferred because it shows a consistent increment in its sensitivity distribution.

6.4 PERFORMANCE ENHANCEMENT OF PCW DEVICE

Optimization technique adopted for the design is shown in Fig. 6.4 using simulation software FDTD or FEM. This software uses optimization techniques with different algorithms [219]. High sensitivity is the major requirement in sensing field. Using FDTD method, we proposed a slotted ring around the sensing area on wafer and CMOS-MEMS are also capable of fabricating using SOI substrate [220]. Highest sensitivity and quality factors are accomplished by varying the ring slot width and radius of PCW design.

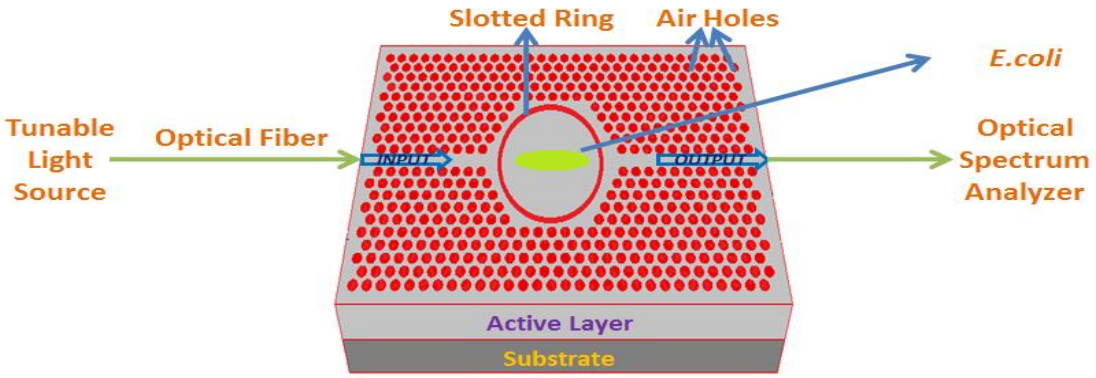

Fig. 6.4 PCW design used for optimization.

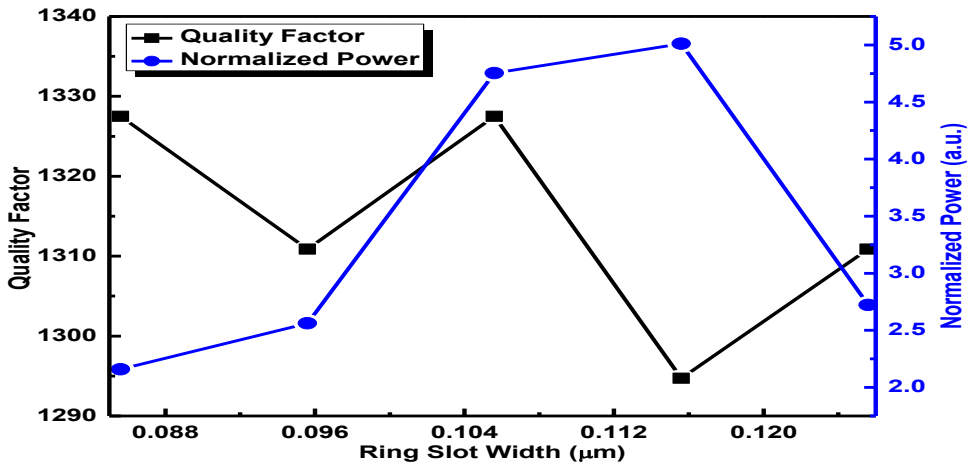

Fig. 6.5 Optimization using changes in ring slot width.

In the above Fig. 6.5 normalized power and quality factor are quantified by varying the ring slot width within the photonic crystal waveguide. At ring slot width 0.104 μm both the normalized power and quality factor seem to reach an optimal value.

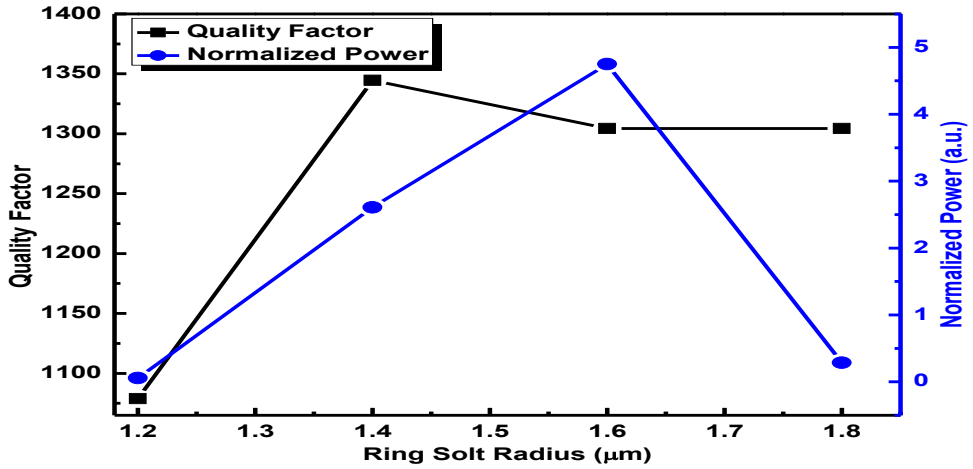

Fig. 6.6 Optimization using changes in ring slot radius.

In the above Fig. 6.6 normalized power and quality factor are quantified by varying the ring slot radius within the photonic crystal waveguide. At ring slot radius from 1.4 to 1.6 μm are showing optimal values for both the normalized power and quality factor.

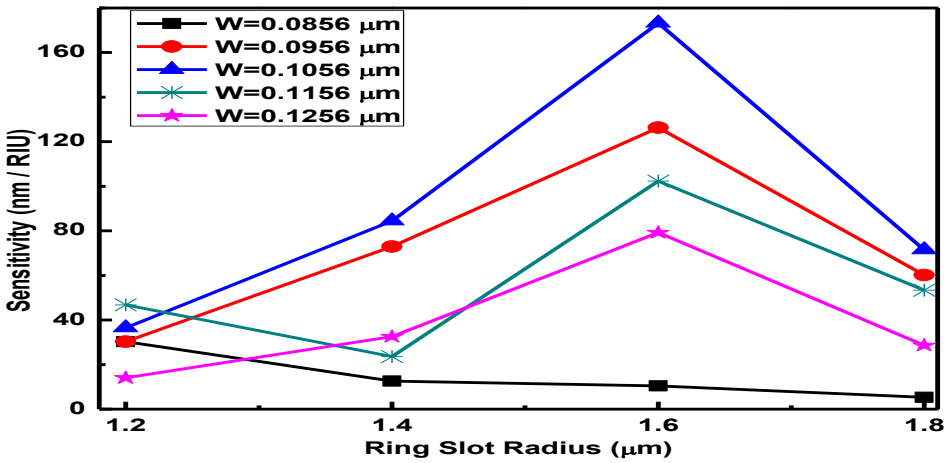

Fig. 6.7 Sensitivity observation using different widths and ring slots radius.

In the above Fig. 6.7 sensitivity is verified by varying the ring slot radius for different ring slot widths of the photonic crystal waveguide. At ring slot radius of 1.6 μm and for the ring slot width 0.1056 μm show the highest sensitivity.

6.5 OUTCOME

The prepared *E. coli* culture is used to verify the length and diameter of pathogens along with refractive index. To trap *E. coli*, central cavity with average length and diameter (1.096 μm and 0.57 μm) is designed. A resonance shift of 1×10^{-4} μm, 6×10^{-4} μm and 6.06×10^{-8} is observed for GaAs/SiO_2, Si/SiO_2 and Si_3N_4/SiO_2 respectively. Though Si/SiO_2, obtaines highest average sensitivity, still not preferred due to inconsistency in sensitivity distribution which initiates from 0 nm/RIU for 1.36 to 1.38 RIU increased to 10.104 nm/RIU and decreased to 6.736 nm/RIU at 1.42 RIU. But, GaAs/SiO_2 had consistent increment due to which it is preferred as active layer for detection of *E. coli*. Optimization of geometrical parameters resulted in highest quality factor and sensitivity.

CHAPTER 7. CONCLUSION, RECOMMENDATIONS AND FUTURE SCOPE

7.1 CONCLUSION

This thesis presents the design and performance enhancement of photonic crystal waveguide (PCW) device for biochemical sensing applications. PCW structure is designed on semiconductor wafer materials. The measurements are analyzed using tunable light source and an optical spectrum analyzer. The PCW design is proposed for both chemical and foodborne pathogens detection applications. The proposed sensing designs are attained by selecting suitable material, one for chemical component concentration detection and another for foodborne pathogen detection along with device optimization.

The selection of suitable material for an on-chip platform based on a 2D photonic crystal waveguide biosensor for the detection of foodborne pathogens is done. The plane wave expansion method is used to achieve band gaps between 0.984 to 0.991 μm^{-1}, at radius (r) of 0.3952 μm and 0.6435 to 0.6459 μm^{-1} at r of 0.465 μm for GaAs. For Si, band gaps are obtained between 0.645 to 0.651 μm^{-1} and 0.925 to 0.927 μm^{-1} at r of 0.48 μm. Two inverted J-shaped defects are introduced to transmit input wavelengths of 1 and 1.55 μm. DH5α strain of *E. coli* foodborne pathogen is considered due to its morphology. SEM and simulation analysis are performed to analyze the average lengths and diameters of *E. coli* pathogen as 2.19 and 0.57 μm. The result shows that Si is best fit with the highest sensitivity and quality factor to build a label-free on-chip platform for optical detection of foodborne pathogens.

For chemical detection in industries, a label-free PCW biochemical sensor based on photonic crystal waveguide is designed for the detection of chemical concentrations. The structure of PCW is engineered to transmit the required wavelength of 1550 nm through the device. Initially, at 0.2 μm cavity radius, concentrations of both sulfuric acid (H_2SO_4) and hydrogen peroxide (H_2O_2) are measured in terms of resonance wavelength shift. For H_2SO_4, average device sensitivity is calculated as 35 nm/RIU and

standard deviation 6.2. Similarly, for H_2O_2, average device sensitivity of 9.4 nm/RIU and standard deviation of 0.62 are obtained. The coefficient of determination obtained as 95.21 and 99.59 % for H_2SO_4 and H_2O_2 is very high. After adopting an optimization technique for the device, both components reach their optimum values at cavity radius 0.2 μm for H_2SO_4 and cavity radius 0.23 μm for H_2O_2 with average sensitivities of 35 nm/RIU and 64.98 nm/RIU and standard deviation of 6.2 and 10.87, respectively. Resolution and limit of detection are calculated as 1.2 nm, 4×10^{-2} RIU for H_2SO_4 solution and 0.2 nm, 2×10^{-2} RIU for H_2O_2 solution. The reported work can be useful in realizing a label-free optical platform for biochemical detection, which has the ability to obtain accurate concentrations of desired chemicals.

Another PCW bio-chemical sensor is engineered to transmit operating wavelength of 589 nm (Sodium-D-Line) through it. Device center cavity radius is set to 0.2μm. Concentrations of H_2SO_4 and H_2O_2 are measured in terms of wavelength shift. At cavity radius 0.2μm H_2SO_4 and H_2O_2 average device sensitivities are calculated as 29.32 nm/RIU and 27.78 nm/RIU with standard deviations of 2.84 and 3.93 respectively. Optimization technique is adopted to derive the optimum values of sensitivity by varying radius from 0.17 μm to 0.23 μm. Subsequently, at center cavity radius of 0.21 μm, H_2SO_4 and H_2O_2 attain optimum average sensitivities of 36.91 nm/RIU and 43.48 nm/RIU and standard deviation of 2.96 and 5.59 respectively. Further, improvement in design sensitivity is achieved by changing the geometry and thickness of waveguide pattern.

For the food industry, an on-chip platform based on a 2D photonic crystal waveguide biosensor for the detection of foodborne pathogens is designed and analyzed. We prepared *Escherichia coli* (*E. coli*) culture to verify the length and diameter of pathogens. Maximum values of *E. coli* length and diameter (2.192 and 0.57 μm respectively) are used to design the central cavity to trap *E. coli*. Resonance shift with and without *E. coli* is observed as 1×10^{-4} μm, 6×10^{-4} μm, and 6.06×10^{-8} μm, respectively, for GaAs/SiO_2, Si/SiO_2, and Si_3N_4/SiO_2 waveguides. Si/SiO_2 PCW obtains the highest sensitivity of 10.10438 nm/RIU and GaAs/SiO_2 PCW shows a medium sensitivity of 2.02 nm/RIU. In bulk RI simulation, Si/SiO_2 obtains the highest average sensitivity of 4.725 nm/RIU, but still it is not preferred due to inconsistency in

sensitivity distribution. From 1.36 to 1.38 RIU, its (Si/SiO_2) sensitivity is 0 nm/RIU; from 1.38 to 1.39 RIU, it reaches to 10.104 nm/RIU and then reduces to 6.736 nm/RIU at refractive index of 1.42 RIU. GaAs/SiO_2 has obtained a moderate average sensitivity of 1.92 nm/RIU and consistent increment in sensitivity with RI. Therefore, by taking the resonance shift and sensitivity into consideration, GaAs is preferred as active layer for identification of *E. coli*. Optimization technique is adopted by changing its geometrical parameters. For ring slot width of 0.104 µm and radius from 1.4 to 1.6 µm results in highest quality factor and for ring slot radius of 1.6 µm along with ring slot width 0.1056 µm results in the highest sensitivity.

7.2 RECOMMENDATIONS

- PCW sensors are accurate and generate precise results in every field of application.

- It is recommended to implement the concept of PCW biochemical sensors in the detection of biological and industrial components to reduce the detection time.

- PCW sensor is specific in its nature and immune to electromagnetic field makes it essentially useful for biosensing applications.

- PCW sensors are designed as per the requirement of test components, such as tailoring of design is possible to allow specific wavelength to transmit through the waveguide.

- As we know that the availability of optical sensors in the market has significantly increased due to reduction in cost. In the same way, bulk production of PCW sensor leads to reduced cost.

- PCW can be designed for multi-point and multi parameter detection system which can further reduce complexity of the sensor system.

7.3 FUTURE SCOPE

- The PCW biochemical sensor can be developed representing a well-adapted solution for very important analytical problem to be deployable in industry.

- Further optimization and assessment in clinical trials should be carried out before exploitation and routine use occur.

- PCW can be designed to overcome the challenges regarding specificity, standardization of methods of collection, treatment and conditioning of samples.

- Lab-on-chip is created in PCW by improving the incorporation of microfluidics.

REFERENCES

[1] D. De Donno, L. Catarinucci, and L. Tarricone, "A battery-assisted sensor-enhanced RFID tag enabling heterogeneous wireless sensor networks," *IEEE Sensors Journal*, vol. 14(4), pp. 1048-1055, 2014.

[2] D. Tandeske, *Pressure Sensors: Selection and Application, 2nd ed.* Taylor & Francis, CRC Press, USA:, pp. 118-119, 1990.

[3] M. I. Baraton, *Sensors for Environment, Health and Security 1ST ed. Advanced Materials and Technologies*: Springer Netherlands, 2008.

[4] D. S. Nyce, *Position Sensors* 1st ed., Wiley, USA, pp. 119-120, 2016.

[5] J. S. Wilson, *Sensor Technology Handbook*: Elsevier Science, pp. 153-154, 2004.

[6] *Vectronav Embedded Navigation Solutions*. Available: http://www.vectornav.com/support/library/calibration accessed at 28/11/2016.

[7] J. Vetelino and A. Reghu, *Introduction to Sensors* 1st ed., Taylor & Francis, CRC Press, pp. 18-19, 2010.

[8] S. Beeby, *MEMS Mechanical Sensors* 1st ed., Artech House, pp. 58-59, 2004.

[9] D. PATRANABI, *SENSORS AND TRANDUCERS*, 2nd ed., PHI Learning, pp. 116-117, 2003.

[10] J. Fraden, *Handbook of Modern Sensors: Physics, Designs, and Applications*, 5th ed. Springer New York, pp. 46-47,2010.

[11] R. Stoney, D. Geraghty, and G. E. O'Donnell, "Characterization of differentially measured strain using passive wireless surface acoustic wave (SAW) strain sensors," *IEEE Sensors Journal*, vol. 14(3), pp. 722-728, 2014.

[12] C. A. Rosen and D. Nilzan, "Use of Sensors in Programmable Automation*," *Computer*, vol. 10(12), pp. 12-23, 1977.

[13] M. A. Fiddy, B. Brames, and J. C. Dainty, "Enforcing irreducibility for phase retrieval in two dimensions," *Optics Letters*, vol. 8(2), pp. 96-98, 1983.

[14] N. Li, R. Wang, Y. Deng, W. Yu, Z. Zhang, and Y. Liu, "Autofocus Correction of Residual RCM for VHR SAR Sensors With Light-Small Aircraft," *IEEE Transactions on Geoscience and Remote Sensing*, vol. 55(1), pp. 441-452, 2017.

[15] J. Ramirez, N. Bottenus, G. Trahey, and J. L. Krolik, "Synthetic aperture imaging with thinned linear sensor arrays for medical ultrasound," in *2016 IEEE Sensor Array and Multichannel Signal Processing Workshop (SAM)*, pp. 1-5, 2016.

[16] M. C. Lina and B. F. Alison, "Smart fabric sensors and e-textile technologies: a review," *Smart Materials and Structures*, vol. 23(5), pp. 053001, 2014.

[17] G. Tschulena and A. Lahrmann, *Sensors Applications, Sensors in Household Appliances*: vol. 5, Wiley, pp. 34, 2006.

[18] D. G. Bailey and C.-S. Bouganis, "Vision Sensor with an Active Digital Fovea," in *Recent Advances in Sensing Technology*, S. C. Mukhopadhyay, G. S. Gupta, and R. Y.-M. Huang, Eds., ed Berlin, Heidelberg: Springer Berlin Heidelberg, pp. 91-111, 2009.

[19] S. Chauhan and L. K. Awasthi, "An energy efficient cycle stealing algorithm for best effort services in wireless sensor networks," *International Journal of Communication Networks and Distributed Systems*, vol. 12(3), pp. 275-298, 2014.

[20] I. Sinclair, *Sensors and Transducers*: 3rd ed., Elsevier Science, pp. 172-173, 2000.

[21] M. Yun, Y. Wan, J. Liang, F. Xia, M. Liu, and L. Ren, "Multi-channel biosensor based on photonic crystal waveguide and microcavities," *Optik - International Journal for Light and Electron Optics*, vol. 123(21), pp. 1920-1922, 2012.
[22] S. H. Tseng, C. L. Fang, P. C. Wu, Y. Z. Juang, and M. S. C. Lu, "A CMOS MEMS thermal sensor with high frequency output," in *IEEE Sensors*, pp. 387-390, 2008.
[23] B. Park, I. W. Jung, J. Provine, A. Gellineau, J. Landry, R. T. Howe, *et al.*, "Double-layer silicon photonic crystal fiber-tip temperature sensors," *IEEE Photonics Technology Letters*, vol. 26(9), pp. 900-903, 2014.
[24] G. C. Righini, *An Introduction to Optoelectronic Sensors*: World Scientific,Singapore, vol 7, pp. 207-208, 2009.
[25] S. Yin, P. B. Ruffin, and F. T. Yu, "Fiber optic sensors,"*Taylor & Francis Group CRC Press New York, pp. 23*, 2008.
26] B. Culshaw, "Fiber-Optic Sensors: Applications and Advances," *Optics and Photonics News*, vol. 16, pp. 24-29, 2005.
[27] V. V. Tuchin, J. S. Skibina, and A. V. Malinin, "Photonic crystal fibers in biophotonics," in *Communications and Photonics Conference and Exhibition, ACP. Asia*, pp. 1-12, *2011*.
[28] S. Yin, P. B. Ruffin, and F. T. S. Yu, *Fiber Optic Sensors, Second Edition*: CRC Press, USA, pp. 23, 2008.
[29] S. Martellucci, A. N. Chester, and A. G. Mignani, *Optical Sensors and Microsystems: 2nd ed. New Concepts, Materials, Technologies*: Springer New York, pp. 159-161, 2007.
[30] B. H. Lee, Y. H. Kim, K. S. Park, J. B. Eom, M. J. Kim, B. S. Rho, *et al.*, "Interferometric fiber optic sensors," *Sensors*, vol. 12(3), pp. 2467-2486, 2012.
[31] B. Gholamzadeh and H. Nabovati, "Fiber optic sensors," *World Academy of Science, Engineering and Technology*, vol. 42(3), pp. 335-340, 2008.
[32] P. M. Tracey, "Intrinsic fiber-optic sensors," *IEEE Transactions on Industry Applications*, vol. 27(1), pp. 96-98, 1991.
[33] M. Yasin, S. W. Harun, and H. Arof, "Fiber optic sensors," ed: InTech, 2012.
[34] S. S. Chong, A. Aziz, and S. W. Harun, "Fibre optic sensors for selected wastewater characteristics," *Sensors*, vol. 13(7), pp. 8640-8668, 2013.
[35] T. Agarwal. (15/10/2016). *Introduction to Fiber Optic Sensors and their Types with Applications*. Available: https://www.elprocus.com/diffrent-types-of-fiber-optic-sensors/
[36] W. Hu, C. Zhu, X. Zheng, M. Gao, D. Guo, and W. Chen, "Polarization-based optical fiber sensor of steel corrosion," *SPIE Nanoscience+ Engineering*. International Society for Optics and Photonics pp. 955510-955510-4,2015.
[37] X. Dong, H. Tam, and P. Shum, "Temperature-insensitive strain sensor with polarization-maintaining photonic crystal fiber based Sagnac interferometer," *Applied Physics Letters*, vol. 90(15), pp. 151113, 2007.
[38] G. E. Sandoval-Romero and E. F. Pinzón-Escobar, "A Simple Detection System for Two Classical Sagnac Interferometer Configurations,"vol.4(12), pp.903-907,2012.

[39] K. Wada, H. Narui, D. Yamamoto, T. Matsuyama, and H. Horinaka, "Balanced polarization maintaining fiber Sagnac interferometer vibration sensor," *Optics express*, vol. 19(2), pp. 21467-21474, 2011.
[40] S. Wu, G. Yan, B. Zhou, E. H. Lee, and S. He, "Open-Cavity Fabry-Perot Interferometer Based on Etched Side-Hole Fiber for Microfluidic Sensing," *IEEE Photonics Technology Letters*, vol. 27(7), pp. 1813-1816, 2015.
[41] T. Yoshino, Y. Sano, D. Ota, K. Fujita, and T. Ikui, "Fiber-Bragg-Grating Based Single Axial Mode Fabry-Perot Interferometer and Its Strain and Acceleration Sensing Applications," *Journal of Lightwave Technology*, vol. 34(9), pp. 2241-2250, 2016.
[42] N. Insturments. (2011, 10/09). *Overview of Fiber Optic Sensing Technologies*. Available: http://www.ni.com/white-paper/12953/en/
[43] J. Dakin, "Multiplexed and distributed optical fibre sensor systems," *Journal of Physics E: Scientific Instruments*, vol. 20(8), pp. 954, 1987.
[44] S. Pevec and D. Donlagic, "Miniature fiber-optic sensor for simultaneous measurement of pressure and refractive index," *Optics Letters*, vol. 39(21), pp. 6221-6224, 2014.
[45] P. Ripka and A. Tipek, *Modern Sensors Handbook*: Vol 3, Wiley,Weinheim, pp. 190-192, 2013.
[46] A. Leung, P. M. Shankar, and R. Mutharasan, "A review of fiber-optic biosensors," *Sensors and Actuators B: Chemical*, vol. 125(2), pp. 688-703, 2007.
[47] M. E. Bosch, A. J. R. Sánchez, F. S. Rojas, and C. B. Ojeda, "Recent Development in Optical Fiber Biosensors," *Sensors (Basel, Switzerland)*, vol. 7(6), pp. 797-859, 2007.
[48] W. Yu, T. Lang, J. Bian, and W. Kong, "Label-free fiber optic biosensor based on thin-core modal interferometer," *Sensors and Actuators B: Chemical*, vol. 228, pp. 322-329, 2016.
[49] S. Singh and B. Sharma, "Immunodeficiency and Microbial Infections," *Journal of Microbiology and Modern Techniques*, vol. 1(1), pp. 1, 2015.
[50] (2015, 01/05/2016). *Centre for Disease Control and Prevention*. Available: http://www.cdc.gov/foodnet/reports/prelim-data-intro.html
[51] P. Chen, Y. B. Li, T. H. Cui, and R. Ruan, "Nanoparticles based sensors for rapid detection of foodborne pathogens," *International Journal of Agricultural and Biological Engineering*, vol. 6(1), pp. 28-35, 2013.
[52] S. M. Tripathi, W. J. Bock, P. Mikulic, R. Chinnappan, A. Ng, M. Tolba, *et al.*, "Long period grating based biosensor for the detection of Escherichia coli bacteria," *Biosensors & Bioelectronics*, vol. 35(1), pp. 308-312, 2012.
[53] M. E. Eissa and A. S. Nouby, "Recovery of Gram-Positive Cocci and Candida albicans from Peroxygen/Silver-Based Disinfectants," *Polish Journal of Microbiology*, vol. 65(1), pp. 13-21, 2016.
[54] V. Suttisunhakul, V. Wuthiekanun, P. J. Brett, S. Khusmith, N. P. Day, M. N. Burtnick, *et al.*, "Development of Rapid Enzyme-Linked Immunosorbent Assays for Detection of Antibodies to Burkholderia pseudomallei," *Journal of clinical microbiology*, vol. 54(5), pp. 1259-1268, 2016.
[55] Y. Sun, J. Yu, X. Lin, and W. Tang, "Inhibition of cyclooxygenase-2 by NS398 attenuates noise-induced hearing loss in mice," *Scientific reports*, vol. 6, 2016.

[56] J. L. Olsen, "Polymerase Chain Reaction," *Encyclopedia of Immunotoxicology*, pp. 715-720, 2016.
[57] A. Subramanian, J. Irudayaraj, and T. Ryan, "A mixed self-assembled monolayer-based surface plasmon immunosensor for detection of E-coli O157 : H7," *Biosensors & Bioelectronics,* vol. 21(7), pp. 998-1006, 2006.
[58] D. Wang, Y. Liu, L. Yuan, J. Lei, X. Li, and S. Hou, "An efficient optical biochemical sensor based on a polyatomic photonic crystal ring resonator," *Optics Communications,* vol. 372, pp. 160-165, 2016.
[59] D. Fraenkel, "Structure and ionization of sulfuric acid in water," *New Journal of Chemistry*, vol. 39(7), pp. 5124-5136, 2015.
[60] B. Painam, P. K. Teotia, R. S. Kaler, and M. Kumar, "Bio-Chemical Sensor Based on Photonic Crystal Waveguide for Estimation of Sulphuric Acid Concentration," in *12th International Conference on Fiber Optics and Photonics*, Kharagpur, p. S5A.48, 2014.
[61] T. N. Das, "Saturation concentration of dissolved O-2 in highly acidic aqueous solutions of H2SO4," *Industrial & Engineering Chemistry Research,* vol. 44(6), pp. 1660-1664, 2005.
[62] L. Buljubasich, B. Blumich, and S. Stapf, "Quantification of H(2)O(2) concentrations in aqueous solutions by means of combined NMR and pH measurements," *Phys Chem Chem Phys*, vol. 12(40), pp. 13166-73, 2010.
[63] J. P. Lafleur, A. Jönsson, S. Senkbeil, and J. P. Kutter, "Recent advances in lab-on-a-chip for biosensing applications," *Biosensors and Bioelectronics,* vol. 76, pp. 213-233, 2016.
[64] M. F. Pineda, L. L.-Y. Chan, T. Kuhlenschmidt, C. J. Choi, M. Kuhlenschmidt, and B. T. Cunningham, "Rapid specific and label-free detection of porcine rotavirus using photonic crystal biosensors," *IEEE Sensors Journal*, vol. 9(4), pp. 470-477, 2009.
[65] R. V. Nair and R. Vijaya, "Photonic crystal sensors: An overview," *Progress in Quantum Electronics,* vol. 34(3), pp. 89-134, 2010.
[66] G. Chen and J. U. Kang, "Waveguide mode converter based on two-dimensional photonic crystals," *Optics Letters*, vol. 30(13), pp. 1656-1658, 2005.
[67] N. M. Gopinath Palai, Santosh K. Sahoo, Sukanta K. Tripathy, Sumanta K. Patanaik, "Realization of Potassium Chloride Sensor Using Photonic Crystal Fiber," *Soft Nanoscience Letters,* vol. 3, pp. 16-19, 2013.
[68] A. Sharma and M. Kumar, "Flat band slow light in silicon photonic crystal waveguide with large delay bandwidth product and low group velocity dispersion," *Iet Optoelectronics,* vol. 9(1), pp. 24-28, 2015.
[69] A. Sharkawy, D. Pustai, S. Y. Shi, and D. W. Prather, "High transmission through waveguide bends by use of polycrystalline photonic-crystal structures," *Optics Letters,* vol. 28(14), pp. 1197-1199, 2003.
[70] N. Janrao and V. Janyani, "Nonlinear performance in silicon nitride slow light photonic crystal waveguides with elliptical holes," *Optik,* vol. 125(13), pp. 3081-3084, 2014.
[71] Q. Gong and X. Hu, *Photonic Crystals: Principles and Applications*: Pan Stanford, 2014.

[72] M. Pisco, A. Ricciardi, I. Gallina, G. Castaldi, S. Campopiano, A. Cutolo, *et al.*, "Tuning efficiency and sensitivity of guided resonances in photonic crystals and quasi-crystals: a comparative study," *Optics Express,* vol. 18(16), pp. 17280-17293, 2010.

[73] K. V. Shanthi and S. Robinson, "Two-dimensional photonic crystal based sensor for pressure sensing," *Photonic Sensors*, vol. 4(3), pp. 248-253, 2014.

[74] T. van Leest and J. Caro, "Cavity-enhanced optical trapping of bacteria using a silicon photonic crystal," *Lab on a Chip,* vol. 13(22), pp. 4358-4365, 2013.

[75] S. Jindal, S. Sobti, M. Kumar, S. Sharma, and M. K. Pal, "Nanocavity-Coupled Photonic Crystal Waveguide as Highly Sensitive Platform for Cancer Detection," *IEEE Sensors Journal*, vol. 16(10), pp. 3705-3710, 2016.

[76] B. E. A. Saleh and M. C. Teich, *Fundamentals of Photonics* 2nd ed. Wiley, pp. 158-159, 2007.

[77] G. S. Rao, *Microwave and Radar Engineering*: 1st ed. Pearson Education India, pp. 125,2014.

[78] J. C. Maxwell, "A dynamical theory of the electromagnetic field," *Philosophical transactions of the Royal Society of London,* vol. 155, pp. 459-512, 1865.

[79] M. Maldovan and E. L. Thomas, *Periodic Materials and Interference Lithography: For Photonics, Phononics and Mechanics*: Wiley, pp. 65-70, 2009.

[80] J. D. Joannopoulos, S. G. Johnson, J. N. Winn, and R. D. Meade, *Photonic Crystals: Molding the Flow of Light (Second Edition)*: 2nd ed. Princeton University Press, pp.44-50, 2011.

[81] J. K. Shaw, *Mathematical Principles of Optical Fiber Communication*: Society for Industrial and Applied Mathematics, vol. 76, Virgina, pp. 19-23, 2004.

[82] J. T. Londergan, J. P. Carini, and D. P. Murdock, *Binding and Scattering in Two-Dimensional Systems: Applications to Quantum Wires, Waveguides and Photonic Crystals*: Springer Berlin Heidelberg, pp.181-193, 2003.

[83] I. A. Sukhoivanov and I. V. Guryev, *Photonic crystals: physics and practical modeling* vol. 152: Springer, New York, pp.1-10, 2009.

[84] B. Pal, "Frontiers in guided wave optics and optoelectronics," in *Frontiers in Guided Wave Optics and Optoelectronics*, 1st ed. InTech, Singapore, pp. 1-10, 2010.

[85] J. D. Joannopoulos, P. R. Villeneuve, and S. Fan, "Photonic crystals: putting a new twist on light," *Nature, USA,* vol. 386, pp. 143-149, 1997.

[86] K. Sakoda, *Optical Properties of Photonic Crystals*,2nd ed. Springer Berlin Heidelberg, pp.13-21, 2013.

[87] S. Noda and T. Baba, *Roadmap on Photonic Crystals*: 2nd ed. Springer US, pp.13-30, 2013.

[88] M. Skorobogatiy and J. Yang, *Fundamentals of photonic crystal guiding*: 2nd ed. Cambridge University Press, pp.93-103, 2009.

[89] J.-M. Lourtioz, H. Benisty, V. Berger, J.-M. Gerard, D. Maystre, and A. Tchelnokov, *Photonic crystals: towards nanoscale photonic devices*, 2nd ed. Springer Science & Business Media, pp. 63-75, 2008.

[90] S. D. Gedney, *Introduction to the Finite-difference Time-domain (FDTD) Method for Electromagnetics*: 1st ed. Morgan & Claypool Publishers, USA, pp.1-5, 2011.

[91] N. V. Kantartzis and T. D. Tsiboukis, *Higher Order FDTD Schemes for Waveguide and Antenna Structures*: 1ST ed. Morgan & Claypool Publishers, USA, pp.1-5, 2006.
[92] U. S. Inan and R. A. Marshall, *Numerical Electromagnetics: The FDTD Method*: 1st ed. Cambridge University Press, Cambridge, pp.1-5, 2011.
[93] I. A. Sukhoivanov and I. V. Guryev, *Photonic Crystals: Physics and Practical Modeling*: Springer Berlin Heidelberg, vol 15(8), 2009.
[94] U. E. Spichiger-Keller, *Chemical Sensors and Biosensors for Medical and Biological Applications*: Wiley, Singapore, pp.1-5, 2008.
[95] W. Gopel, T. A. Jones, M. Kleitz, I. Lundstrom, T. Seiyama, J. Hesse, *et al.*, *Sensors, Chemical and Biochemical Sensors*: VCH, Germany, vol. 2(1), pp. 1-2, 2008.
[96] G. Rajan, *Optical Fiber Sensors: Advanced Techniques and Applications*: 1st ed. CRC Press, New York, pp.137-139, 2015.
[97] A. Mekis, J. Chen, I. Kurland, S. Fan, P. R. Villeneuve, and J. Joannopoulos, "High transmission through sharp bends in photonic crystal waveguides," *Physical Review Letters,* vol. 77(18), pp. 3787, 1996.
[98] A. Mekis, S. Fan, and J. Joannopoulos, "Bound states in photonic crystal waveguides and waveguide bends," *Physical Review B,* vol. 58(8), pp. 4809, 1998.
[99] J. Broeng, D. Mogilevstev, S. E. Barkou, and A. Bjarklev, "Photonic crystal fibers: A new class of optical waveguides," *Optical fiber technology*, vol. 5(3), pp. 305-330, 1999.
[100] M. Loncar, T. Doll, J. Vuckovic, and A. Scherer, "Design and fabrication of silicon photonic crystal optical waveguides," *Journal of lightwave technology*, vol. 18(10), pp. 1402-1411, 2000.
[101] S. Fan, S. G. Johnson, J. Joannopoulos, C. Manolatou, and H. Haus, "Waveguide branches in photonic crystals," *JOSA B,* vol. 18(2), pp. 162-165, 2001.
[102] M. Koshiba, "Wavelength division multiplexing and demultiplexing with photonic crystal waveguide couplers," *journal of lightwave technology*, vol. 19(12), pp. 1970-1975, 2001.
[103] P. Lalanne, "Electromagnetic analysis of photonic crystal waveguides operating above the light cone," *IEEE Journal of Quantum Electronics*, vol. 38(7), pp. 800-804, 2002.
[104] S. Boscolo, M. Midrio, and C. G. Someda, "Coupling and decoupling of electromagnetic waves in parallel 2D photonic crystal waveguides," *IEEE Journal of Quantum Electronics,* vol. 38(1), pp. 47-53, 2002.
[105] S. Boscolo, C. Conti, M. Midrio, and C. G. Someda, "Numerical analysis of propagation and impedance matching in 2-D photonic crystal waveguides with finite length," *Journal of Lightwave Technology,* vol. 20(2), p. 304, 2002.
[106] M. Imada, S. Noda, A. Chutinan, M. Mochizuki, and T. Tanaka, "Channel drop filter using a single defect in a 2-D photonic crystal slab waveguide," *Journal of Lightwave Technology*, vol. 20(5), pp. 873-878, 2002.
[107] T. Sondergaard, J. Arentoft, and M. Kristensen, "Theoretical analysis of finite-height semiconductor-on-insulator-based planar photonic crystal waveguides," *Journal of lightwave technology,* vol. 20(8), pp. 1619-1626, 2002.

[108] M. Soljačić and J. D. Joannopoulos, "Enhancement of nonlinear effects using photonic crystals," *Nature materials,* vol. 3(4), pp. 211-219, 2004.
[109] M. Notomi, A. Shinya, S. Mitsugi, E. Kuramochi, and H. Ryu, "Waveguides, resonators and their coupled elements in photonic crystal slabs," *Optics express,* vol. 12(8), pp. 1551-1561, 2004.
[110] M. Patterson, S. Hughes, S. Combrié, N.-V.-Q. Tran, A. De Rossi, R. Gabet, *et al.*, "Disorder-induced coherent scattering in slow-light photonic crystal waveguides," *Physical review letters,* vol. 102(25), pp. 253903, 2009.
[111] N. C. Panoiu, J. F. McMillan, and C. W. Wong, "Theoretical analysis of pulse dynamics in silicon photonic crystal wire waveguides," *IEEE Journal of Selected Topics in Quantum Electronics,* vol. 16(1), pp. 257-266, 2010.
[112] F. Long, H. Tian, and Y. Ji, "A study of dynamic modulation and buffer capability in low dispersion photonic crystal waveguides," *Journal of lightwave technology,* vol. 28(8), pp. 1139-1143, 2010.
[113] S. Kocaman, M. Aras, P. Hsieh, J. McMillan, C. Biris, N. Panoiu, *et al.*, "Zero phase delay in negative-refractive-index photonic crystal superlattices," *Nature Photonics,* vol. 5(8), pp. 499-505, 2011.
[114] S. L. Portalupi, M. Galli, M. Belotti, L. C. Andreani, T. F. Krauss, and L. O'Faolain, "Deliberate versus intrinsic disorder in photonic crystal nanocavities investigated by resonant light scattering," *Physical Review B,* vol. 84(4), p. 045423, 2011.
[115] H. Lin, Z. Yi, and J. Hu, "Double resonance 1-D photonic crystal cavities for single-molecule mid-infrared photothermal spectroscopy: theory and design," *Optics letters,* vol. 37(8), pp. 1304-1306, 2012.
[116] W. S. Fegadolli, J. E. Oliveira, V. R. Almeida, and A. Scherer, "Compact and low power consumption tunable photonic crystal nanobeam cavity," *Optics express,* vol. 21(3), pp. 3861-3871, 2013.
[117] K. Ishizaki, M. Koumura, K. Suzuki, K. Gondaira, and S. Noda, "Realization of three-dimensional guiding of photons in photonic crystals," *Nature Photonics,* vol. 7(2), pp. 133-137, 2013.
[118] M. Radulaski, T. M. Babinec, S. Buckley, A. Rundquist, J. Provine, K. Alassaad, *et al.*, "Photonic crystal cavities in cubic (3C) polytype silicon carbide films," *Optics express,* vol. 21(26), pp. 32623-32629, 2013.
[119] M. Minkov and V. Savona, "Automated optimization of photonic crystal slab cavities," *Scientific reports,* vol. 4, p. 5124, 2014.
[120] X. Zhang, H. Subbaraman, A. Hosseini, and R. T. Chen, "Highly efficient mode converter for coupling light into wide slot photonic crystal waveguide," *Optics express,* vol. 22(17), pp. 20678-20690, 2014.
[121] R. S. Savelev, D. S. Filonov, P. V. Kapitanova, A. E. Krasnok, A. E. Miroshnichenko, P. A. Belov, *et al.*, "Bending of electromagnetic waves in all-dielectric particle array waveguides," *Applied Physics Letters,* vol. 105(18), pp. 181116, 2014.
[122] B. K. Ofori-Okai, P. Sivarajah, C. A. Werley, S. M. Teo, and K. A. Nelson, "Direct experimental visualization of waves and band structure in 2D photonic crystal slabs," *New Journal of Physics,* vol. 16(5), pp. 053003, 2014.

[123] A. González-Tudela, C.-L. Hung, D. E. Chang, J. I. Cirac, and H. Kimble, "Subwavelength vacuum lattices and atom–atom interactions in two-dimensional photonic crystals," *Nature Photonics*, vol. 9(5), pp. 320-325, 2015.
[124] J. E. Baker, R. Sriram, and B. L. Miller, "Two-dimensional photonic crystals for sensitive microscale chemical and biochemical sensing," *Lab on a Chip*, vol. 15(4) pp. 971-990, 2015.
[125] A. Tavousi and M. A. Mansouri-Birjandi, "Performance evaluation of photonic crystal ring resonators based optical channel add-drop filters with the aid of whispering gallery modes and their Q-factor," *Optical and Quantum Electronics*, vol. 47(7), pp. 1613-1625, 2015.
[126] S. Shen, K. Wu, L. Sun, and C. Jiang, "Theoretical study of graphene-silicon nitride-silicon hybrid photonic crystal waveguides for four-wave mixing enhancement," *Applied Optics*, vol. 54(12), pp. 3640-3644, 2015.
[127] L. Gan and Z. Li, "Photonic crystal cavities and integrated optical devices," *Science China Physics, Mechanics & Astronomy*, vol. 58(11), pp. 114203, 2015.
[128] Z. Hayran, M. Turduev, M. Botey, R. Herrero, K. Staliunas, and H. Kurt, "Numerical and experimental demonstration of a wavelength demultiplexer design by point-defect cavity coupled to a tapered photonic crystal waveguide," *Optics letters*, vol. 41(1) pp. 119-122, 2016.
[129] B. Liu, Y.-F. Liu, S.-J. Li, and X.-D. He, "High efficiency all-optical diode based on photonic crystal waveguide," *Optics Communications*, vol. 368, pp. 7-11, 2016.
[130] K. I. Zaytsev, G. M. Katyba, V. N. Kurlov, I. A. Shikunova, V. E. Karasik, and S. O. Yurchenko, "Terahertz photonic crystal waveguides based on sapphire shaped crystals," *IEEE Transactions on Terahertz Science and Technology*, vol. 6(4), pp. 576-582, 2016.
[131] S. Lavdas and N. C. Panoiu, "Theory of pulsed four-wave mixing in one-dimensional silicon photonic crystal slab waveguides," *Physical Review B*, vol. 93(11), pp. 115435, 2016.
[132] Y. Liu and A. A. Houck, "Quantum electrodynamics near a photonic bandgap," *Nature Physics*, vol. 13(1), pp. 48-52, 2017.
[133] F. Xue, S.-B. Liu, H.-F. Zhang, X.-K. Kong, Y.-D. Wen, L.-L. Wang, *et al.*, "The theoretical analysis of omnidirectional photonic band gaps in the one-dimensional ternary plasma photonic crystals based on Pell quasi-periodic structure," *Optical and Quantum Electronics*, vol. 49(1), pp. 19, 2017.
[134] A. Massaro, M. Grande, R. Cingolani, A. Passaseo, and M. De Vittorio, "Design and modeling of tapered waveguide for photonic crystal slab coupling by using time-domain Hertzian potentials formulation," *Optics express*, vol. 15(25), pp. 16484-16499, 2007.
[135] C. Lee, R. Radhakrishnan, C.-C. Chen, J. Li, J. Thillaigovindan, and N. Balasubramanian, "Design and modeling of a nanomechanical sensor using silicon photonic crystals," *Journal of lightwave technology*, vol. 26(7), pp. 839-846, 2008.
[136] S. Haxha, I. Dayoub, F. AbdelMalek, W. Aroua, J. Trombi, and H. Bouchriha, "Light Coupling Between Photonic Crystal and Standard Photonic Waveguides in

a Compact Photonic Integrated Circuitry Using 2D FDTD," *Open Optics Journal*, vol. 3, pp. 44-51, 2009.
[137] H. Ling-Juan, X. Xu-Ming, L. Nian-Hua, Y. Tian-Bao, F. Li-Guang, and L. Qing-Hua, "Proposal of an ultracompact triplexer using photonic crystal waveguide with an air holes array," *Chinese Physics Letters*, vol. 27(8), pp. 084201, 2010.
[138] K. Üstün and H. Kurt, "Compact coupling of light from conventional photonic wire to slow light waveguides," *Journal of Applied Physics*, vol. 110(11), pp. 113109, 2011.
[139] L. Gan and Z. Li, "Designs and experiments on infrared two-dimensional silicon photonic crystal slab devices," *Frontiers of Optoelectronics*, vol. 5(1), pp. 21-40, 2012.
[140] W. Shimizu, N. Nagai, K. Kohno, K. Hirakawa, and M. Nomura, "Waveguide coupled air-slot photonic crystal nanocavity for optomechanics," *Optics express*, vol. 21(19), pp. 21961-21969, 2013.
[141] P.-T. Lin, T.-W. Lu, and P.-T. Lee, "Photonic crystal waveguide cavity with waist design for efficient trapping and detection of nanoparticles," *Optics express*, vol. 22(6), pp. 6791-6800, 2014.
[142] H. Liu, L. Leng, H. Ma, and L. Li, "Stress sensing characteristics of two-dimensional photonic crystal cross-waveguide geometry," *Optical and Quantum Electronics*, vol. 47(12), pp. 3825-3835, 2015.
[143] L. Athanasekos, A. Christofi, G. Gantzounis, E. Bolomyti, G. Papageorgiou, M.-C. Skoulikidou, *et al.*, "Design and fabrication of suspended Si 3 N 4 nanobeam cavities," *Microelectronic Engineering*, vol. 159, pp. 42-45, 2016.
[144] S. Feng, T.-H. Xiao, L. Gan, and Y.-Q. Wang, "Tuning beam power-splitting characteristics through modulating a photonic crystal slab's output surface," *Journal of Physics D: Applied Physics*, vol. 50(2), pp. 025107, 2016.
[145] E. Chow, A. Grot, L. Mirkarimi, M. Sigalas, and G. Girolami, "Ultracompact biochemical sensor built with two-dimensional photonic crystal microcavity," *Optics letters*, vol. 29(10), pp. 1093-1095, 2004.
[146] J. B. Jensen, L. H. Pedersen, P. E. Hoiby, L. B. Nielsen, T. P. Hansen, J. R. Folkenberg, *et al.*, "Photonic crystal fiber based evanescent-wave sensor for detection of biomolecules in aqueous solutions," *Optics letters*, vol. 29(17), pp. 1974-1976, 2004.
[147] A. C. Sharma, T. Jana, R. Kesavamoorthy, L. Shi, M. A. Virji, D. N. Finegold, *et al.*, "A general photonic crystal sensing motif: creatinine in bodily fluids," *Journal of the American Chemical Society*, vol. 126(9), pp. 2971-2977, 2004.
[148] S. O. Konorov, A. M. Zheltikov, and M. Scalora, "Photonic-crystal fiber as a multifunctional optical sensor and sample collector," *Optics Express*, vol. 13(9), pp. 3454-3459, 2005.
[149] J. P. Walker and S. A. Asher, "Acetylcholinesterase-based organophosphate nerve agent sensing photonic crystal," *Analytical chemistry*, vol. 77(6), pp. 1596-1600, 2005.
[150] H. Kurt and D. Citrin, "Photonic crystals for biochemical sensing in the terahertz region," *Applied Physics Letters*, vol. 87(4), p. 041108, 2005.

[151] L. Rindorf, J. B. Jensen, M. Dufva, L. H. Pedersen, P. E. Høiby, and O. Bang, "Photonic crystal fiber long-period gratings for biochemical sensing," *Optics Express,* vol. 14(18), pp. 8224-8231, 2006.
[152] I. D. Block, L. L. Chan, and B. T. Cunningham, "Photonic crystal optical biosensor incorporating structured low-index porous dielectric," *Sensors and Actuators B: Chemical,* vol. 120(1), pp. 187-193, 2006.
[153] M. P. Schwartz, A. M. Derfus, S. D. Alvarez, S. N. Bhatia, and M. J. Sailor, "The smart petri dish: a nanostructured photonic crystal for real-time monitoring of living cells," *Langmuir,* vol. 22, pp. 7084-7090, 2006.
[154] Y. Nishijima, K. Ueno, S. Juodkazis, V. Mizeikis, H. Misawa, T. Tanimura, *et al.*, "Inverse silica opal photonic crystals for optical sensing applications," *Optics express,* vol. 15(20), pp. 12979-12988, 2007.
[155] J. Sun, C.-C. Chan, X.-Y. Dong, and P. Shum, "High-resolution photonic bandgap fiber-based biochemical sensor," *Journal of biomedical optics,* vol. 12(4), pp. 044022, 2007.
[156] P. C. Mathias, N. Ganesh, L. L. Chan, and B. T. Cunningham, "Combined enhanced fluorescence and label-free biomolecular detection with a photonic crystal surface," *Applied Optics,* vol. 46(12), pp. 2351-2360, 2007.
[157] J. Wu, D. Day, and M. Gu, "A microfluidic refractive index sensor based on an integrated three-dimensional photonic crystal," *Applied Physics Letters,* vol. 92(12), pp. 071108, 2008.
[158] S. Buswell, V. Wright, J. Buriak, V. Van, and S. Evoy, "Specific detection of proteins using photonic crystal waveguides," *Optics express,* vol. 16(20), pp. 15949-15957, 2008.
[159] L. Rindorf and O. Bang, "Sensitivity of photonic crystal fiber grating sensors: biosensing, refractive index, strain, and temperature sensing," *JOSA B,* vol. 25(3), pp. 310-324, 2008.
[160] F.-L. Hsiao and C. Lee, "Novel biosensor based on photonic crystal nano-ring resonator," *Procedia Chemistry,* vol. 1(1), pp. 417-420, 2009.
[161] S. Zlatanovic, L. W. Mirkarimi, M. M. Sigalas, M. A. Bynum, E. Chow, K. M. Robotti, *et al.*, "Photonic crystal microcavity sensor for ultracompact monitoring of reaction kinetics and protein concentration," *Sensors and Actuators B: Chemical,* vol. 141(1), pp. 13-19, 2009.
[162] J. Dahdah, N. Courjal, and F. I. Baida, "Analysis of a photonic crystal cavity based on absorbent layer for sensing applications," *JOSA B,* vol. 27(2), pp. 305-310, 2010.
[163] F.-l. Hsiao and C. Lee, "Computational study of photonic crystals nano-ring resonator for biochemical sensing," *IEEE Sensors Journal,* vol. 10(7), pp. 1185-1191, 2010.
[164] Y. Guo, J. Y. Ye, C. Divin, B. Huang, T. P. Thomas, J. Baker, James R, *et al.*, "Real-time biomolecular binding detection using a sensitive photonic crystal biosensor," *Analytical chemistry,* vol. 82(12), pp. 5211-5218, 2010.
[165] M. Scullion, A. Di Falco, and T. Krauss, "Slotted photonic crystal cavities with integrated microfluidics for biosensing applications," *Biosensors and Bioelectronics,* vol. 27(1), pp. 101-105, 2011.

[166] B. Sun, M.-Y. Chen, Y.-K. Zhang, J.-c. Yang, J.-q. Yao, and H.-X. Cui, "Microstructured-core photonic-crystal fiber for ultra-sensitive refractive index sensing," *Optics express*, vol. 19(5), pp. 4091-4100, 2011.
[167] L. Junhua, K. Qiang, W. Chunxia, S. Baoqing, X. Yiyang, and C. Hongda, "Design of a photonic crystal microcavity for biosensing," *Journal of Semiconductors*, vol. 32(3), pp. 034008, 2011.
[168] Y. Liu and H. Salemink, "Photonic crystal-based all-optical on-chip sensor," *Optics express*, vol. 20(18), pp. 19912-19920, 2012.
[169] F. Bougriou, T. Boumaza, M. Bouchemat, and N. Paraire, "Sensitivity analysis of a photonic crystal waveguide for refraction index sensing," *Physica Scripta*, vol. 2012(T151), pp. 014064, 2012.
[170] J. L. Lim, D. J. J. Hu, P. P. Shum, and Y. Wang, "Cascaded photonic crystal fiber interferometers for refractive index sensing," *IEEE Photonics Journal*, vol. 4(4), pp. 1163-1169, 2012.
[171] Q. Quan, D. L. Floyd, I. B. Burgess, P. B. Deotare, I. W. Frank, S. K. Tang, *et al.*, "Single particle detection in CMOS compatible photonic crystal nanobeam cavities," *Optics express*, vol. 21(26), pp. 32225-32233, 2013.
[172] F. Liang, N. Clarke, P. Patel, M. Loncar, and Q. Quan, "Scalable photonic crystal chips for high sensitivity protein detection," *Optics express*, vol. 21(26), pp. 32306-32312, 2013.
[173] P. Xu, K. Yao, J. Zheng, X. Guan, and Y. Shi, "Slotted photonic crystal nanobeam cavity with parabolic modulated width stack for refractive index sensing," *Optics express*, vol. 21(22), pp. 26908-26913, 2013.
[174] Y. Zou, S. Chakravarty, D. N. Kwong, W.-C. Lai, X. Xu, X. Lin, *et al.*, "Cavity-waveguide coupling engineered high sensitivity silicon photonic crystal microcavity biosensors with high yield," *IEEE Journal of Selected Topics in Quantum Electronics*, vol. 20(4), pp. 1-10, 2014.
[175] Y. Zhao, Z.-q. Deng, and J. Li, "Photonic crystal fiber based surface plasmon resonance chemical sensors," *Sensors and Actuators B: Chemical*, vol. 202, pp. 557-567, 2014.
[176] H. Guo and J. Guo, "Hybrid plasmon photonic crystal resonance grating for integrated spectrometer biosensor," *Optics letters*, vol. 40(2), pp. 249-252, 2015.
[177] E. Eftekhari, X. Li, T. H. Kim, Z. Gan, I. S. Cole, D. Zhao, *et al.*, "Anomalous Fluorescence Enhancement from Double Heterostructure 3D Colloidal Photonic Crystals–A Multifunctional Fluorescence-Based Sensor Platform," *Scientific reports*, vol. 5, 2015.
[178] A. Rifat, G. A. Mahdiraji, Y. Sua, Y. Shee, R. Ahmed, D. M. Chow, *et al.*, "Surface plasmon resonance photonic crystal fiber biosensor: a practical sensing approach," *IEEE Photon. Technol. Lett.*, vol. 27(15), pp. 1628-1631, 2015.
[179] D. Yang, C. Wang, W. Yuan, B. Wang, Y. Yang, and Y. Ji, "Silicon on-chip side-coupled high-Q micro-cavities for the multiplexing of high sensitivity photonic crystal integrated sensors array," *Optics Communications*, vol. 374, pp. 1-7, 2016.
[180] D. Men, D. Liu, and Y. Li, "Visualized optical sensors based on two/three-dimensional photonic crystals for biochemicals," *Science Bulletin*, vol. 61(17), pp. 1358-1371, 2016.

[181] M. F. O. Hameed, Y. K. Alrayk, and S. Obayya, "Self-calibration highly sensitive photonic crystal fiber biosensor," *IEEE Photonics Journal,* vol. 8(3), pp. 1-12, 2016.
[182] W. Peng, Y. Chen, and W. Ai, "Higher-order mode photonic crystal based nanofluidic sensor," *Optics Communications,* vol. 382, pp. 105-112, 2017.
[183] M. R. Lee and P. M. Fauchet, "Nanoscale microcavity sensor for single particle detection," *Optics letters,* vol. 32(22), pp. 3284-3286, 2007.
[184] D. Dorfner, T. Hürlimann, T. Zabel, L. H. Frandsen, G. Abstreiter, and J. Finley, "Silicon photonic crystal nanostructures for refractive index sensing," *Applied Physics Letters,* vol. 93(18), pp. 181103, 2008.
[185] A. Di Falco, L. O'Faolain, and T. Krauss, "Chemical sensing in slotted photonic crystal heterostructure cavities," *Applied physics letters,* vol. 94(6), pp. 063503, 2009.
[186] J. Jágerská, H. Zhang, Z. Diao, N. Le Thomas, and R. Houdré, "Refractive index sensing with an air-slot photonic crystal nanocavity," *Optics letters,* vol. 35(15), pp. 2523-2525, 2010.
[187] W.-C. Lai, S. Chakravarty, X. Wang, C. Lin, and R. T. Chen, "Photonic crystal slot waveguide absorption spectrometer for on-chip near-infrared spectroscopy of xylene in water," *Applied Physics Letters,* vol. 98(2), p. 7, 2011.
[188] W. C. Wong, C. C. Chan, L. H. Chen, T. Li, K. X. Lee, and K. C. Leong, "Polyvinyl alcohol coated photonic crystal optical fiber sensor for humidity measurement," *Sensors and Actuators B: Chemical,* vol. 174, pp. 563-569, 2012.
[189] C. Nicolaou, W. T. Lau, R. Gad, H. Akhavan, R. Schilling, and O. Levi, "Enhanced detection limit by dark mode perturbation in 2D photonic crystal slab refractive index sensors," *Optics express,* vol. 21(25), pp. 31698-31712, 2013.
[190] D. Yang, S. Kita, F. Liang, C. Wang, H. Tian, Y. Ji, *et al.*, "High sensitivity and high Q-factor nanoslotted parallel quadrabeam photonic crystal cavity for real-time and label-free sensing," *Applied Physics Letters,* vol. 105(6), pp. 063118, 2014.
[191] Y. Tan, T. Tang, H. Xu, C. Zhu, and B. T. Cunningham, "High sensitivity automated multiplexed immunoassays using photonic crystal enhanced fluorescence microfluidic system," *Biosensors and Bioelectronics,* vol. 73, pp. 32-40, 2015.
[192] X. Zhang, G. Zhou, P. Shi, H. Du, T. Lin, J. Teng, *et al.*, "On-chip integrated optofluidic complex refractive index sensing using silicon photonic crystal nanobeam cavities," *Optics letters,* vol. 41(6), pp. 1197-1200, 2016.
[193] S. Arafa, M. Bouchemat, T. Bouchemat, A. Benmerkhi, and A. Hocini, "Infiltrated photonic crystal cavity as a highly sensitive platform for glucose concentration detection," *Optics Communications,* vol. 384, pp. 93-100, 2017.
[194] L. Novotny and B. Hecht, *Principles of Nano-Optics,* 2nd ed. Cambridge University Press, Cambridge, pp. 338-339, 2012.
[195] R. V. Nair, "Observation of wavelength-dependent Brewster angle shift in 3D photonic crystals," *arXiv preprint arXiv:1611.09693,* 2016.
[196] X. Fu, B. Zhang, X. Kang, J. Xu, C. Xiong, and G. Zhang, "Lattice constant effects of photonic crystals on the extraction of guided mode of GaN based light

emitting diodes," *Science China Technological Sciences*, vol. 54(1), pp. 1-5, 2011.
[197] M. Boroditsky, "Modification of spontaneous emission in photonic crystals," UNIVERSITY OF CALIFORNIA Los Angeles, 1999.
[198] B. Rezaei, I. Giden, and H. Kurt, "Tuning light focusing with liquid crystal infiltrated graded index photonic crystals," *Optics Communications*, vol. 382, pp. 28-35, 2017.
[199] R. Srivastava, R. K. Singh, and Y. N. Singh, "Large capacity optical router based on arrayed waveguide gratings and optical loop buffer," *Optical and quantum electronics*, vol. 41(6), pp. 463-480, 2009.
[200] S. Olyaee, S. Najafgholinezhad, and H. A. Banaei, "Four-channel label-free photonic crystal biosensor using nanocavity resonators," *Photonic Sensors*, vol. 3(3), pp. 231-236, 2013.
[201] S. G. Johnson, P. R. Villeneuve, S. Fan, and J. D. Joannopoulos, "Linear waveguides in photonic-crystal slabs," *Physical Review B*, vol. 62(12), p. 8212, 2000.
[202] A. Chutinan and S. Noda, "Waveguides and waveguide bends in two-dimensional photonic crystal slabs," *Physical review B*, vol. 62(7), p. 4488, 2000.
[203] K. Bayat, S. K. Chaudhuri, and S. Safavi-Naeini, "Polarization and thickness dependent guiding in the photonic crystal slab waveguide," *Optics express*, vol. 15(13), pp. 8391-8400, 2007.
[204] W. Amorntep and P. Wanchai, "Guided mode for enhanced spontaneous emission using finite thickness photonic crystal waveguides," *Physics Procedia*, vol. 22, pp. 186-190, 2011.
[205] J. Hou, D. S. Citrin, H. Wu, D. Gao, Z. Zhou, and S. Chen, "Slab-thickness dependence of photonic bandgap in photonic-crystal slabs," *IEEE Journal of Selected Topics in Quantum Electronics*, vol. 18(6), pp. 1636-1642, 2012.
[206] V. Sharma, A. Singh, and A. K. Sharma, "Analysis of the Impact of P-Ratio on BER, Q-Factor and OSNR of Radio over Fiber (RoF) System," *Optics and Photonics Journal*, vol. 1(4), pp. 179, 2011.
[207] R. Soref, "Mid-infrared photonics in silicon and germanium," *Nature photonics*, vol. 4(8), pp. 495-497, 2010.
[208] R. A. Soref, S. J. Emelett, and W. R. Buchwald, "Silicon waveguided components for the long-wave infrared region," *Journal of Optics A: Pure and Applied Optics*, vol. 8(10), pp. 840, 2006.
[209] S. Combrié, A. De Rossi, Q. V. Tran, and H. Benisty, "GaAs photonic crystal cavity with ultrahigh Q: microwatt nonlinearity at 1.55 μm," *Optics letters*, vol. 33(16), pp. 1908-1910, 2008.
[210] Y. Li, H. W. Fu, X. L. Li, and M. Shao, "Contribution of strain and elasto-optical effect to resonant mode in the two-dimensional photonic crystals force sensor," in *Advanced Materials Research*, pp. 148-152, 2011.
[211] K. Crozier, V. Lousse, O. Kilic, S. Kim, S. Fan, and O. Solgaard, "Air-bridged photonic crystal slabs at visible and near-infrared wavelengths," *Physical Review B*, vol. 73(11), pp. 115126, 2006.
[212] J. Lee, B. Zhen, S.-L. Chua, W. Qiu, J. D. Joannopoulos, M. Soljačić, *et al.*, "Observation and differentiation of unique high-Q optical resonances near zero

wave vector in macroscopic photonic crystal slabs," *Physical review letters*, vol. 109(6), pp. 067401, 2012.
[213] J. Franz and V. K. Jain, *Optical Communications: Components and Systems: Analysis--design--optimization--application*: CRC press, 2000.
[214] B. J. Eggleton, "Chalcogenide photonics: fabrication, devices and applications Introduction," *Optics express*, vol. 18(25), pp. 26632-26634, 2010.
[215] B. Painam, R. S. Kaler, and M. Kumar, "Label Free Chemical and Biochemical Sensing using Photonic Crystal Waveguide at Sodium-D Line," *Journal of Nanoelectronics and Optoelectronics*, vol. 12(2), pp. 184-188, 2017.
[216] T. Li, D. Gao, D. Zhang, and E. Cassan, "High-and High-Sensitivity One-Dimensional Photonic Crystal Slot Nanobeam Cavity Sensors," *IEEE Photonics Technology Letters*, vol. 28, pp. 689-692, 2016.
[217] I. M. White and X. Fan, "On the performance quantification of resonant refractive index sensors," *Optics Express*, vol. 16, pp. 1020-1028, 2008.
[218] J. W. Zeller and F. Jain, "Photonic crystal coupled-cavity waveguides with asymmetric-defect structure for narrow spectral widths at 1.55 microns," in *Integrated Optoelectronic Devices 2005*, 2005, pp. 414-421.
[219] G. Hura, A. Khan, D. Grover, H. Singh, and N. Nanda, "Optimization of assembly code generation using Petri nets," *International Journal of Electronics Theoretical and Experimental*, vol. 49, pp. 427-431, 1980.
[220] A. Solanki, K. Prasad, K. Nunan, and R. Oreilly, "Comparing process flow of monolithic CMOS-MEMS intergration on SOI wafers with monolithic BiMOS-MEMS integration on Silicon wafer," in *Circuits and Systems (MWSCAS), 2010 53rd IEEE International Midwest Symposium on*, 2010, pp. 1189-1192.

Plasmonics
DOI 10.1007/s11468-017-0529-x

On-Chip Oval-Shaped Nanocavity Photonic Crystal Waveguide Biosensor for Detection of Foodborne Pathogens

Balveer Painam[1] · **R. S. Kaler**[1] · **Mukesh Kumar**[2]

Received: 15 October 2016 / Accepted: 3 February 2017

Abstract A photonic crystal waveguide (PCW) biosensor is proposed for the detection of foodborne pathogens. Various semiconductor materials and insulator with higher to lower refractive indices (Si, GaAs, Si_3N_4, and SiO_2) are analyzed to fix the choice of material in PCW design. The design and analysis are performed using finite difference time domain (FDTD) simulation method. The design exhibits two inverted J-shaped defects with center cavity designed in the shape of *Escherichia coli*. In this research, DH5α strain of *E. coli* foodborne pathogens is considered as a model due to its shape. Simulation of PCW design is performed using infrared radiation (1 and 1.55 μm) wavelengths. Simulation analysis reports larger resonance wavelength shifts, higher sensitivities, and quality factors for Si-based PCW biosensor at an operating wavelength of 1.55 μm.

Keywords Optical sensors · Biophotonics · Waveguides · Photonic crystal waveguide · Biosensors

Introduction

According to the 2015 reports by the Foodborne Diseases Active Surveillance Network (Food Net) of US Center for Disease Control and Prevention (CDC), foodborne diseases caused 20,107 confirmed cases, 4531 hospitalizations, and 77 deaths [1]. Maximum number of deaths are caused by *Salmonella*, *Listeria*, *Escherichia coli* O157:H7, and *Toxoplasma* [2], among them, pathogenic *E. coli* is one of the most dangerous agents of foodborne disease, Tripathi et al. reported *E. coli* detection mechanism, as low as 10^3 cfu/ml with an experimental accuracy greater than 99% [3]. Several detection techniques have been employed for the detection of gram-positive foodborne pathogens, including biochemical systems [4]. To improve the assay specificity and minimize the time for diagnosis, enzyme-linked immunosorbent assays (ELISAs) are developed [5], Western blot analysis (WBA) is used in research to separate and identify the proteins [6, 7], and polymerase chain reaction (PCR) technique is used to detect and characterize genes [8].

The above mentioned conventional detection methods often require extraction, isolation, enrichment, counting, etc., prior to measurement, testing, and resulting and take longer time to arrive at a quantitative conclusion [9]. Optical biosensors have come up with solutions for all the existing problems with conventional test methods. Surface plasmon resonance and surface-enhanced Raman scattering are two recent methods in optical biosensors [10]. Both technologies offer the advantages of label-free biosensing and high sensitivity, but they are limited by a combination of factors that include sensor cost, instrumentation complexity, and low assay multiplexing throughput [11]. Derived from the same optical biosensor family, photonic crystal waveguide (PCW) biosensor technology is rapid, pathogen-specific, and does not require chemical modification of the test sample. PCW slabs with a submicron scale periodic modulation of the refractive index form a versatile platform to control the

✉ Balveer Painam
balveer.pv@gmail.com

[1] Optical Fiber Communication Research Laboratory (OFCR Lab), ECE Department, Thapar University, Patiala 147004, India

[2] Optoelectronic Nanodevice Research Laboratory, Department of Electrical Engineering, Indian Institute of Technology (IIT), Indore 453446, India

Published online: 20 February 2017

Plasmonics
DOI 10.1007/s11468-016-0341-z

Photonic Crystal Waveguide Biochemical Sensor for the Approximation of Chemical Components Concentrations

Balveer Painam[1] · **R. S. Kaler**[1] · **Mukesh Kumar**[2]

Received: 18 April 2016 / Accepted: 15 July 2016

Abstract The rapid progress in chemical and biochemical applications with optical interfaces has motivated an ever-increasing demand for highly sensitive, accurate, and disposable photonic components. We propose a design of biochemical sensor to identify the chemical components acid concentrations with a greater accuracy using photonic crystal waveguide (PCW). It consists of circular air holes of radius 0.44 *a* (*a* being the lattice constant), arranged in a hexagonal structure on silicon on insulator (SOI). Due to change in refractive index of the sample, resonance wavelength shifts towards higher wavelengths (red shift) with a higher coefficient of determination. The proposed design allows desired input wavelength of 1550 nm to be guided in the waveguide for an effective identification of chemical component concentration. Resolution and limit of detection are calculated as 1.2 nm and 4×10^{-2} RIU for sulfuric acid (H_2SO_4) solution and 0.2 nm and 2×10^{-2} RIU for hydrogen peroxide (H_2O_2) solution. Improved sensitivities with increased standard deviations are achieved after structural optimization.

Keywords Photonic bandgap materials · Photonic crystals · Waveguide · Optical sensing and sensors · Optical properties

✉ Balveer Painam
balveer.pv@gmail.com

[1] Optical Fiber Communication Research Laboratory (OFCR Lab), ECE Department, Thapar Institute of Engineering and Technology University, Patiala 147004, Punjab, India

[2] Integrated Photonics Laboratory, Department of Electrical Engineering, Indian Institute of Technology, Indore 453446, Madhya Pradesh, India

Introduction

Aqueous sulfuric acid (H_2SO_4) is the world's most commonly adopted industrial chemical. Its applications are diversified in many areas of science and technology and in laboratories such as in resin manufacturing, ore and mineral dissolution and processing, fertilizer production, catalytic processes, and storage batteries [1]. H_2SO_4 offers a wide range of acidity values for different types of requirements in industries [2, 3]. Due to its high density, oily, and corrosive nature, it needs to be diluted to certain concentration to acquire the desired results. Similarly, hydrogen peroxide (H_2O_2) also has an exceptional significance as a chemical compound. It is used in large areas of research, industrial, and manufacturing applications all-around the world. Due to its oxidizing capabilities, it is used as bleaching agent in textiles, paper, and mineral industries. Waste water treatment, removal of organic, and inorganic contaminants are the most common applications [4].

A standard technique for chemical sensing is absorbance spectroscopy [5]. Recent technologies utilize surface plasmon resonance and micro-mechanical systems to reduce complexity, but high sensitivity (S) and reduction in cost are also a major requirement of a measuring system which can be fulfilled by photonic crystal waveguide (PCW) structure. The photonic crystal concept was introduced about 25 years ago. Photonic structures deliver a new approach for guiding light and to make integrated photonic devices [6]. The PCW operation is based on the photonic band gap (PBG) concept. Permittivity variation as a function of position leads to PBG. The variation of periodicity can be in 1D, 2D, or 3D structures which can be operated by regulating the period of permittivity. Apart from these parameters, PCW operation also depends on the defect availability. The PCW with a defect (line or point) controls the electric field distribution within the waveguide

Published online: 27 July 2016

Journal of
Nanoelectronics and Optoelectronics
Vol. 11, pp. 1–5, 2016
www.aspbs.com/jno

ARTICLE

Label Free Chemical and Biochemical Sensing Using Photonic Crystal Waveguide at Sodium-D Line

Balveer Painam[1,*], R. S. Kaler[1], and Mukesh Kumar[2]

Photonic crystal waveguide (PCW) sensors represents an efficient and accurate solution for chemical and biochemical sensing. Here, we propose a design of photonic crystal waveguide sensor for chemical sensing applications. The proposed PCW sensor is patterned on 10×10 μm silicon on insulator (SOI) wafer. PCW designed with circular air holes of radius $r = 0.35a$ where a is the lattice constant of 0.45 μm, arranged in hexagonal structure. The principle of measurement is based on variation in refractive index of sample that causes change in effective refractive index (ERI) in guided mode leading to blue shift. Experimental results of refractive index are used in sensing analysis. Proposed design is capable of allowing sodium doublet line (Sodium D line) wavelength through structure to work as chemical and biochemical sensor. Better results are achieved after optimization of center cavity.

Keywords: Photonic Crystal Waveguide, Bio-Chemical Sensor, Wavelength Shift, Sodium D Line.

1. INTRODUCTION

The main challenges in sensing system these days are related to fast response, simultaneous detection of several compounds in clinical, food and environmental samples.[1] For these purposes, the advancements in chemical and biochemical fields has influenced the design of diagnostic sensors.[2] Ultrafast response of biochemical sensors is utilized in ultrasmall analyte requirements, higher sensitivity and selectivity plays a prominent role in various fields.[3] The sensing mechanism is categorized in to two types one is effective refractive index (RI) sensing and second one is surface sensing.[4] The optical sensors responses depend upon the changes in effective refractive index of the guided modes.[5] The refractive indices are usually reported at sodium doublet (sodium D lines) due to its enhanced optical properties.

Optical instruments are playing important role in field of communication[6–9] and are also focused in the field of optical sensing.[10–12] Optical sensing mechanisms receive considerable attention in the applications of chemical and biochemical sensors.

Numerous chemical and biochemical optical sensors employ different sensing mechanisms.[13] Even though there are many optical sensors available in the market such as fiber optic biochemical sensor,[14] internal reflection spectroscopy,[15] attenuated total reflection,[16] reflectometric interference,[17] total internal reflection[18] and surface plasmon resonance,[19] they are facing selectivity, sensitivity and time consuming issues. Out of all these sensors photonic crystal waveguide (PCW) biosensors is the best alternative to overcome all the above mentioned problems.

Miniature size and photonic bandgap properties make photonic crystal waveguides more suitable for label free sensing and gas sensing.[20] The properties of PCW can be engineered through the process of doping which is achieved by either adding or removing dielectric material in a certain area.[21] The dielectric materials then act as a defect region that can be used to localize an electromagnetic wave.[22] If the difference between the dielectric constants of the materials composing the photonic crystal is high enough, a photonic bandgap occurs.[23] A 2D PCW with dense arrays of functionalized spots for multiplexed sensing technique is used to achieve the highest sensitivity and quality factor.[24] Various designs in PCW are reported for biosensing application.[25,26] PCW has strong

[1]Optical Fiber Communication Research Laboratory (OFCRLab), ECE Department, Thapar University, Patiala 147004, Punjab, India
[2]Integrated Photonics Laboratory, Department of Electrical Engineering, Indian Institute of Technology, Indore 453446, Madhya Pradesh, India
*Author to whom correspondence should be addressed.
Email: balveer.pv@gmail.com
Received: 2 May 2016
Accepted: 17 June 2016

Optical Engineering 55(7), 077105 (July 2016)

Active layer identification of photonic crystal waveguide biosensor chip for the detection of *Escherichia coli*

Balveer Painam,[a,*] Rajinder S. Kaler,[a] and Mukesh Kumar[b]
[a]Thapar University, ECE Department, Optical Fiber Communication Research Laboratory (OFCR Lab), Patiala, Punjab 147004, India
[b]Indian Institute of Technology, Department of Electrical Engineering, Integrated Photonics Laboratory, Indore, Madhya Pradesh 453446, India

Abstract. This work represents experimental and simulation analysis of photonic crystal waveguide (PCW)-based biosensor structures, which is used for detection of the *Escherichia coli* (*E. coli*) cell. A method is adopted for *E. coli* culture to measure length, diameter, and refractive index to finalize the structural design and to verify the suitability of PCW as a biosensor. This method is tested using DH5α strains of *E. coli*. The typical precisions of measurements are varied in ranges from 1.132 to 1.825 μm and from 0.447 to 0.66 μm for pathogen's length and diameter, respectively. The measured distribution of samples over length and diameter are in correlation with the measurements performed by scanning electron microscope. After obtaining average length and diameter of cylindrical shaped *E. coli* cell, we consider these values for simulation analysis of designed PCW biosensor. *E. coli* cell is trapped in the middle of the PCW biosensor having three different types of waveguides, i.e., gallium arsenide/silicon dioxide ($GaAs/SiO_2$), silicon/silicon dioxide (Si/SiO_2), or silicon nitride/silicon dioxide (Si_3N_4/SiO_2) to observe the maximum resonance shift and sensitivity. It is observed from the simulation data analysis that $GaAs/SiO_2$ is the preferred PCW biosensor for the identification of *E. coli*. [DOI: 10.1117/1.OE.55.7.077105]

Keywords: wafers; biophotonics; waveguides; photonics; sensors and fiber optic sensors.

Paper 160562 received Apr. 18, 2016; accepted for publication Jul. 1, 2016; published online Jul. 28, 2016.

1 Introduction

Detection of pathogens in food is an emerging trend. The infections caused by foodborne pathogens is a major public health concern and a major cause of death.[1] Rapid detection tests are required to detect contaminations during preparation, handling, and transportation. Varieties of contaminations come from various organisms, the most important ones being *Aeromonas hydrophila*, *Escherichia coli* (*E. coli*), *Shigella* spp., *Salmonella typhimurium*, *Pseudomonas*, *Campylobacter jejuni*, and *Staphylococcus aureus*. Protection of health is a major concern, for that various approaches and methodologies have been employed to detect foodborne pathogens.[2]

In this report, *E. coli* strain is used as a model and morphology of this prepared strain is determined by scanning electron microscope (SEM). The small size and structural "simplicity" of *E. coli* is certainly an advantage in making *E. coli* a model organism for the study of living matter. The envelope of *E. coli* contains three layers: the cytoplasmic membrane, the peptidoglycan or murein layer, and the outer membrane.[3] To detect *E. coli*, a biosensor is a better alternative instead of traditional and time-consuming culturing methods. Optical biosensors are in great demand in recent years due to their sensitivity and selectivity.[4] There are numerous optical biosensors readily available these days based on refractive index (RI) detection, such as surface plasmon resonance-based biosensors,[5] interferometer-based biosensors,[6] optical waveguide-based biosensors,[7] optical ring resonator-based biosensors,[8,9] and optical fiber-based biosensors.[10] All these above-mentioned biosensors detect changes in RI of the sensing sample using an evanescent wave sensing technique.[11,12] Evanescent wave fields have a property of exponential decay from sensor surface to sample analyte and only changes within the penetration depth of evanescent field are probed. Under normal conditions this penetration depth has an upper limit of 100 to 200 nm. Typical bacterial cell sizes vary from 1 to 3 μm in length, where a minimum portion of the bacteria is affected by the evanescent field, which leads to reduction in sensitivity. In contrast, enzyme-linked immunosorbent assay is popular in market. Although, it was introduced to market more than two decades ago, it is experiencing sensitivity issues as its incubation time is in hours.[13] Liquid chromatography–mass spectrometry is also an effective system whereby the mass spectrometry component functions by transforming the ionized (charged) state of molecules using the mass-to-charge ratio. This system is also costly and time consuming.[14] Among all these sensing techniques, a class of optical materials known as photonic crystal waveguide (PCW) may hold the key to the continued progress. Photonic crystals offer the possibility of controlling and manipulating light by opening a gap in the waveguide within a given range of frequencies. Structures with periodic variations in dielectric constant can influence the nature of photonic modes in the material. Yablonovitch's[15] aim was to control the radiative properties of materials, while John[16] reported that photon localization was caused by introducing a random RI variation.[17] PCW biosensor is advantageous for rapid, accurate, label-free, and sensitive detection.[18] Moreover, it offers dispersion free propagation, having compatibility with on-chip integration and room temperature operations.[19] Silicon dioxide (SiO_2) layer is used as a base

*Address all correspondence to: Balveer Painam, E-mail: balveer.pv@gmail.com

0091-3286/2016/$25.00 © 2016 SPIE